8-2008

Microstructural Control and Alloy Design of the Ti-Al-Nb-W-B Alloys

Lan Huang
University of Tennessee - Knoxville

To the Graduate Council:

I am submitting herewith a dissertation written by Lan Huang entitled "Microstructural Control and Alloy Design of the Ti-Al-Nb-W-B Alloys." I have examined the final electronic copy of this dissertation for form and content and recommend that it be accepted in partial fulfillment of the requirements for the degree of Doctor of Philosophy, with a major in Materials Science and Engineering.

Peter K. Liaw, Major Professor

We have read this dissertation and recommend its acceptance:

Chain T. Liu, James R. Morris, John D. Landes

Accepted for the Council:
Dixie L. Thompson

Vice Provost and Dean of the Graduate School

(Original signatures are on file with official student records.)

To the Graduate Council:

I am submitting herewith a dissertation written by Lan Huang entitled "Microstructural Control and Alloy Design of the Ti-Al-Nb-W-B Alloys". I have examined the final electronic copy of this dissertation for form and content and recommend that it be accepted in partial fulfillment of the requirements for the degree of Doctor of Philosophy, with a major in Materials Science and Engineering.

Peter K. Liaw, Major Professor

We have read this thesis
and recommend its acceptance:

Chain T. Liu

James R. Morris

John D. Landes

Acceptance for the Council:

Carloyn R. Hodges, Vice Provost
and Dean of the Graduate School

Original signatures are on file with official student records

Microstructural Control and Alloy Design of the Ti-Al-Nb-W-B Alloys

A Dissertation
Presented for the
Doctor of Philosophy Degree
The University of Tennessee, Knoxville

Lan Huang
May 2008

Dedication

This work is dedicated to my parents, Dr. Boyun Huang and Mrs. Qinglan Yu,
for their love

Acknowledgement

I would like to thank many of those who have help, advised, and cared for me during my Ph.D. study at the University of Tennessee. If it were not because of them, I would not have been able to experience the exciting world of materials science, and enjoy the journey of gaining goals after hard working. My advisor, Dr. Peter K. Liaw, has always been a great guidance through my research work. Not only has he created an environment for me to extend my intellectual skills, but also inspired me to make full use of my potentials, so as to build up a "rich and famous" dream in the scientific world. Dr. C. T. Liu of the Oak Ridge National Laboratory and at the University of Tennessee has given precious instructions on my research work, providing all the necessary materials for my project, and transferring sparkles of wisdom into my research study. Dr. James R. Morris and Dr. John D. Landes, who kindly agreed to be on my committee, have been giving all kinds of help to me, making it possible for me to finish my Ph.D. study. They have been encouraging me on my research work and on every step of my progress.

Many thanks to Mr. Douglas E. Fielden at the machine shop of the Materials Sciences & Engineering Department, Dr. Gongyao Wang, Mr. Fengxiao Liu, and Ms. Migri Stoica for their kind helps.

Many thanks to my family who has always been of great support to me, never letting me down and standing by me at all times.

Acknowledgements are due to the financial support of the Oak Ridge National Laboratory (ORNL), with the late Dr. R. Judkins, Dr. J. Zollar, and Dr. I. Wright as

Program managers, under the contact number of 11X-SP173V; and the United States National Science Foundation (NSF), the Combined Research-Curriculum Development (CRCD) Program, with Ms. Mary Poats as the Program Director, under the contract number of DGE 0203415.

Abstract

The TiAl alloys have been considered as promising candidates for structural-materials applications at around 800^0C. The major concern for the structural use of the TiAl alloys is their low ductility and poor fracture resistance at ambient temperature. Refining the grain size of the TiAl alloys can be an effective way to improve the mechanical properties of the alloys. In this work, new TiAl alloys, containing tungsten (W) and boron (B), have been developed. Using the scanning-electron microscopy (SEM), electron-microprobe, and transmission-electron microscopy (TEM), the effects of W and B on the microstructural evolution of TiAl alloys, including the grain size and lamellar spacing, were analyzed. It is important to point out that fine uniform microstructures (with the grain size smaller than 50 μm) can be conveniently developed after Hot-Isostatic Pressing (HIP) the as-cast alloys at $1{,}250^0$C and 130 MPa for 5 h, produced through arc-melting.

With the increase of the tungsten content, the microstructure of the TiAl-based alloy can be refined. The addition of tungsten can restrain the grain coarsening and stabilize the microstructure up to $1{,}280^0$C by hindering the migration of grain boundaries at high temperatures. It is also noteworthy that the beta phase, a high-temperature residual phase, forms when the tungsten content exceeds 0.4 atomic percent (at.%). The α-phase transus temperature, T_α, has been determined through differential-thermal analyses (DTA) and further proved by the investigation of the microstructural changes during various heat treatments. Different microstructures meeting desirable needs can be developed through heat treatments beyond and below the α-phase transus

temperature. The mass production of the TiAl-based alloy, with the optimal composition developed through arc-melting, has been made through a magnetic-floatation-melting method.

A comparison in the microstructures of the mass production and arc-melting small production has been made. A larger grain size, with a significant amount of the β phase, has been observed in the large ingot. Heat treatments have been conducted in order to obtain desirable microstructures and to minimize the amount of the β phase in the alloy. Hot forging is another effective method chosen to refine the grain size and eliminate the β phase in the alloy. Hot simulation has been conducted to the alloy in order to obtain the optimal parameters for the hot deformation of the TiAl-based alloy. Mechanical testing, such as hardness measurements and tensile tests, have been performed on the alloys.

The addition of the alloying element, such as tungsten, increases the hardness of TiAl alloys by the solution strengthening and refinement of grain sizes. The room-temperature ductility and yield strength of the alloy have been enhanced through the alloy development and heat treatments. A ductility as high as 1.9% has been obtained in the newly-developed TiAl-based alloy at ambient temperature in the heat-treated cast samples. This result demonstrates the potential use of the cast material for structural applications of TiAl-based alloys with controlled compositions and optimal heat treatments.

Table of Contents

List of Tables

List of Figures

1. Introduction

Two-phase TiAl alloys have been receiving considerable attentions because of their attractive properties, such as low density, excellent high-temperature strength, and good oxidation resistance. However, TiAl alloys are quite brittle at room temperature and have relatively low fracture toughness. The mechanical properties of the TiAl-based alloys with lamellar structures depend on three factors: the colony size, interlamellar spacing, and alloying addition. The tensile elongation at room temperature is strongly dependent on the lamellar colony size, showing the increased ductility with decreasing the colony size. The strength at room and elevated temperatures is sensitive to the interlamellar spacing, showing the increased strength with decreasing the interlamellar spacing [1].

The as-cast TiAl-based alloys are usually coarse in the grain size. A refinement in the microstructures is necessary to meet the desirable applications. Additional elements, such as W, B etc., added into the TiAl-based alloy can help refine the grain size. Related heat treatments can facilitate the development of the desirable microstructures. In general, the fully-lamellar (FL) structure has a better overall property than the other microstructures. But it has the low room-temperature tensile ductility. The duplex structure (DP) tends to have the good room-temperature tensile ductility, but its fracture toughness is low. This dilemma has not been satisfactorily solved recently. For the DP structure, it is hard to enhance its fracture toughness and creep resistance. On the other hand, the room-temperature ductility can be enhanced by refining the grain size of the FL structure. A fine fully-lamellar microstructure has both

good ductilities and fracture strengths, and the fracture toughness and creep resistance are also better than the duplex microstructure.

For deformed TiAl-based alloys, the most optimal selection of the microstructures can be obtained by different kinds of deformation techniques for the microstructural control, and by additional heat treatments for the microstructural rearrangement [1]. Some deformation methods, such as isothermal forging, may initiate small cracks. Since most deformation techniques are costly, optimal solutions are in the search.

With the understanding of the relationship among the fabrication technique, the microstructure, and the related mechanical properties, optimal processing methods can be developed so as to control the microstructures of the TiAl intermetallics, and to improve the associated mechanical behaviors.

In this research, an optimal composition of the TiAl-based alloy has been suggested. A refinement in the colony size of the TiAl-based alloy is obtained by alloying. An investigation regarding the effect of the additional elements on the phase formation, and the microstructural features has been conducted. Heat treatments have been designed to obtain desirable microstructures for excellent mechanical properties. A comparison in the as-cast alloy and hot-deformed alloy has been made. Mechanical properties related to the microstructures are studied through the hardness measurements and tensile tests of the alloys. A room temperature ductility of 1.9% can be reached in the cast and heat-treated TiAl-based alloy.

2. Literature Review

2.1 Research and Development of the TiAl-based Intermetallic Alloys

In the early 1950's, as the uses of titanium alloys in jet-turbine engines for their excellent properties, such as the low density, high strength, high-temperature resistance, and high corrosion resistance, increase, research efforts on the phase diagram, phase composition, phase relationships of TiAl-based alloys, and their mechanical properties, oxidation resistances, had been conducted. Ti-50Al alloys had been studied first, but were abandoned for their low ductility at room temperature. Fifteen years later, 1975 ~ 1982, the Pratt & Whitney (P&W) laboratory in the United States found Ti-48A1-1V-0.3C (atomic percent, at.%), which was the first generation of TiAl-based alloys, to have the best properties, after investigating nearly one hundred other TiAl-based alloy compositions. By the end of the 1980's, the second generation of TiAl-based alloys, Ti-48Al-2Cr-2Nb (at.%) [2], was developed by Dr. S. C. Huang at the General Electric Company. For nearly ten years, the relationship among the alloy composition-processing-microstructure-mechanical properties had been investigated. A complete study of the overall properties of this alloy, such as the physical, mechanical, and chemical properties, had been conducted. The room-temperature ductility of the alloy can reach 1%, which is still not enough for engineering applications. The fracture toughness and the high-temperature creep resistance are low. However, the results had still drawn a worldwide interest in the research of TiAl-based alloys. The Pacific Western Airlines (PWA) developed the 47XD TiAl-based alloy for the high-pressure F119 engine [3]. One outstanding characteristic of this alloy is that it has a great

fatigue-crack-propagation resistance. It has superior creep strength than the IN100, but the highest ductility at room temperature reaches only 1.2%.

Based on the COST 501 Round project, Europe developed Ti-47 at.% Al-2 at.% W-0.5 at.% Si [4], a TiAl-based alloy with a high creep resistance, which exceeds the nickel-based alloy IN738LC. But Ti-47 at.% Al-2 at.% W-0.5 at.% Si has a low tensile ductility of 0.5%. Following the research work of many investigators, there is a great improvement in the understanding of fundamental principles, fabrication techniques, microstructures, and overall properties of the γ-TiAl alloys [5]. The first three generations of the γ-TiAl alloys are listed in Table 1*.

2.2 Microstructures of the TiAl-based Alloys

2.2.1 Crystal Structures

The binary phase diagram of the γ-TiAl alloy is shown in Fig. 1*, with the range of Al from 45 to 52 at.%. The basic phase is the γ-TiAl, and the second phase is the α_2-Ti_3Al. γ-TiAl belongs to the Berthollide type of intermetallics. This type of structure remains ordered at any temperature, and its compositions can change within a specific range. γ-TiAl has the Ll_0 crystal structure, with a Pearson sign of TP4, and a lattice space of P4/mmm. Its lattice structure is shown in Fig. 2(a), composed of alternative atomic planes piling between each other, with either only Al or Ti atoms in the [001]

* All tables are located in Appendix A
* All figures are located in Appendix B

direction. The lattice constant in the [100] and [010] directions is different from that in the [001] direction. The crystal structure of the γ-TiAl is face centered tetragonal (FCT), and its lattice constant changes with the content of Al and compositions, in the range of: a = 0.397 - 0.401 nm, c = 0.404 - 0.408 nm, and c/a = 1.01 - 1.05 [6] (a and c represent, respectively, the short and long unit-cell dimensions). The ratio of the axis constant (c/a) can affect the dislocation movement of the crystal. With the addition of V, Mn, and Cr, the value of the ratio can be lowered, and the ductility of the alloy can be enhanced. For those non-stoichiometric γ phases**,** the additional Ti or Al atoms occupy the position of each other, and no vacancy is formed.

Even though in the early stages, the research concerning the ductility of the γ-TiAl-based alloy focused on the high Al-containing single-phase range. It was shown that the lower amount the Al content, the better the tensile ductility of the two-phase alloy would be [7]. Up to now, the most practical TiAl-based alloy in progress consists of the two phases of the α_2-Ti_3Al and γ-TiAl. When there is a small amount of the α_2 phase, oxygen and carbon impurities dissolve in it, thus enhancing the purity of the γ phase, which leads to an increase in the tensile ductility of the γ-TiAl-based alloy. The α_2-Ti_3Al is a Kurnakov type of intermetallic, and the order-to-disorder temperature is about $1{,}125^0$C. Above this critical temperature, the α_2-Ti_3Al is of the disordered hexagonal close-packed (HCP) structure, while below this critical temperature, it is of the ordered $D0_{19}$ structure, and the lattice constants are a = 0.5782 nm, and c = 0.4629 nm. The crystal structure is shown in Fig. 2(b).

Generally speaking, the Ti-rich two-phase alloy is composed of two phases, the $\gamma + \alpha_2$ lamellae. In the lamellar structure, the γ-TiAl and α_2-Ti_3Al laths are alternatively arranged, and they have an orientation relationship as: $(111)_\gamma$ // $(0001)\alpha_2$,$[110]_\gamma$ // $<11\bar{2}0>\alpha_2$. The hexagonal $D0_{19}$ structure of the Ti_3Al phase is equivalent in three $<11\bar{2}0>$ directions; but as for the cubic structure of the TiAl phase, its [110] and [011] directions on the (111) plane are not equivalent. There are three different orientation relationships in the γ lamellae, twins (180^0 rotation axis), 120^0 rotation axis, and the pseudo twins (60^0 rotation axis) [6].

2.2.2 Phase Structures of the TiAl-based Alloys

Four important microstructures of TiAl-based alloys [7], as shown in Fig. 3, are: near-gamma (NG) microstructures, γ [Fig. 3(a)]; duplex microstructures (DP), $\alpha_2 + \gamma$ and γ [Fig. 3(b)]; near-lamellar microstructures (NL) [Fig.3(c)]; and fully lamellar (FL) microstructures, $\alpha_2 + \gamma$ [Fig. 3(d)]. NG are generally inhomogeneous microstructures, it is composed of bulk γ crystals, and fine γ crystals, which are restrained by small α_2 phases. DP is usually the most refined microstructure compared to the other three microstructures, and it is composed of the lamellar colony and equiaxed γ phase, which are of the same volume proportion. NL is composed of the bulk lamellar colony, which occupies most of the volume fraction, and a very small amount of the primary γ phase. FL is composed of completely bulk lamellar structures.

The FL microstructure consists of equiaxed polycrystalline grains with densely packed lamellae, which are always called lamellar colonies. The lamellar colonies are

composed of α_2 and γ laths. The DP microstructure, however, is made up of lamellar colonies with single-phase γ grains distributed around them.

The coarse FL structures with a grain size (d), $d > 500$ μm, exhibit adequate fracture toughnesses, but are usually brittle at room temperature. On the other hand, the DP structures with fine grain sizes ($d < 50$μm) show adequate tensile ductilities but poor fracture toughnesses, and more importantly, worse high-temperature strengths and creep resistances, as compared with the FL materials. The room-temperature tensile yield strength (σ_y), fracture strength (σ_f), and ductility (δ) of TiAl-based alloys increase with decreasing the colony size of the fully-lamellar structure. Based on these results, a material with fine fully lamellar (FFL) microstructures would be expected to have balanced mechanical properties.

After heat treating the TiAl-based alloys at a temperature above $1{,}000^0$C, three phase transformations may take place: $\alpha_2 + \gamma \rightarrow \alpha + \gamma \rightarrow \alpha$, and the single α-phase region extends to $1{,}470^0$C. Thus, different microstructures can be obtained through different kinds of heat-treatments.

(1) As-cast microstructure:

The as-cast microstructure is a structure formed when the liquid metal solidifies in the casting mold. Thus, the grain size is usually large and non-uniform in the compositions. Columnar crystals and cellular structures are found to grow toward the center of the casting mold.

(2) Equaixed near-gamma microstructure:

Following heat treating the TiAl-based alloy in the $\alpha + \gamma$ two-phase region, at a temperature slightly above the eutectoid temperature (T_e), an equaixed near-gamma microstructure with a small amount of α_2-phase grains can be obtained. With a combination of heat treatments, the microstructure can be refined.

(3) Duplex microstructure:

After heat treating the TiAl-based alloy in a temperature range below T_α, the duplex structure can be developed. At the heat-treatment temperature, the equiaxed α and γ phase are formed. The α phase is a high-temperature disordered structure, which can transform into a α_2/γ lamellar structure through the eutectic reaction after air or furnace cooling. Since the α and γ phases restrict each other during the heat treatments, the grain growth is very slow, thus leading to small colony sizes (30 μm - 150 μm).

(4) Near-lamellar microstructure:

Following heat treating the TiAl-based alloys at a temperature range slightly below the α-trasnsus temperature, $T_\alpha - 10^0$C, in the $\alpha + \gamma$ two-phase region, a α_2/γ lamellar structure and a small amount of the equiaxed γ phase can be developed after air or furnace cooling. Since the amount of the γ phase is small, its effect on restraining the α phase is hindered. The colony size is larger than the DP microstructure (200 μm ~ 500 μm). The γ crystal is usually smaller than 30 μm. The larger the temperature far from T_α, the smaller the colony size, but the more the amount of γ crystals.

(5) Fully-lamellar microstructure:

Following heat treating the TiAl-based alloy at a temperature slightly higher than the T_α, $T_\alpha + 20^0C$, the high-temperature α phase can completely turn into a α_2/γ lamellar structure after furnace cooling. Since the heat-treatment temperature is high, and there is no γ phase restraining at the grain boundaries, the α phase grows very fast. Thus, the colony size of the FL microstructure is coarse. For the as-cast fully-lamellar microstructure, the grain size is normally 600 ~ 1,000 μm. With additional heat-treatments and thermo-mechanical processing, the grain size of the FL microstructure can be refined.

The heat treatments of TiAl alloys can be divided into three categories, as shown in Fig. 4. Processes I and II consist of annealing, at a temperature slightly above T_α, and aging afterwards, while Process III contains only aging. The heat-treatment temperature, holding time, heating rate, cooling rate, and final properties are determined by the alloy compositions and the desired microstructures. In Process I, alloys are usually annealed at high temperatures for 0.5 ~ 5 h, cooled to room temperature at a rate of 30 ~ 150°C/min., reheated to an aging temperature, then aged for 4 ~ 100 h. In Process II, alloys are either furnace cooled after annealing, or moved directly from the annealing furnace to the aging furnace. In order to obtain refined and uniformed grains, a fast heating rate is preferred; while in order to avoid crack initiation and supersaturation in phases, a slow cooling rate is preferred. Two-step heat treatments (I and II) are for heat-treating non-lamellar structural alloys. Process III heats the alloy directly to the aging temperature without annealing. This process is used for alloys,

which do not need to change their as-cast structures, or alloys with stabilized microstructures (fully lamellar), which only needs the aging control. The aging temperature in Fig. 4 can be chosen either above T_e or below T_e [8].

For different TiAl alloys, the general principles for the heat treatment are the same, but since there are differences in the compositions, specific heat-treatment schedules can be designed to develop the best overall properties.

2.2.3 The β phase of the TiAl-based Alloys

Adding a β phase stabilizer, such as Cr, Nb, W, and Mo, to γ-TiAl-based alloys can form a β phase, which usually appears to be a bulk structure or contains small precipitates. Generally, the β phases, which grow along the grain boundary, decrease the creep resistance of the alloy. The β phase commonly exists in the TiAl alloys. Research had been conducted on Ti-49Al-2W (at.%), and small particles had been found at the grain boundaries between the equiaxed γ phases and $\alpha_2 + \gamma$ lamellar microstructures [9]. A discontinuous β phase was found to be rich in W and Si in Ti-47Al-2W-0.5Si [10].

The orientation relationships among the β, α_2, and γ phases are: $(0001)\alpha_2$ // {111}γ // {110}β and 〈1120〉 α_2// 〈110〉 γ // 〈111〉 β. The β phase has a cubic structure with 8 atoms as its nearest neighbors, which are all different atoms. The lattice constant at 900^0C is $a_0 = 0.33065$ nm. Its crystal structure is shown in Fig. 2(c). The β phase cannot exist at room temperature without alloying the intermetallics.

Experiments on the ABB-23 alloy showed that when there are beta-phase stabilizers, such as W, in the TiAl-based alloy [11], the β phase tends to precipitate with

the dissolution of the α_2 phase, which is rich in W, during heat-treatments and creep deformations. The lamellar microstructures of the TiAl-based alloys are grown through ledges [12]. Since the α_2 phase has a higher amount of W than the γ phase, the excessive amount of W formed during the dissolving process of the α_2 lamellae (the growth of the γ lamellae) would go into the undissolved α_2 lamellae, especially at the α_2/γ boundaries and between the α_2/γ ledges. Once the amount of W at these places outgrows a critical value, β phase would precipitate. Thus, the α_2/γ boundaries and phase ledges are the favorable locations for the β-phase nucleation. Research on the Ti-Al-W-Mo-Si alloy showed that between 760^0C-$1{,}050^0$C, there is a three-phase ($\alpha_2 + \gamma + \beta$) region, where W, Si, Mo will be rich in lamellar boundaries, there is a phase-transformation action of $\alpha_2 + \gamma \rightarrow \alpha_2 + \gamma + \beta$ [13].

The morphology of the β phase may vary with the alloy compositions and the processing states. The β phase formed at the interface of the α_2/γ lamellae may be of an oval sphere shape [13]. In the ABB-23 alloy after the hot isostatic pressing (HIP) and heat treatment, discontinuous bar-shaped and massive Ti (Al, W) phases with the β crystal structure were found [14].

With the calculations and analyses of the dielectric structure and phase structure factors of the alloy with β-stabilizing elements, W is the best β-stabilizer, V, Mo, and Nb are the next, and Ta, Hf, and Zr are the weakest. Mn, Fe, and Cr are β-phase eutectoid elements, which can easily form compounds through the eutectoid reaction. These compounds tend to make the alloy brittle. Even though Zr and Hf can stabilize the β phase, they are also α phase stabilizer, so they are not very effective in extending

the β-phase region. In this case, V, Mo, and Nb are more often chosen as alloying elements.

2.3 Mechanical Properties of the TiAl-based Alloys

2.3.1 Tensile Ductility

At room temperature, the yield strength of the TiAl-based alloy is usually between 250 ~ 600 MPa, and the fracture strength is around 300 ~ 700 MPa [17]. These values are affected by the grain size, lamellar spacing, and microstructures. For the FL microstructure, when the lamellar colony size refines from 1,200 μm to 300 μm, the yield strength changes from 300 MPa to 500 MPa [18]. This trend can be explained by the Hall-Patch equation: $\sigma_{0.2} = \sigma_0 + k_\lambda \lambda^{-1/2}$, where $\sigma_{0.2}$ is the 0.2% offset yield strength, σ_0 and k_λ are material constants, and λ is the lamellar spacing. For the polysynthetically twinned (PST) single crystal, its yield strength is related to the tensile angle, ϕ (the angle between the lamellar interface and the tensile hard direction). Since the deformation appears on the {111} plane, $\phi = 45^o$ is the deforming direction (soft direction), and the yield strength is approximately 90 MPa. At $\phi = 0^o$ and $\phi = 90^o$, which is known as the hard direction, the yield strengths are 290 MPa and 500 MPa, respectively [18].

To increase the room-temperature ductility, the microstructures of the binary-phase intermetallic alloy should have a uniformed fine grain size. With the thermo-mechanical processing (TMP), and additional heat treatments, the grain size can be refined to 30 ~ 60 μm, the room-temperature ductility can reach 1.7%, which is much

higher than the original as-cast alloys that have a large grain size and are usually difficult to refine through heat treatments. The tensile ductility of the FL microstructure, which is usually low, together with its yield strength, can be increased, when the grain size is refined. For PST crystals, its tensile ductility is related to the tensile angle. The tensile ductility reaches the highest point at the soft direction ($\phi = 30^o$), since in this direction, the shearing deformation is not subjected to the lamellar interface, thus exceeding the ductility of the fully lamellar structure. Moreover, the γ/α_2 dual phase alloy has a better tensile ductility, which is related to the transferring of the oxygen from the γ phase into the α_2 phase, since the solubility of oxygen in the α_2 phase is much higher than that in the γ phase [20].

There is a significant brittle-ductile transition point in the dual-phase intermetallic alloys. For a typical tensile strain rate of 1×10^{-4} s^{-1}, the brittle-ductile transition temperature (BDTT) is around 620 ~ 800^0C, and is related to the microstructure. For PST crystals, when the tensile orientation angle is $\phi = 0^o$ or $\phi = 30^o$, there is also a brittle-ductile transition point, but for $\phi = 30^o$, the transition is not so obvious. When $\phi = 90^o$, the tensile ductility of the PST is small, and there is no brittle-ductile transition found even when the temperature is raised to $1{,}100^0$C [21]. This is similar to the polycrystalline intermetallic alloy with the FL structure. Under the BDTT temperature, there is not much influence of temperature on the yield strength of the TiAl-based alloy. Above the BDTT temperature, the yield strength drops dramatically with the increase of the temperature.

The room-temperature ductility is always low, which is generally an obstacle to the application of the TiAl-based alloys. Recently, methods used to improve the ductility of the intermetallic alloys are:

(1) Control the composition of the alloy, so that the atomic percent of the Al is between 45% ~ 49%. Induce a small amount of the α_2-Ti_3Al phase to form the binary-phase TiAl-based alloy. The fine microstructure of the alloy has the better ductility.

(2) Alloy the TiAl-based intermetallic with elements, such as Cr, V, Mn, Si, C, and B, to increase the room-temperature ductility.

(3) Improve the processing techniques of the alloying procedure. Combining high-temperature mechanical processing, such as isothermal forging and hot extrusion, with a heat treatment, the final microstructures of the alloy can be controlled. With the use of the directional-solidification method, the rapid solidification technique, and HIP, microstructures of the alloy can be improved.

(4) Refine the colony size of the alloys.

(5) Reducing the ratio of c/a in a single-phase γ-TiAl can increase the tensile ductility. But for the dual-phase alloy, reports have shown that there is a little relation between the c/a value and the ductility [21].

(6) Improving the purity of the alloy can be an effective way to enhance the tensile ductility at room temperature.

(7) Adding ductile particles or fibers into the intermetallic alloy can increase the tensile ductility.

2.3.2 Fracture Toughness of the TiAl-based Alloys

The microstructure of the TiAl-based alloy has a great effect on the fracture toughness of the material. It has been concluded that, as the volume fraction of the lamellar colony increases, the fracture toughness of the TiAl-based alloy increases. For the four typical microstructures of the TiAl-based alloy, the fully-lamellar structure has the best fracture toughness. The duplex structure has a better fracture toughness than the equiaxed single-phase γ-TiAl alloy. The reason that the FL structure has the best fracture toughness is as follows:

(1) a fully-lamellar structure can initiate a large plastic strain at crack tips, and can increase the resistance to the crack propagation;

(2) the difference in the structure and the orientation between the neighboring lamellae can restrain the slip bands and the cleavage cracks to cross the interface, thus deterring the crack from propagation;

(3) when the crack is stopped at the interface, there is a resolving shear stress along the interface, which causes the interface to slip and, thus, passivate the major crack tip;

(4) microcracks are initiated at the tip of the main crack, which causes a formation of a shear zone between the main crack and the microcracks. These shear zones restrain the expansion of the cracks. Only when the shear zone is deformed and broken down, the major crack could, then, propagate through. In this case, the deformation and rupture of the shear zone enhanced the toughness.

Decreasing the lamellar spacing of the TiAl-based alloy can enhance the crack-initiation toughness, K_{IC}, and the crack-growth toughness, K_S. But for the grain size, it has a more complicated influence on K_{IC} and K_S. Based on the research of Ti-46.8at.%A1-2.3 at.%Nb-1.6 at.%Cr-0.9at.%V [23], when the colony size is smaller than 600 μm, both K_{IC} and K_S increase with increasing the colony size; when the colony size increases to 600 μm, the fracture toughness is no longer dependant on the colony size; when the colony size exceeds 600 μm, the fracture toughness is related to the size of the shear zone, which is influenced by the lamellar spacing and the orientation of the lamellar colony.

Additional alloying elements and adjusting processing techniques can change the mincrostructure, thus influencing the fracture toughness. The addition of Cr into the TiAl-based alloy can obviously increase the amount of the lamellar structures, which can lead to the formation of the lamellar fracture zone in order to increase the resistance of the fracture propagation, thus, increasing the fracture toughness [24]. The addition of Nb deters the fracture toughness, and this trend might be caused by the influence of Nb on the grain boundaries. With the addition of Nb, deposits have been found at the grain boundaries. The failure of the TiAl-based alloy is related to the microcracks, which are nucleated, propagated, and gathered at the grain boundaries or phase boundaries. Depositions along the grain boundaries can weaken the bonding strength between the grains. On the other hand, they can facilitate the nucleation of the microcracks, which can increase the possibility of the fracture along the grain boundaries. The effect of

processing techniques and heat treatments on the fracture toughness of the TiAl-based alloy lies in the influence of these procedures on the microstructures [25].

2.3.3 Creep Resistance of the TiAl-based Alloys

The fully-lamellar structure does not only have the best toughness, but also the highest creep resistance among the other three microstructures (shown in Fig. 5) [26]. Its transient-creep and steady-state creep rates are both lower than the other microstructures. The time needed for the FL structure alloy to reach the 0.2% strain is two magnitudes longer than the duplex structure. For high creep-resistant TiAl-based alloys, they either are a fully-lamellar structure or contain a large fraction of the lamellar structure [27]. Research indicates that during creep, deformation twins occur in the γ phase and, then, refines the grain. For the α_2 lamellae, it tends to dissolve and spheroidize, which leads to an increase in the lamellar spacing.

2.3.4 Fatigue Behavior of the TiAl-based Alloys

At a temperature below 850^0C, the DP structure has a better low-cycle-fatigue life (LCF) than the FL structure, and shows a good high-cycle-fatigue life (HCF). But at a higher temperature, the FL structure has a longer fatigue life. In the DP structure, cracks are formed at the surface of the alloy. For the FL structure, cracks are usually developed inside the alloy, and these cracks go through a propagation stage. The non-uniformed microstructures hinder the fatigue behavior.

The research on TiAl-based-alloy plates showed that fatigue cracks first nucleate at the shear zones and the grain boundaries, which are impacted by the shear bands [23]. But due to cyclic hardening, most microcracks are in a closed state, and are unable to move. At room temperature, microcracks are more likely to nucleate in the FL structure than in the equiaxed γ structure. But just like fracture toughness, the propagation and gathering of microcracks is much faster in the equiaxed γ structure than in the FL structure [28]. In the FL structure, the initiation of microcracks is a continuous procedure, but the newly-formed microcracks are separated by the shear band, and the already-existing expanding or non-expanding microcracks. The shear zone between the microcracks can stop the cracks from propagating, only when the alloy is under a quasi-static load. When the alloy is under the cyclic load, the shear zone is destructed by fatigue, and loses its protection from the crack propagation. In the FL structure, expanding microcracks, stable microcracks, and newly-nucleated microcracks form up the macrocracks of the alloy.

2.3.5 Superplasticity of the TiAl-based Alloys

Starting in the 1990's, researchers have become interested in the superplasticity of the TiAl-based alloys. The superplasticity of the TiAl-based alloy usually occurs at a temperature above $1{,}000^0$C. At this high temperature, expensive mold materials are needed, and the alloy oxidizes severely. Thus, finding a way to lower the superplasticity temperature has become a critical issue. Now, the superplasticity temperature has been lowered to $700 \sim 900^0$C [29], or even lower. Usually, equiaxed fine microstructures are

needed to obtain the superplasticity. But to transform as-cast bulk TiAl-based alloys into fine equiaxed structures needs complicated thermo-mechanical processing, which causes a dramatic increase in the cost. This trend leads to another critical issue, how to develop the superplasticity under the condition of large TiAl-based alloy grains [30]. Research has been conducted, and the superplasticity has been found in TiAl-based alloys with a grain size of 20 ~ 95 μm [31].

The un-equiaxed thermally-deformed microstructure (including deformed metastable structures) also shows a good superplasticity. Besides lowering the superplasticity temperature of the alloy, enhancing the rate of the superplasticity can also strengthen the mechanical property of the alloy. This trend not only reduces the oxidation resistance of the alloy, which sensitively influences the mechanical property of the TiAl-based alloy; but also enhances the production efficiency, which is very much of practical use. The strain rate of the TiAl-based alloy under superplasticity is in the range of $10^{-2} \sim 10^{-5}s^{-1}$, there are rates, which are higher than $10^{-2}s^{-1}$ that is close to the practical use.

Two applications of the superplasticity are: (1) shaping the parts; and (2) solid-state welding. At the temperature of $1{,}150^{0}$C [32], hemisphere-shaped, arc-shaped, and wave-shaped parts were obtained from a 1 mm sheet of Ti-48 at.% Al-2 at.% Cr. At the temperature of $1{,}000^{0}$C, a box shape was obtained from Ti-47 at.% Al- 2 at.% Cr- 0.2 at.% Si and Ti-48 at.% Al-3.5 at.% (Cr, Mn, Nb, Si, B); more complicated shapes were obtained from the Ti-47 at.% Al-2 at.% Cr-0.2 at.% Si sheet. The application of the superplasticity in the TiAl-based alloy is rising. We can predict that the superplasticity

is a useful technique, which can overcome the difficulty of metal working of the TiAl-based alloy, and it will turn into an essential technique in processing the alloy.

2.4 Composition Design of the TiAl-based Alloys

The first step in designing the TiAl-based alloys is to control the Al content. The amount of Al has to be less than 53 at.% in order to obtain a two-phase alloy. Experimental results show that, the best ductility lies in the region of 45 ~ 47 at.% Al [35].

Recently, research has been focused on the alloying of the intermetallic, in order to enhance the properties of the alloy. Major points are on the improvement in the ductility and oxidation resistance. Generally, alloying elements can affect the alloys through the intrinsic and extrinsic effects. The intrinsic effect changes the properties of the alloy directly, while the extrinsic effect affects the alloy indirectly through the change of microstructures. The objects of the following additional elements are [7, 36]:

(1) enhance the ductility and oxidation resistance: Nb, Ta, W, Mo, etc.;

(2) enhance the ductility but decrease the oxidation resistance: Cr, V, Mn, etc.;

(3) enhance the strength: Cr, V, Mn, Mo, Ta, Hf, Sn, W, Ca, Sb, La, B, C, N, etc.;

(4) enhance the ductility: Si, C, B, N, P, Se, Fe, Ni, Ca, Sb, La, Mo, Fe, etc.;

Since there are differences in production methods, machining techniques, and heat-treatments, different effects can be obtained even if the same kind of element is added [35], and the explanation may vary. But the effects of niobium (Nb), boron (B), tungsten (W), and silicon (Si) are clear: Nb is a beta-phase stabilizer, and it can enhance

the ductility and oxidation resistance of the alloy [37]; B forms borides in the TiAl-based alloy, and it tends to refine the grain size, and enhance the mechanical properties [38, 39]; W can stabilize the beta phase, and a small amount of W can enhance the strength and creep resistances of the TiAl-based alloy [40, 41]; Si can notably strengthen the creep and oxidation resistances of the alloy. The distribution and existing arrangements of the Nb, B, W, and Si are controlled by processing procedures, machining techniques, and heat treatments. They are very important in changing the properties of the intermetallic alloys [42]. Below is a summarization of the effects of alloying elements in TiAl-based alloys:

2.4.1 Nb in TiAl-based Alloys

Nb has a high melting point (2,468°C), and good resistance to oxidation. The addition of Nb in the TiAl alloy can increase its high-temperature strength and oxidation resistance [47]. Depending on the amount of Nb, there are high-Nb TiAl alloys (~ 23 at.% Nb and ~ 20 at.% Al), medium-Nb TiAl alloys (17 ~ 18 at.%Nb and 20 ~ 30 at.% Al), low-Nb TiAl alloys (10 at.% Nb and 40 at.% Al), and less-Nb TiAl alloys (~ 2 at.% Nb).

With the method of the substitutional solid-solution strengthening, the moving Peierls-Nabarro (P-N) force of dislocations (the force required to move a dislocation through the crystal lattice), and the critical resolved shear stress, τ_{CRSS} (the threshold value of the shearing stress on the slip plane in the slip direction when slip begins), of the γ-TiAl-based alloys have been enhanced [45]. The Nb content in the high Nb-

containing TiAl-based alloys significantly increases the elevated-temperature strength. The main effect of high Nb contents on high-temperature strengths relies on the increase of the value of σ_0 in the Hall-Petch equation:

$$\sigma_{0.2} = \sigma_0 + k_\lambda \lambda^{-1/2}$$

where $\sigma_{0.2}$ is the 0.2% offset yield strength, σ_0 and k_λ are material constants, and λ is the lamellar spacing. It means that the friction stress of moving dislocations arises mainly from the Peierls stress of the lattice, and the interactions between dislocations are much stronger than those for TiAl-based alloys with less Nb contents. The high Nb content also improves the elevated-temperature stability of microstructures of the TiAl-based alloys, resulting in the improvement of the high-temperature strength.

Niobium can improve the oxidation resistance of the alloy, because Nb^{5+} can replace Ti^{4+} in TiO_2, reduce the amount of anions, improve the protection of TiO_2, and facilitate the formation of Al_2O_3 [47]. Nb can lower the solubility of oxygen in the alloy, which can restrain the interior oxidation and improve the structure of the Al_2O_3 in order to form an interlinked reticulate structure. The structure change of the inner Al_2O_3 and the stability change of the outer Al_2O_3, which is linked to the TiO_2 layer, can lead to a large decrease in the oxidation resistance of the alloy. The amount of Nb to be added is generally determined from the oxidation resistance required.

2.4.2 W in TiAl-based Alloys

The addition of W may increase the room-temperature strength and high-temperature strengths of the TiAl alloy [48-49]. Furthermore, the addition of W improves the oxidation resistance [47] and enhances the creep resistance [52].

The W addition in the Ti-Al-Nb alloy tends to segregate between the dendrites and facilitate the formation of the β phase, which can refine the lamellar colony. After the heat treatment, W is enriched in the β-precipitated phase. The β phase can precipitate either in the grain, or at the boundaries of the equiaxed γ crystals [50]. A small amount of W can enhance the room-temperature and high-temperature strengths of the Ti-Al-Nb-W alloy [48, 49]. But the addition of W can lead to structural segregations in the as-cast alloy. These segregations, such as the dendrites structures formed in the as-cast alloy, can initiate cracks [50], which deter the ductility of the alloy.

The mechanism of enhancing the high-temperature oxidation resistance by W is similar to that of Nb [47]. W can effectively improve the oxidation resistance of the TiAl-based alloy, especially at 900^0C. With the increasing amount of W, the oxidation mass decreases. The oxidization surface, from the outer to inner sides, of the TiAl-based alloy, with the W addition, is: TiO_2/Al_2O_3 (continuous)/Al_2O_3 (reticular) + TiO_2/Ti_3Al/TiAl base alloy. At 900^0C, there is no oxidization occuring inside the alloy. The inner reticular Al_2O_3 is combined with the outer Al_2O_3 layer. This extended Al_2O_3 screen enhances the oxidation resistance of the alloy. At $1{,}000^0$C, a small amount of oxides are found in the TiAl-2 at.% W alloy. The addition of W can reduce the amount

of oxygen in the alloy. W represses the initial growth of TiO_2, and facilitates the formation of the outer Al_2O_3 layer, especially the inner reticular Al_2O_3 layer, thus enhancing the oxidation resistance.

Tungsten was found to improve the creep properties significantly [52]. The dynamic deformation controlled by dispersion slowed down by the W solute, and the creep resistivity of the alloy increased.

2.4.3 B in TiAl-based Alloys

B has a significant effect on the grain refinement of TiAl alloys [54, 55]. Also the addition of B can strengthen the alloy by forming secondary TiB_2 particles [56]. B can evidently restrain the grain growth of the α phase at and above the α phase transus temperature. The addition of B has become an effective way to refine the grain size of the TiAl-based alloy. The mechanism of refining the alloy by B can be explained in many ways. The most accepted explanation is that, as the alloy solidifies, the high melting-point borides formed in the alloy will become the grain nucleation nucleus, which facilitates the refinement of the alloy. Boron is added into the TiAl-based alloys as an in-situ ceramic phase. It exists as borides, such as TiB_2, TiB etc., and segregate along γ/γ or α_2/γ interfaces, in order to refine the grain size [57]. A small amount of boron tends to dissolve in the α_2 and γ phase as strengthening phases, which can enhance the properties of the alloy. Any refinement in titanium-boride precipitates, i.e., breaking down long titanium-boride precipitates by thermomechanical processing, or

limiting the boride-precipitate growth by fast cooling during solidification, will increase the ductility significantly [58].

Pu et al. found that the TiB_2 phase can be easily formed in the TiAl-based alloys [59], and no typical grain-boundary segregation of B in the as-cast alloys was found. The thermal deformation can facilitate the grain-boundary segregation of B, which leads to a restraint in the growth of grains. If the boron segregates along the γ/γ or α_2/γ phases as TiB_2, TiB, etc. in order to refine the grain size, the restraint mechanism is due to the formation of the second phase. If B dissolves in the α_2 and γ phases in the atomic state, which refines the lamellar phase, and improves the properties of the alloy, the restraint mechanism is due to the atomic aggregation. The combination of B and W in TiAl-based alloys can refine the lamellar structure, homogenize the lamellar spacing, and effectively enhance the thermal stability [60]. The B addition has a great effect on the grain uniformity. The research in the CTI-8 alloy by Liu et al. showed that, B has an important control over the lamellar structure of the TiAl-based alloy [61]. The amount of 0.1 at.% of B can help develop uniform microstructures in the alloy. With a less amount of B, the abnormal growth of grains will occur during thermal processing. The tensile ductility of the sample with a uniform grain structure more than doubles that with an abnormal grain structure.

2.5 Powder-Metallurgy Technique

The powder metallurgy technique is a near net shaping method. It is also an important technique to produce alloys of refined microstructures. It is suitable for

various materials, especially the brittle materials, which are difficult to deform, such as the ceramics, sintered-carbides, and intermetallics.

The powder-metallurgy (PM) technique includes the powder production and consolidation. The source of the powders for TiAl-based alloys includes: the mixture of the Ti and Al powders, mechanical-alloying powders, the rapid solidification of pre-alloy powders, rotation-electrode-atomization powders, and other additional elemental powders. The consolidation of the TiAl-based alloys includes: the sinter-reaction method, the high-temperature exploding method, the hot-pressing method, and the hot iso-thermal pressing, etc. Usually, the smaller the original powder, the more refined the TiAl-based alloy microstructures are. Consolidated alloys can be hot forged, hot extruded, and hot rolled. With the use of PM, sub-micron crystalline TiAl-based alloys can be obtained.

The powder metallurgy includes “sintering + thermo-mechanical processing” and “sintering into a near-net shape” [62]. Since the original grain size of this method is small, the heat-treatment temperature is not as high as the IM procedure, and its final grain size is much smaller. But since the impurities of the TiAl-based alloys produced by this method are hard to control, the use of PM is limited.

2.6 Casting Technique

The casting method for producing the TiAl-based alloy, is a low-cost production, and is able to produce complicatedly-shaped samples. Due to these reasons, it is one of the most useful methods, which are often used in aircraft and automobile

industries. But cast alloys usually have coarse crystal structures, even though they have high fracture toughness and creep resistivity, and the room-temperature ductility is low. Cast alloys are aeolotropism, and have porosities. How to refine the microstructure of the as-cast alloys, and enhance their ductility and density, has become a critical issue.

2.7 Cyclic Heat Treatment (CHT)

The most practically used TiAl-based alloys are the as-cast ones. But since as-cast alloys usually have large grain sizes, refining the intermetallic alloy is an essential subject. There are mainly three methods used in the refinement of the TiAl alloys.

One of the methods used is the cyclic heat treatment (CHT). The CHT of the TiAl-based alloy refers to the cyclic heat-treatment of the steel, and it is based on the phase transformation during heating and cooling. In the TiAl-based alloy, the cyclic heat-treatment temperature is chosen at the transformation temperature, T_α, or eutectic temperature, T_e. γ-TiAl has a FCT structure, α_2-Ti_3Al and α-TiAl have HCP structures. During the heat treatment, the HCP structures, α_2, and the α phase precipitate from the four faces of the FCT γ phase. Since the growth of the α_2 and α phases are different in the directions, the growth is restricted, and thus, the α_2 and α particles from the γ phase are refined. During cooling, the γ phase precipitates from the α_2 and α phases, with a refined grain size than before. When heat-treated afterwards, the α_2 and α phases will, then, again precipitate from the γ phase in four favorable directions. The grain size is, then, refined. So, as the cycle goes on, the more refined the alloy will be.

It is well known that the uniform fine-grain duplex γ-TiAl alloys can be obtained by CHT. Fine full lamellar (FFL) microstructures could be obtained by the method of the cyclic heat treatment in the α + γ phase field. But its difficulty in controlling the tendency to form cracks has impeded its wide industrial applications. Using the improved cyclic heat-treatment technology, a series of fine duplex microstructures were obtained. With the increase of the number of heat-treatment cycles, the uniformity and the spheroidicity of the materials were largely improved, and a duplex microstructure of the γ-TiAl alloy with varied fractions of lamellar structures could be obtained by changing the time and temperature of the cyclic heat treatment [63]. The mechanism of the cyclic heat treatment is: (1) For each cycle of the heat treatment, the concentration of the two phases, α and γ, will change. This kind of change depends on the nucleation and growth of the new grains, subject to the new phase balance. (2) Dislocations, twins, stacking faults, which were trapped in the α + γ phases through the heating and cooling procedures, are the nucleation spots for new grains. As the new grains are generated, the number of grains per unit volume will increase, thus, refining the grain size of the alloy. The merits of CHT are: this procedure of the refinement does not need any mechanical process, so that the usage of the material is more efficient. Since the alloys used in CHT are the as-cast material, the shape of the alloys can be complicated, and the casting equipments could be simple. The disadvantages of CHT are: cyclic procedures can cause the over-consumption of energy; the multiple procedures can lead to crack initiation since the alloys are usually

large in size, the homogenization of microstructures in the alloys is hard to obtain [64, 65].

2.8 Dynamic Recrystallization Technique

In thermal-deformation techniques, the original ingots can be the as-cast or powder-metallurgy sintered ones. For the isothermal forging, the grain size of the TiAl alloys is refined through the dynamical recrystallization. It is a dynamic pressing procedure to refine the grain size, which is conducted at a static high temperature. The shear strain in the lamellar structure of the γ-TiAl alloy can be induced by the heavy deformation during hot working. The shear strain, which is parallel to the boundaries of the lamellar structure, can make the lamellar structure produce a great amount of dynamic recrystallization structures. The grain size of the TiAl alloys is refined through the dynamical recrystallization. The merit of this procedure is: it is a preferable way to process brittle materials, since the alloy is kept at a higher temperature, and the speed of pressing is kept even. But iso-thermal forging will initiate microcracks, and microstructures are not homogenized [66]. As-cast ingots needed more procedures in the iso-thermal forging than powder-metallurgy ingots. The previous ones need 15 ~ 20 times of forging, while the later ones need only 3 ~ 5 times.

The merit of this procedure is: it is a preferable way to process brittle materials, since the alloy is kept at a higher temperature, and the speed of pressing is kept even.

But the iso-thermal forging will initiate small cracks, and microstructures are not homogenized [66].

2.9 Thermal-Mechanical Deformation Technique

Thermal-mechanical methods, such as hot extrusion and rapid canned forging, are the most commonly used techniques in grain refinements. With the use of this method, the grain size can be efficiently reduced from hundreds to tens of micrometers.

In TiAl-based alloys, the temperature for hot extrusion is usually higher than the temperature used for iso-thermal forging. The parameters for hot extrusion are: a handspike speed of 15 ~ 50 mm/s; a compression ratio of 4:1 ~ 12:1; a preheated temperature of 1,050 ~ 1,450^{0}C. As reported in the research group of Dr. C. T. Liu, the hot-extruded CTI-8 alloy has a better strength and ductility than other lamellar or duplex structured alloys. At the same time, it also bears a better high-temperature creep resistance than other lamellar or duplex structured alloys [67]. The greatest problem of the hot extrusion technique is that the microstructure of the alloy is not uniform. This trend leads to an uneven distribution of grains. With the use of coating, this tend can be reduced, but not eliminated. Equal-angle pressing is a newly developed technique, which is useful to refine the grain size of the TiAl-based alloy. But through this technique, the extent of cracking of alloys is severe, and the improvements need to be conducted.

The rapid canned forging of TiAl alloys is a repeated treatment of the rapid forging and heat treatment. It can refine the grain size and obtain different kinds of microstructures at the same time. With the use of this method, the grain size can be efficiently reduced from thousands of micrometers to ten micrometers. The microstructures of the alloy can be homogenized. Because of the coating, there is no crack initiated [68].

3. Experimental Procedures

3.1 Small Drop-casting Alloy Preparation

3.1.1 Alloy Composition Preparation

In order to strengthen TiAl alloys, reducing the Al concentration is effective in increasing the ratio of the α_2 phase composition. However, the toughness deteriorates, if the Al concentration is reduced too much. More than 45 at.% Al is required in order to secure toughness. The strength of the TiAl alloy is improved with the increase of the Nb concentration, but the elongation decreases. The oxidation resistance of TiAl-Nb alloys is improved up to 7.5 at.% Nb, suggesting that 7.5 at.% is an optimal concentration of Nb. The B addition alone refines the lamellar structure, but causes fragmental and discontinuous α_2 lamellae. In contrast, the W + B addition refines the lamellar structure and produces more uniform and continuous α_2 lamellae [50]. In this research, the base TiAl intermetallic alloy was selected as, Ti-45at.%Al-7at.%Nb-0.15at.%B-χat.%W, where W at the level (χ) of 0.2, 0.4, 0.7, 1.1, or 1.5 was added to the base composition. TiAl-based samples fabricated at the Oak Ridge National Laboratory (ORNL) are [69]:

- Ti-45at.%Al-7at.%Nb-0.15at.%B (base composition)
- Ti-45at.%Al-7at.%Nb-0.15at.%B-0.2at.%W
- Ti-45at.%Al-7at.%Nb-0.15at.%B-0.4at.%W
- Ti-45at.%Al-7at.%Nb-0.15at.%B-0.7at.%W
- Ti-45at.%Al-7at.%Nb-0.15at.%B-1.1at.%W
- Ti-45at.%Al-7at.%Nb-0.15at.%B-1.5at.%W

All alloys were prepared by arc melting and drop casting, using pure Ti, Al, W, and Nb metal lumps together with the semiconductor-grade boron. Alloy buttons were melted at least 5 times and then drop cast into a copper mold with an ingot size of 12.7 x 12.7 x 76.2 mm.

3.1.2 Hot Isostatic Pressing (HIP) and Homogenization Treatments

The equipment used for HIPing is QIF-6 produced by the ABB company. Samples are HIPed under the conditions of: argon atmosphere, 1,250^{0}C, 130 MPa, 5 h, and furnace cooling. After HIPing, a homogenization treatment is conducted at 1,250^{0}C for 16 h in air, followed by furnace cool to room temperature.

3.1.3 Differential Thermal Analyses (DTA)

Based on the differential thermal analyses (DTA), the phase-transformation temperatures were roughly estimated. Combining the microstructure with the desirable grain size, proper heat-treatment temperatures can be determined. With the comparison of microstructures after each heat treatment, a more accurate phase-transformation temperature, such as T_α, can be obtained. The DTA & DSC machine is used for the test. The experimental conditions are: a heating rate of 20^{0}C / min. with an argon atmosphere, and the reference sample is an Al_2O_3 powder.

3.1.4 Heat Treatments

For the alloy heat treatment, it is separated into two steps: first quench the alloy at a temperature above T_α, and then let the alloy slow cool at a temperature above T_α, in the $\gamma + \alpha$ two-phase region or the $\gamma+\alpha_2$ two-phase region. In this technique, microstructures obtained during quenching are essential to the refinement of the alloy, and the non-continuous coarsening of microstructures during slow cooling is also important to the refinement.

The TiAl-based sample alloys are hot-isostatic pressed (HIPed) at $1{,}250^0$C, for 5 h at a pressure of 130 MPa, and then, heat-treated at $1{,}250^0$C for 16 h for homogenization. The heat-treatment temperatures for the sample alloys have been scheduled as: at 900^0C for 360 h; at $1{,}265^0$C for 18 h; at $1{,}280^0$C for 14 h; at $1{,}295^0$C for 10 h; and at $1{,}310^0$C for 5 h. The specimens were encapsulated in quartz tubes with argon gas at 0.1 atmosphere pressure, and then furnace cooled after heat treatments.

3.1.5 Hardness Tests

Hardnesses of the metallographically-mounted specimens were measured, using a diamond-pyramid hardness tester under a 10 Kg load.

3.2 Large Ingot Alloy Preparation

3.2.1 Alloy Preparation

The Ti-45Al-7Nb-0.15B-0.4W (at.%, atomic percent) ingot of 15kg was produced by the magnetic-floatation-melting method, using the German magnetic

floatation cold crucible furnace. High purity Nb, W, B, powders, Ti particles (99.6% purity), and Al pieces (99.99% purity), were uniformly placed in the copper crucible for magnetic floatation melting. The large ingot sample is levitated and melted in the middle of the magnetic field created by the induction coils.

3.2.2 Heat Treatment of the Large Ingot Samples

After HIPping at 1,250^{0}C / 130 MPa / 5h, heat treatments have been conducted to the large ingot samples in order to reduce the amount of the β phase, and obtain the desirable microstructure for mechanical testing later on. As indicated in the phase diagram, heat treating the TiAl-based alloy above 1,250^{0}C can reduce the remaining β phase. Since above this temperature, $\beta \rightarrow \alpha + \gamma$, can take place. Besides reducing the amount of β phase, the grain size is also a very important parameter to consider when heat treating the alloy. In order to control the grain size, heat treating the alloy around T_α-10^{0}C is required. An optimal heat-treating method, including heat-treating temperature, heat treating time, and cooling rate, is to be determined in order to obtain desirable microstructures for the as-cast alloy.

3.2.3 Mechanical Tests

Tensile tests have been conducted to the large TiAl-based ingot samples with the optimal microstructure. After the heat treatments, a fine near fully lamellar microstructure can be obtained, and the amount of β phase can be minimized. Tensile tests have been preformed in order to test the liability of this newly-developed,

massively produced TiAl-based alloy. Tensile tests have been conducted at room temperature, 300^0C, 600^0C, and 800^0C in air on the MTS testing machine, at a strain rate of 1 x $10^{-4}s^{-1}$. The geometry of the specimens is of a bar shape shown in Fig. 53, with a gauge length of 12.7 mm, and a cross section of 2.49 mm.

3.3 Hot Deformation

3.3.1 Hot Simulation and Hot Deformation

Small samples, *d(*10 mm) × *l(*10 mm) [10 mm in diameter and 10 mm in length] were spark-eroded from the large ingot for hot simulation experiments. The small samples were canned in the carbon steel, and then hot-pressed on the Gleeble1500 hot simulator for the hot-simulation experiments. The hot-compression temperatures range from $1{,}050^0$C to $1{,}230^0$C, with a deformation of 50%, at a strain rate of 0.02 s^{-1}. The optimal hot deformation temperature of the TiAl alloy is between $1{,}180^0$C - $1{,}200^0$C. Hot deformation had been conduced to the TiAl-based alloy after the hot simulation experiments. The TiAl alloy had been hot deformed twice, first at $1{,}180^0$C, with a deformation of 60%, and a strain rate of 0.02 s^{-1}; and then at $1{,}180^0$C, with a deformation of 50%, and a strain rate of 0.02 s^{-1}. After the first hot-deformation procedure, the samples had been annealed. Second hot-deformation had been conduced on the TiAl-based after the heat treatment. Following the second deformation procedure of the TiAl-based alloys, heat treatments had been performed on the alloys in order to obtain different kinds of microstructures.

3.3.2 Mechanical Tests

Tensile tests have been preformed on the hot-forged alloy, in order to understand the effect of hot forging on the TiAl-based alloy. After hot deformation and different heat treatments, the microstructure of the TiAl-based alloy changes, the mechanical properties of the alloy have been compared to that of the as-cast, heat-treated alloys. Tensile tests have been conducted at room temperature in air on the MTS testing machine, at a strain rate of $1 \times 10^{-4} s^{-1}$. The geometry of the specimens is of a bar shape shown in Fig. 53, with a gauge length of 12.7 mm, and a cross section of 2.49 mm.

3.4 Nondestructive Detection

3.4.1 X-ray Diffraction Analyses (XRD)

The Rigaku D/max 2550VB + X X-ray diffraction machine is employed for the analyses. Testing conditions are: Cu Kα radiation; nickel filter; voltage 40 KV; electrical current 300 mA; scanning rate 8^0/min.

3.4.2 Metallographic Analyses

Specimens were prepared for optical microscopy by conventional grinding and polishing, using a 0.5 μm diamond paste, followed by etching with Kroll solution, $1\%HNO_3+1\%HF+98\%H_2O$ (vol.%). Metallography was done on the REICHERT MeF3A optical microscope.

3.4.3 Scanning-Electron Microscope (SEM) and Electron Microprobe

The SEM and electron microprobe are used for more detailed analyses of the specimens. The preparation for the specimens is the same as that for the metallography. For the backscattering detection, specimens do not need any etching. For the secondary-electron detection, a Kroll solution is used for etching. JSM-5600LV is employed for the SEM analyses, with an acceleration voltage of 20 KV. The JCXA-733 Microprobe is used for more detailed microprobe analyses. The electron beam used is 2 μm in size, the electric current is 100 μA, and the working voltage is 20 KV.

3.4.4 Transmission-Electron Microscopy (TEM)

In order to obtain the more detailed structure information of the specimens, the TEM analyses are performed. Specimens are spark eroded into slices with a diameter of 3 mm, and a thickness of 0.3 mm, then mechanically thinned into 35 - 45 μm. Foils for TEM are prepared with a twin jet electropolishing, using a solution of a 30% nitric acid plus 70% methanol (volume percent), operating at -20^{0}C, 100 mA, and 30 V. Hitachi H-800 TEM (200 KV) is used for the TEM analyses.

4. Microstructure of Small Arc-melting TiAlNbWB Alloy: Results and Discussions

4.1 As-cast Microstructure of Small Arc-Melting Samples

From the Ti-Al binary phase diagram (Fig. 1), the equilibrium condition of the TiAl-based alloy containing 45 at.% Al mainly consists of two phases, the α_2 and γ phases, resulting in the formation of the lamellar structure. The as-cast TiAl-based alloys contain defects, such as porosities and composition segregations. In the as-cast condition, the TiAl-based alloy is composed of typical non-equilibrium structures, such as cellular structures and dendrites. As shown in Fig. 6, the as-cast Ti-Al-Nb-W-B contains cellular structures, lamellar structures, and dendrites. The addition of B in the TiAl-based alloy can cause the in-situ formation of TiB_2 in the melt. Since the melting temperature of TiB_2 is high ($3{,}253^0$C), it is surround by the TiAl melt during casting and can induce the heterogeneity nucleation during cooling. Under the condition of drop casting, the cooling rate of the Ti-Al-Nb-W-B alloy is very fast, and a peritectoid reaction is involved, as the TiAl alloy cools down. This trend made the compositions within the colony and between the colonies not uniform, thus non-uniform as-cast structures, such as the cellular structures and dendrites, are formed. W and other solutes are enriched at the cellular boundaries and the peripheries of the dendrites.

Figure 7 presents the backscattered images of the as-cast Ti-Al-Nb-W-B alloys. Small amounts of casting defects and porosities are shown by the arrows. Under the backscattering condition, the contrast grade is in the positive correlation with the atomic number of the elements. The greater the coordinate number, the brighter the image is. In

Fig. 7, the boundary of the cellular structure is bright, which indicates that heavy metal elements, such as Nb and W, are enriched in this area. Furthermore, ribbon-shaped phases can be found in the structure of the alloys. These phases are consistent with the boride structures mentioned in references [46, 47]. They are the Ti-B boride phases, shown in the area A of Fig. 7(b), as the ribbon shaped phase. Since these boride phases are bright, heavy metals must be present. Comparing the Figs. 7(a), (b), (c), and (d) as the amount of W differs, the structure of the as-cast alloys varies. In Fig. 7(a), when no W is added into the alloy, the cellular interfaces of the alloy are bright, indicating that there is a strong segregation of Nb at the grain boundaries. As the amount of W increases, cellular structures also tend to grow, and the brightness of the interface increases. Since the composition of Nb is kept constant, W tends to segregate more in the dendrites, as its amount increases.

4.2 Microstructure of HIPed and Homogenized Small Arc-melting Samples

The defects in the TiAl-based alloy under as-cast condition can be eliminated after HIPing and homogenization. Since the Ti-Al-Nb-W-B alloys are kept at a high temperature ($1{,}250^{0}$C) and high pressure (130 MPa) during HIPing. The diffusion process takes place, and the defects, such as porosities in the as-cast material, are eliminated. Figure 8 shows the backscattered-electron images of the Ti-Al-Nb-W-B alloys after HIPing and homogenization. A comparison of Figs. 7 and 8 shows that structure defects, such as cellular structures, dendrites, and composition segregations all have disappeared. From the above results, HIPing and homogenization are effective

ways to eliminate the defects from casting. The lamellar structure after the treatments is more continuous, and the colony size of the lamellae refines. As-cast microstructures are non-uniform, and Nb and W are richly dispersed in the α_2 phase and in the borides. During Hipping and homogenization, the α phase preferentially nucleates at the metastable lamellae-colony boundaries, thus refining the as-cast coarse microstructure. After the homogenization treatment, the Ti-Al-Nb-W-B alloy is fast cooled. The high-temperature α phase turns into a lamellar structure with the remaining of the primary γ phase. This trend made the inhomogeneous as-cast microstructure develops into a duplex structure. As shown in Fig. 8, the microstructure is composed of the lamellar structure, which is composed of the black (γ phase) and white (α phase) lamella; bulky black primary γ phase; and the bright needle-shaped structures, which are borides, distributed in the grains or at the grain boundaries.

As shown as in Figs. 8(a), (b), (c), and (d), as the content of W differs, the equilibrium structure of the TiAl-based alloys varies. Presented in Fig. 9, with the content of W increasing from 0 at.% to 0.2 at.%, 0.4 at.%, and 0.7 at.%, the colony sizes are 70 μm, 50 μm, 32 μm, and 25 μm, respectively; and the interlamellar spacings are 2.46 μm, 2.35 μm , 2.28 μm, and 2.08 μm, respectively. With the addition of W, the microstructure of the Ti-Al-Nb-W-B alloy refines. As the content of W increases, the grain size and the interlamellar spacing decrease. As the amount of W exceeds 0.4 at.%, the trend of the refinement slows down. More accurate analysis has been conducted on TEM on the change of interlamellar spacing of the alloy, shown in Fig. 10, the interlamellar spacing of the alloy decreases as the amount of W addition increases.

From Fig. 9, the colony size tends to change, as the amount of W varies. However, the size of the equiaxed γ phase does not change much. The difference in the W content leads to changes in the shapes of bright phases (later identified as the β phase and borides), especially in the amount of these phases. The volume fraction of these phases increases, as W increases.

To obtain more information of the phase compositions, the energy-dispersive X-ray spectroscopy (EDS) and the electron microprobe are employed. In the lamellar structure, the γ lamellae has a higher Al content and lower W content; the α_2 lamellae has a higher W content and a lower Al content (Figs. 11 and 12). More accurate analyses in structure are conducted using the SEM. In Fig. 13(a), bright needle-shaped phases contain 7.74 at.% of Al, 20.27 at.% of Nb, and 6.79 at.% of W. From the shape and content, these phases could be borides. Beside these needle-shaped phases is the hexagonal phase, which has the same composition as the boride, and, thus, could be the cross-section of the boride. The gray phase in Fig. 13(b) contains 49.54 at.% of Al, which exceeds the amount of 42.45 at.% of Ti, and the amount of other elements are the same as the base alloy. Small cracks are also observed. The gray phase is determined to be the γ phase. γ twin-phases can be triggered to form in regions beside the borides, as exhibited in Fig. 13(c). This trend might be caused by the capture of Ti by B, which can lead to a fast decrease of Ti in the boride-surrounding region, and trigger the formation of the high-Al, low-Ti γ twins. A more clear segregation of these phases is shown through the TEM analysis. Figure 14(a) exhibits the γ twins segregated from the α/γ

lamellae grains, and Fig. 14(b) shows the borides formed in the α/γ lamellae and the triggered γ twins.

4.3 β Phase in the Small Alloy

The composition and structure of the β phase differ as the alloy composition and heat treatment change in the alloy. Particles at the α_2/γ boundaries appear to be the β phase ellipsoids [12]. This is because, the α_2/γ interface, which is enriched in W, is a favorable nucleation site for the β_2 phase. The composition of the β phase in the ABB-23 alloy is 48.9 at.% Ti, 36.4 at.% Al, and 14.7 at.% W. Compared with the nominal composition, nearly 1/3 of the Al has been substituted by W, while the amount of Ti is similar to that in the γ-TiAl. The β phase composition of the Ti-45Al-6Cr (at.%) alloy after the heat treatment at $1{,}200^0$C for 168 h is: 46.7 at.% Ti, 39.3 at.% Al, and 13.9 at.% Cr. For Ti-46Al-2Cr- 2Mo-0.25Si-0.3B (at.%) after the heat treatment at $1{,}150^0$C for 48 h, the composition of the β phase is: 52.16 at.% Ti, 37.58 at.% Al, 3.7 at.% Cr, and 5.19 at.% Mo. From the above results, the β phase has a low Al content, and high contents of alloying elements, such as W, etc [14]. Figure 15 exhibits microstructures of the Ti-45Al-7Nb-0.7W-0.15B (at.%) alloy after HIPing and homogenization. Bright ellipsoid-shaped phases are observed in the figure, which contain greater amounts of W (3.46 at.%) and Nb (12.95 at.%), a lower amount of Al (31.77 at.%), and about the same amount of Ti, relative to the base alloy. The shape of these phases differs from the borides (which are usually long in shape and have polygon cross sections). These phases contain more Al than in the borides, and, thus, identified as the β phases.

The β phase is a high-temperature residual phase. The orientation relationships among the α_2 phase, γ phase and β phase are: (0001)α_2 // {111}γ // {110}β, and 〈1120〉 α_2 // 〈110〉 γ // 〈111〉 β. Compared with the γ phase, the composition of the β phase is closer to that of the α phase. This trend assumes that, when the β phase precipitates from the α phase, the composition fluctuation requirement is easier to meet, which is the reason why the β phase precipitated more often from the ends of the α phase. The research regarding the effect of Ru on the Ti-47Al alloy showed that for the Ti-47Al-1Ru (at.%) heat treated at 1,200^{0}C for 24 h, the formation of the β phase relies on the consumption of the α_2 phase. In the region where the β phase forms greatly, the α_2 phase decreases accordingly. When the heat-treatment temperature exceeds the α phase transus temperature, T_α, the reaction, $\gamma \rightarrow \alpha$, happens. The grain coarsens fast in the single-α phase region. When the β phase precipitates dispersedly, the atoms do not need to move and diffuse in the alloy, and the energy needed is small. This is why the β phase disperses separately in the alloy at high temperatures.

Figure 16, using a more accurate electron superprobe (15 KV), with the alloy containing 0.7 at.% W, shows detailed compositions of the boride and β phase. The bright phase with compositions of Ti-1.0 at.% Al-9.6 at.% Nb-3.6 at.% W-51.9 at.% B can be determined as borides. The other bright blocky phases, which have different shapes, as compared with the boride, composed of Ti-35.7 at.% Al-8.5 at.% Nb-1.7 at.% W, can be determined as the β phase. No β phases with these characteristics are found in the samples containing 0.4 at.% W. Thus, the β phase tends to form at an amount above 0.4 at.% of W.

4.4 Microstructure of Small Arc-melting Samples after Heat Treatments

For quench-temper/aging heat treatments, it is separated into two steps: first quench the alloy at a temperature above T_α, and then let the alloy slow cool at a temperature below T_α, in the $\gamma + \alpha$ two-phase region or the $\gamma + \alpha_2$ two-phase region. In this technique, microstructures obtained during quenching are essential to the refinement of the alloy, and the non-continuous coarsening of microstructures during slow cooling is also important to the refinement. After HIPing and homogenization, Ti-Al-Nb-W-B alloys are heat-treated at scheduled temperatures of: 900^0C for 360 h; $1{,}265^0$C for 18 h; $1{,}280^0$C for 14 h; $1{,}295^0$C for 10 h; and $1{,}310^0$C for 5 h. Microstructures and their evolution are examined.

Microstructures of the Ti-Al-Nb-W-B alloys heat treated at 900^0C for 360 h after HIP and homogenization are shown in Fig. 17. Compared with microstructures before the heat treatment, there is not much difference. It is still mostly composed of lamellar structures. According to the binary phase diagram of the Ti-Al alloy, above the eutectoid temperature (T_e, approximately $1{,}175^0$C), as the heating temperature increases, the fraction of the γ phase tends to decrease, as the amount of the α phase increases in the Ti-45 at.% Al alloy. Heat treating the alloys below T_e, at 900^0C for 360 h, after the redistribution of the elements, the microstructure of the alloy is in an equilibrium condition. The microstructure of the alloy contains a blocky γ phase and α_2/γ lamellae, with the γ phase as the matrix. There is not much change in the grain size.

After the heat treatment at 1,265^{0}C for 18 h, Ti-Al-Nb-W-B alloys contain a less amount of γ lamellae structures, Fig. 18 as compared with that in Fig. 17. Since specimens are kept in the α + γ two-phase region for some time, the α_2 and γ phases tend to grow, and the lamellar structure coarsens. After heat treating the alloy above T_e, at 1,265^{0}C for 18 h, the matrix of the alloy tends to change from the γ matrix to α matrix. The microstructure of the alloy is made up of the blocky γ phase and α_2/γ lamellae. The grain size does not change much in the alloy, but the interlamellar spacing tends to increase (Fig. 18). This is because above the eutectoid point, the concentration of the α (α_2) phase is higher than at room temperature. Since the γ phase is the $L1_0$ structure, it has four close-packed {111} planes. The α_2 phase has a $D0_{19}$ structure with only one close-packed plane (0001). At a heat treating temperature above the eutectoid point, the α phase tends to precipitate from the four close-packed planes of the γ phase. The lamellar structure is formed from the α phase at the eutectoid point of 1,175^{0}C, $\alpha \rightarrow \alpha_2 + \gamma$, with an orientation relation of: $\{111\}_\gamma$ // $(0001)\alpha_2$ $<110>_\gamma$ // $<1120>\alpha_2$. Since the $\alpha \rightarrow \alpha_2$ change is an ordered transformation, the required degree of the supercooling and energy is small. But the γ phase has a different crystal structure from the α phase, and a large amount of supercooling and energy is needed for atoms to transfer and diffuse to nucleate and grow. In a large amount of supercooling, the γ phase does not have enough time to precipitate from the α phase, nor to grow. Thus the volume fraction of the α_2 phase increases. In a region approaching the single-α phase region, it is more difficult for the γ phase to grow, and a greater volume fraction of the α_2 phase forms. When heat-

treating the alloy below T_α, there is little difference in the colony size, but as the α_2/γ lamellae inside the colony tend to be equiaxed, the lamellae coarsen.

Microstructures of the Ti-Al-Nb-W-B alloys, after the heat treatment at $1{,}280^0$C for 14 h, indicate that the lamellar structure tends to coarsen greatly, and the grain size also grows (Fig. 19). When the Ti-Al-Nb-W-B alloy is heat treated at $1{,}280^0$C, the microstructures are composed of mostly lamellae and a small amount of the equiaxed γ phase, which belong to a nearly fully lamellar structure. Even though the specimens are annealed for a long time, there is not much change in the colony size of the alloys, but the lamellae tend to coarsen, and the interlamellar spacing increases.

Figure 20 presents the microstructures of the Ti-Al-Nb-W-B alloys after the heat treatment at $1{,}295^0$C for 10 h. Fine equiaxed γ phase almost disappeared, and the structure is mainly composed of the fully lamellae $\alpha_2 + \gamma$. The colony size of the alloy coarsens significantly, and the average grain size reaches 400 μm.

After the heat treatment at $1{,}310^0$C for 5 h, the microstructure of the alloy, composed of fully lamellae, further coarsens. The grain size reaches 500 μm, shown in Fig. 21.

When heat-treating the alloy at $1{,}295^0$C for 10 h and at $1{,}310^0$C for 5 h, the microstructure of the alloy is composed of only a fully lamellar structure. No primary γ phase is found in the alloy. The grain size tends to grow fast. This is because when the heat-treatment temperature exceeds the α transus temperature, T_α, the alloy enters the single-α phase region. Since the reaction $\gamma \rightarrow \alpha$ takes place, almost all of the γ phase transforms into the α phase, and the α crystals tend to grow rapidly. During cooling, the

reactions, such as $\alpha \rightarrow \alpha + \gamma$, and $\alpha \rightarrow \alpha_2 + \gamma$ take place. The microstructure of the alloy, being heat treated at a temperature above $T_{\alpha,}$ depends mainly on the cooling rate of the alloy. When the alloy is being cooled very fast, the phase transformation has been suppressed, and no γ phase will form. The microstructure of the alloy is composed of the supersaturated α phase, which later on will tend to decompose into martensite structures. If the alloy is cooled down in a medium pace, fine fully lamellae of α_2/γ lamellae will be formed. When the alloy is cooled down slowly, the reaction, $\alpha \rightarrow \alpha_2 + \gamma$, takes place completely, and the α_2/γ lamellae is equiaxed, a fully lamellar structure will be formed.

In summary, the phase compositions of the TiAl alloys, related to the heat treatments and tungsten contents are listed in Table 2. Heat treating the TiAl-based alloys below the α transus temperature, T_α, the phase composition of the 0 to 0.4 at.% W alloys consist of the primary γ phase and $\alpha_2 + \gamma$ lamellae. The 0.7 at.% W alloy contains the β phase, in addition to the primary γ phase and $\alpha_2 + \gamma$ lamellae. When the alloys are heat treated at a temperature above T_α, the phase composition of the 0 to 0.4 at.% W alloys consist of fully lamellar structure $\alpha_2 + \gamma$. The 0.7 at.% W alloy contains a small amount of the β phase which tends to decrease as the heat-treating temperature increases, in addition to the fully lamellar structure $\alpha_2 + \gamma$.

4.5 Differential-Thermal Analyses (DTA)

In order to determine the α-transus temperature, T_α, of the alloy, the heat treatments in the $\alpha + \gamma$ phase region and single-α phase region are previously conducted.

Through the differential-thermal analyses (DTA), T_α, can be determined by the decalescence during the phase transformation of the alloy. From the differential thermal analyses, the Ti-Al-Nb-W-B alloy shows an endothermic reaction around the temperature range of $1{,}280^0$C ~ $1{,}295^0$C, and the peak appears at a temperature around $1{,}290^0$C. This reaction indicates that, a phase transformation occurs at $1{,}290^0$C in the Ti-Al-Nb-W-B alloys. Comparing the microstructures in Figs. 17 to 21, obtained from different heat-treatment temperatures (900^0C, $1{,}265^0$C, $1{,}280^0$C, $1{,}295^0$C, $1{,}310^0$C), the grain size does not change much for the 900^0C, $1{,}265^0$C, and $1{,}280^0$C heat-treatments, but it coarsens significantly at temperatures above $1{,}280^0$C. Apparently, there is a phase transformation in the Ti-Al-Nb-W-B alloy at a temperature above $1{,}280^0$C and below $1{,}295^0$C, which involves $\alpha + \gamma \rightarrow \alpha$. Based on the results from the heat treatments and differential thermal analyses, the α phase transus temperature, T_α, of the Ti-Al-Nb-W-B alloy is around $1{,}290 \pm 5^0$C, and not sensitive to the W concentration. The phase transformation of the Ti-Al-Nb-W-B alloy is consistent with the TiAl7Nb phase diagram, Fig. 22. Thus this phase diagram can be used as a guide for phase information of the alloys in later heat-treatment designs.

4.6 Effect of W and B on the Microstructure of the Alloys

W tends to segregate between the dendrites of the TiAl alloy. In the as-cast lamellar structure of the alloy, W is enriched at the phase interface. W can deter the growth of the new phase and, thus, refine the colony size and the interlamellar spacing. As the content of W increases, this effect becomes more obvious. W is a beta-phase

stabilizer, which is distributed mainly in the β phase. The segregation of the β phase increases with the increase of W. During heat treatments, the growth of the β phase mainly relies on the α_2 phase. Hence, the β phase is usually formed at the ends of α_2 phases, hindering the growth of the grain size and reducing the interlamellar spacing. From the wave-spectrum analyses, the solubility of W in the α phase is high. W has little influence on the precipitation and growth of the γ phase. Thus, W does not affect the size of the equiaxed γ crystal.

Borides can be found in the grains of different TiAl-based alloys. They are usually added into the alloy as alternatives to refine the grains. Borides in the TiAl-based alloys might refine the grain size through a heterogeneous nucleation mechanism.

In the present research, W can refine the microstructure of the alloy. However, as the content of W increases to 0.4 at.%, the effectiveness of the refinement slows down. W is enriched in the borides and tends to make borides locate at the grain boundaries, hindering the growth of the grains. A small amount of W can effectively impede the grain growth, and it is found that 0.4 at.% is most effective in refining the microstructures of the alloy.

4.7 Conclusions

1. A small additional amount of W can refine the grain size of the Ti-Al-Nb-W-B alloys. The lamellar spacing also decreases with increasing the W concentration.

2. The addition of W promotes the formation of the β phase in the base alloy. When the amount of W exceeds 0.4 at.%, the β phase precipitates. The β phase in the

blocky form mainly distributes along the grain boundary. Its composition is close to the α_2 phase, but with a less amount of Al.

3. From the results of microstructural changes related to different kinds of heat treatments, and differential-thermal analyses (DTA), the α transus temperature, T_α, is estimated to be $1{,}290 \pm 5^0$C.

4. The Ti-45Al-7Nb-0.15B-0.4W alloy is a newly-developed TiAl-based alloy, which a fine grain size can be obtained using this composition without any hot deformations or cyclic heat treatments.

5. Related heat treatments can be selected to obtain desirable microstructures for the Ti-45Al-7Nb-0.15B-0.4W alloy. Fine fully lamellae, with good overall properties, can be obtained through heat treatments at temperatures slightly below T_α (T_α - 10^0C). Duplex microstructures can be obtained through heat treatments at temperatures slightly above the eutectoid temperature, T_e (T_e + 10^0C).

5. Microstructure of Large Magnetic-Floatation-Melting TiAlNbWB Alloy: Results and Discussions

5.1 Microstructures of the Large Ingot

As shown in Fig. 23, the as-cast microstructure is composed of an equiaxed fully lamellar structure with an average grain size of 60 μm. A significant amount of residual β phase can be observed in the alloy. After HIPping at 1250^0C / 130MPa / 5h, the porosities in the as-cast alloy have been eliminated, the alloy is more densified. The average grain size of the alloy tends to increase into 80 μm after HIPping. Homogenization treatment has been conducted on the HIPped alloy at 1250^0C / 16h, the average grain size of the alloy grows to 110 μm while the annealing time extends at 1250^0C. The residual β phase also tends to congregate and precipitate more when annealing at 1250^0C.

5.2 β phase in the Large Alloy

For the mass production large ingot, with a weight of 15 kg, the solidification of the alloy is slow during cooling. When the requirements of structural fluctuation, energy fluctuation and composition fluctuation of the alloy have been met, borides with a very high melting point, act as a nucleation core for the β-phase to form and grow. The β-crystal casting structure is finer than the α-crystal casting structure in the way that, for α-crystal the solidification direction is only in the C-axis, which is easy to form columnar structures in the heat conducting direction, and the grains in the alloy tend to combine and grow large. For the β-crystal the solidification direction is

along the <110> direction, which has three equivalent directions, such as [100], [010], and [001], thus different from the C-axis solidification, it is easier to form equiaxed crystals. During cooling, the β phase transforms into the α phase in the relationships as: $\{1\bar{1}0\}_\beta$ // $(0001)_\alpha$<111>$_\beta$<11$\bar{2}$0>$_\alpha$. The transformation starts in the grains toward the grain boundaries, since the transformation can not be completed, the remaining β phase exists at the grain boundaries. Furthermore, since Nb and W are β phase stabilizers, the segregation of Nb and W in the residual β phase tends to grow, which makes it more difficult for the transformation to proceed under the as-cast condition of the large ingot. Thus the remaining bulky β phase can be easily observed at the grain boundaries of the alloy.

In order to reduce the amount of the bulky β phase, heat treatments have been conducted to the TiAl-based alloy after HIPping. When annealing the alloy at a higher temperature for a sufficient time, the driving force for atomic diffusion can be increased, the residual β phase in the alloy thus can be reduced. When the alloy is heat-treated at a lower temperature, above the eutectoid temperature, T_e, at $1{,}240^0$C / 16h / FC, in the α + γ phase region, as shown in Fig. 24, a large amount of the β phase still remains in the alloy. Indicating that at a lower heat treating temperature, even heat treating for a longer time, the β phase can be not eliminated. When the annealing temperature rises higher to $1{,}280^0$C, the amount of the β phase can be reduced, Fig. 25, showing that the dissolving of the high-temperature residual β phase has taken place. But since the annealing time is limited to only 30 min, the amount of the β phase can only be reduced but not eliminated, due to the insufficient time for the alloy to reach

an equilibrium balance. As the heat treating temperature increases above the T_α point, at 1310^0C, and the heat treating time extends to 8h, shown in Fig. 26, the residual β phase can almost be eliminated. Therefore heat treating at a higher temperature and annealed for long enough time, the kinetic energy is sufficient for the atom diffusion to take place, thus the residual β phase can mostly be eliminated. When the alloy reaches an equilibrium condition, the residual β phase can be transformed into the α phase and the γ phase. When the cooling rate is slow, a lamellar structure composed of $\alpha_2 + \gamma$ can be obtained.

The transformation of the β phase in the TiAl-based alloy is related to the heat-treating temperature, the heat-treating time, and the cooling rate. When the heat-treating temperature is above the single-phase region ($1{,}295^0$C), and kept for a sufficient amount of time, the dissolving of β phase can take place. When the heat treating temperature is lower, for instance at $1{,}240^0$C, the annealing time should be held longer, and the cooling rate should be very slow, in order to reduce the amount of the β phase. Figure 27 shows the dissolving procedure of the β phase. The bulky β phase, which is precipitated along the grain boundary of the lamellar grain, reduces as the alloy is heat treated at $1{,}310^0$C for 8 hours. While heat treating the TiAl-based alloy, the residual β phase dissolves mainly in the α phase. Since the concentration of Nb and W is high in the α phase, the concentration gradient between the α phase and the β phase is small, and thus the required driving force for the β phase to dissolve is also small. The β phase is usually dispersed at the ends of the α lamellae. When the alloy is cooled down slowly, such as furnace cooled, the time for atomic diffusion is

sufficient, almost no β phase can be observed in the alloy.

5.3 Microstructure of the Large Ingot Samples after Heat Treatments

The microstructure of the TiAl-based alloy is closely related to the heat-treating temperature and the cooling rate. The phase structure of the alloy is more affected by the heat-treating temperature, while the interlamellar spacing is more sensitive to the cooling rate of the alloy. The grain size of the alloy is closely related to both. Since heat treating above and below the T_α temperature, a fully-lamellar structure and duplex structure can be obtained, respectively. The grain size of the alloy changes dramatically at this temperature point. In order to obtain fine-sized lamellar structure, the heat-treating temperature must be close to T_α, but not exceeding it. The formation of the interlamellar spacing is mainly during the cooling of the alloy, thus different cooling rate can result in different interlamellar spacings. When the cooling is too rapid, the formation of the lamellae can be suppressed. While the cooling rate slows down more lamellae precipitates out, the lamellar structure starts to form. When the cooling rate is reduced more, the interlamellar spacing refines since more lamellae has been formed. If the TiAl-based alloy is annealed above the T_α temperature for a sufficient time and cooled down very slowly, the interlamellar spacing of the alloy tends to widen since the grains of the alloy tends to be equiaxed.

After heat-treating the HIPed TiAl-based alloy at $1{,}190^0$C, 14h, and then air cooled, a duplex structure can be obtained, as shown in Fig. 28. The heat-treating temperature is under T_α, and thus, bulky γ phase combined with the lamellar structure

can be observed. A large amount of the β phase still remains in the alloy. After heat-treating the HIPped TiAl-based alloy at 1,290^{0}C, 8h, and then air cooled, a fully-lamellar structure can be obtained, as shown in Fig. 29. Since the heat-treating temperature is approximately at the T_α point, the microstructure of the alloy is composed of a large-sized lamellar structure. The residual β phase can still be observed in the alloy.

After HIPping the TiAl-based alloy has been heat treated at 1,310^{0}C / 8h, and then cooled down through different methods, exhibited in Fig. 30, in order to understand the effect of the cooling rate on the microstructures of the alloy. When the TiAl-based alloy is heat treated at 1,310^{0}C / 8h and then cooled in salt-ice water, there is no lamellar structure found in the microstructure. As shown in Fig. 30(a), grain boundaries cannot be observed in the alloy, and no β phase is shown in the microstructure. Since the cooling rate of the alloy is too rapid, no lamellar structure is being able to be formed, and no grain boundaries are able to show under this condition. When the TiAl-based alloy is heat treated at 1,310^{0}C / 8h and then oil cooled, no obvious grain boundaries and grains can be observed in the alloy. A lamellar structure starts to appear, Fig. 30(b), but the lamellae are non-uniform and non-continuous. The space between each lamella is large and different. The lamellar structure begins to precipitate in grains under this condition, and the microstructure is composed of the large α phase and a very small amount of lamellae under this condition. When the TiAl-based alloy is heat treated at 1,310^{0}C / 8h and, then, fan cooled, Fig. 30(c), the lamellar structure can be observed. The interlamellar spacing is quite large and not

uniform under this cooling condition. When the TiAl-based alloy is heat treated at $1{,}310^0$C / 8h and then air cooled, lamellar colonies with uniform lamellar spacings can be obtained, Fig. 30(d). When the TiAl-based alloy is heat treated at $1{,}310^0$C / 8h and, then, furnace cooled, the lamellar grains precipitate out completely, a fully-lamellar structure can be observed, Fig. 30(e). The grain size has grown under this condition.

The formation and growth of the new phase depends on nucleation rate, forming rate and growing rate. When the TiAl-based alloy is heat treated at $1{,}310^0$C / 8h, and, then, cooled down, there's not much difference in the nucleation rate of the new phase, but the cooling rate of the alloy has a great effect on the growing rate of the phase. When the cooling rate is too rapid, the new phase does not has sufficient time to grow, and the grain size of alloy is small. When the cooling rate is slowed down, after sufficient diffusion and transformation, the new phase tends to form completely, and the grain size grows. The formation of the lamellar structure is: 1) the crystal-structure change from HCP → FCC; 2) the change in the chemical composition by atom diffusion; 3) the transformation of FCC crystal structure into the γ-phase Ll_0 crystal structure. The precipitation of the γ phase from the α phase is a kind of dissociation of a Shockley-partial dislocation from the hexagonal-crystal structure. This mechanism was firstly found by Blackburn from the observation of the eutectic composition (40 mol.%, mole percent, of Al) of the TiAl alloys. When the $Ti_{54}Al_{46}$ alloy is cooled down from the α phase into the α + γ phase region at $1{,}250^0$C, there is a large amount of stacking faults in the hexagonal structure. The transformation from the HCP into FCC structure starts with the decomposition of the

a/3<110> into two Shockley partial dislocations with one stacking fault in between, this kind of stacking fault forms the FCC-stacking sequence from the hexagonal structure. Whether the stacking sequence is ABC or ACB depends on the sign of the Shockley partial dislocation. For each repeating of such mechanism on two planes in the hexagonal structure, the transformation of HCP→FCC structure is accomplished. The stacking sequence of the HCP structure, ABABAB…, has been turned into the stacking sequence of FCC structure of ABCABC…or ACBACB…. This trend induces the formation of twins or pseudo-twin structures between two γ lamellae. Since the close-packed plane and close-packed direction of the FCC structure is parallel to that of HCP structure, they have coherent boundaries. If the transformation of the γ lamella only relates to the transformation of the crystal structure, then the self-diffusion of Shockley partial dislocations can alone accomplish the formation of the lamellar structure. The Gibbs-free energy of the phase transformation drives the separation of the Shockley partial dislocations, just like the transformation in the cobalt (Co) allotropy. But the changes in the chemical composition and the ordering of the FCC structure are involved in this transformation. The formation of the FCC stacking fault, and the coherent boundaries formed between the FCC stacking fault and the HCP crystal structure, help form a "pre-nucleation" stage, which lower the obstacle for the nucleation of the γ phase. The atomic diffusion during the nucleation of the γ phase leads to the changes in the chemical composition and the ordering of the FCC structure. The low energy, high stability, and smooth boundary between the lamellae structure made it favorable for the atomic diffusion, which is essential in the

nucleation and growth of the new phase. Since it is difficult for one atom to diffuse into the lamellae, the preferable way of the atomic diffusion is as follows: the lateral growth of the lamellae is due to the Shockley partial dislocation, which induces the formation of steps between the phase boundaries. The growth of the lamella is due to the diffusion of the atoms at the torsion of the steps. The Shockley partial dislocation forms the FCC stacking fault area, at which the γ phase starts to nucleate. In order to obtain the ordered γ-phase $L1_0$ structure, the atoms must rearrange. The transformation of FCC → $L1_0$ will lower the symmetry of the structure, which induces three possible directions along the <001> for the C axis in $L1_0$ structure.

The precipitation of the γ phase is related to the supersaturation of Al in the TiAl-based alloy. When the alloy is heat treated at $1{,}310^0$C / 8h, the alloy has been transformed into the α-single phase, and the elements are evenly distributed. When the alloy is cooled down through the salt-ice water, the α phase has been transformed into the α_2 phase, the concentration of Al is even, and the saturation of Al is small, which does not favor the formation the γ phase. More importantly, the cooling time is rapid, thus there is not sufficient time for the γ phase to precipitate, and the lamellar structure can not be observed. When the TiAl-based alloy is cooled through oil, the cooling rate is fast, the α phase has been transformed into the α_2 phase, and the γ phase starts to form, but the lamellar structure is not obvious, and the length and thickness of the lamella is not uniform. When the TiAl-based alloy is cooled by fan, the reaction, $\alpha \rightarrow \alpha_2 + \gamma$ need time to take place, the γ phase precipitates out more and the lamellar structure appears. When the TiAl-based alloy is cooled down through air and furnace-

cooled conditions, the cooling time is sufficient for the reactions, $\alpha \rightarrow \alpha + \gamma$, and $\alpha \rightarrow \alpha_2 + \gamma$, to take place, the lamellar structure is fully formed and uniform. The interlamellar spacing tends to be refined but the grain size tends to grow.

5.4 Conclusions

1. A large amount of the β phase can be observed in the 15 kg-alloy ingot produced through the magnetic-flotation-melting method with the composition of Ti-45Al-7Nb-0.15B-0.4W.
2. The β phase in the large ingot can be reduced after heat treatments. In order to induce a sufficient kinetic energy for the atomic diffusion to reach an equilibrium condition, both the heat-treating temperature and heat-treating time are essential for the elimination of the β phase.
3. The cooling rate of the heat-treated TiAl-based alloy has a great effect on the formation of the lamellar structure of the alloy. The lamellar structure forms more completely as the cooling rate slows down.
4. The grain size of the alloy is related to the cooling condition of the alloy. When the cooling rate of the alloy decreases, the grain size of the alloy tends to grow, showing a faster cooling rate to a smaller grain size.

6. The Microstructure Comparison Between Small Arc-melting Ingot and Large Magnetic-Floatation-Melting Ingot: Results and Discussions

6.1 The Different Microstructure Between the Small and Large Ingot

From the TiA7lNb phase diagram, Fig. 22, the equilibrium condition of the TiAl-based alloy under room temperature is composed of the α_2 and γ phases. As for the arc-melting small ingot, the cooling rate is rapid, and there is not much atomic diffusion in the alloy. The microstructure of the as-cast condition is non-equilibrium. The microstructure feature of the as-cast TiAl-based alloy produced by arc-melting is: 1) no lamellar structure can be determined in the alloy, dendrite structures can be observed; 2) no bulky primary β phase can be found in the alloy; 3) ribbon shaped borides can be observed in the alloy. When the cooling rate of the alloy is very fast, the concentration of the elements remains almost same as of the liquefied state, there is no strong microsegregation in the alloy. The β phase is a high-temperature stable phase, which requires time to nucleate and grow; it transfers into the α phase at a temperature below $1{,}430^0$C. When the cooling rate of the alloy is rapid, the β phase is not able to form or limitedly formed. As the temperature lowers, it mostly transfers into the α phase, and, thus, no bulky primary β phase can be found in the as-cast alloy. Since the formation of the γ lamellae relates to the chemical composition difference in the alloy, which is due to the atomic diffusion, the kinetic energy for the lamellar growth is not sufficient in the as-cast alloy, the precipitation of the γ lamellae is not

obvious, and no lamellar structure can be determined. Nb is highly dissolvable in Ti and also in the β phase. Since the atomic-diameter difference in Nb and Ti atoms is large, the distortion energy is quite different in the grain and at the grain boundaries. Nb tends to disperse at the grain boundaries to lower the distortion energy. Thus, a white dendrite structure can be observed in the as-cast alloy. The melting point of TiB_2 is high ($3{,}253^0$C), and it is surrounded by the solid solute during cooling. The grain size of the alloy tends to be refined, since TiB_2 act as heterogeneous nucleation sites.

The flowability of the liquid TiAl-based alloy is poor, since the cooling speed is fast under the drop-casting condition, porosities form at the places, which last solidified while no liquid metal can refill the shrank spots. Both the density and atomic diameter of W are large, when W is added into the TiAl-based alloy, the viscosity of the melt increases, and the flowability of the liquid decrease. Therefore, the porosities in the alloy increase. Since the porosities are randomly distributed in the as-cast alloy, mechanical properties are lowered by these defects, HIPping and homogenization treatments are required.

The microstructure of the large ingot produced through the magnetic-floatation-melting method is, 1) macro-defects, such as porosities, are not obvious in the alloy; 2) a equiaxed lamellar structure can be observed in the as-cast alloy with evident grain boundaries; 3) a bulky β phase can be found in the as-cast condition; 4) needle-shaped borides can be seen in the alloy. Since the large ingot solidifies in the direction of heat conducting, which is from the outside to the inner part, the last place to solidify, which is the upper open part of the ingot tends to form porosities. When

the upper part has been cut off, the remaining parts of the ingot are mostly less of macro-defects. A lamellar structure can be observed under the as-cast condition is because for the large ingot, 15 kg, the β phase first nucleates and grows during the solidification. Heavy elements tend to disperse at the grain boundaries of β crystals. As the temperature lowers, the β phase decomposes into the α phase. Since Nb and W addition elements are β-phase stabilizers, the remaining bulky β phase, which has not been transformed into the α phase, can be observed at the grain boundaries. Due to size of the ingot, the cooling rate is sufficient for the phase transformation: $\alpha \rightarrow \alpha_2 + \gamma$ to take place. Thus, a lamellar structure can be formed. On the other hand, when Nb is added into the alloy, as indicated in the TiAl7Nb phase diagram, shown in Fig. 22, the region of the β phase has been extended. The alloy solidifies from the β phase favoring in the crystal direction of <110>, which has three-equally directions of: [100], [010], and [001]. This trend differs from the solidification of the α crystal, which only favors the direction of the C axis. During cooling, the β phase transforms into the α phase, in the following relation: $\{1\bar{1}0\}_\beta$ // $(0001)_\alpha<111>_\beta<11\bar{2}0>_\alpha$. The difference in the alloy solidified from the β phase and the α phase is that for the later, it is easy to form column crystal in the heat conducting direction, while the former usually forms equiaxed crystals. Borides, such as TiB_2, act as heterogeneous-nucleation spots during cooling. This trend can refine the as-cast grain size of the alloy. The TiAl-based alloy in this research has an equiaxed structure with an average grain size of 60 μm.

6.2 The Similar Microstructure Between the Small and Large Ingot

The microstructural difference in the samples produced through arc-melting and magnetic-flotation-melting is due to the different conditions in the solidification. It strongly depends on the cooling rate of the material. Thus, under specific circumstances, similar microstructures with the small arc-malted alloy can be obtained in the large magnetic-flotation-melted alloy. When heat-treating the small sample, which is cut from the large ingot, at $1{,}450^0$C / 2h, and then salt-ice water cooled, a non-equilibrium cellular microstructure can be obtained, as shown in Fig. 31. This kind of structure is similar to the arc-melting as-cast microstructure exhibited in Fig. 32. When the alloy is heat treated at $1{,}450^0$C, a temperature reaching the single-β-phase region, and slightly above the α + β phase region, the microstructure of the alloy transfers into the single-β phase. When the alloy is cooled down rapidly, the microstructure of the alloy transfers from the β phase into the α phase, but the formation of a lamellar structure, $\alpha \rightarrow \alpha_2 + \gamma$, is suppressed due to rapid cooling. As shown in Fig. 31, the microstructure of the alloy is composed of non-lamellar cellular structures. No primary bulky β phase can be observed in the alloy, white dendrites are randomly formed under this condition. The formation of the dendrite, the microsegregation of Nb and W, is related to the concentration of vacancies. As shown in the equation, $\frac{N_D}{N} = \exp\left(\frac{-Q_D}{KT}\right)$, whereas N_D is the number of defects, N is the number of potential defect sites, $-Q_D$ is the activation energy, K is the Boltzmann's constant, and T is the temperature. The number of vacancies in the alloy is strongly

dependent on the temperature. The higher the temperature the more concentration of the vacancies. Therefore, when the TiAl-based alloy is heat treated at 1,450^{0}C for 2h, and, then, rapidly cooled down, oversaturated vacancy sites are formed. These vacancies tend to move toward the grain boundaries, while dragging the Nb and W atoms to move along. Thus Nb and W atoms are enriched at the grain boundaries, forming the dendrite structures. This kind of non-equilibrium segregation is strongly dependent on the cooling rate of the alloy. It happens under certain cooling rates, showing large segregations while the vacancies increase due to the increase in both the annealing temperature and the cooling rate.

When the above 1,450^{0}C, 2h, the salt-ice water cooled specimen is, then, annealed at 1,260^{0}C / 14h / FC, Fig. 33, it has a duplex structure, similar to the arc-melted TiAl-based alloy heat treated at 1,250^{0}C / 16h / AC, Fig. 34. Except that, there is a significant amount of the residual β phase in the large ingot alloy. The microstructure of both specimens is composed of a lamellar structure and a primary γ phase. The lamellar structure of the annealed sample from the large ingot tends to have a larger grain size than the heat-treated small ingot. When heat treating the TiAl-based alloy, produced by magnetic floatation, at 1,295^{0}C, 10h, and, then, air cooled, a fully-lamellar structure can be observed, Fig. 35. Under a similar condition of the heat treatment, above the T_α temperature, at 1,295^{0}C, 10h, and, then, air cooled, a fully-lamellar structure can also be obtained in the arc-melted TiAl-based alloy, as shown in Fig. 36. It is noteworthy that the amount of the residual β phase has been largely reduced, after this high-temperature long-time annealing heat treatment, in the large

ingot sample.

Hence, similar microstructure can be obtained in the large ingot sample and the small arc-melting sample after different heat-treatments.

In order to have a more accurate comparison in the microstructures of the arc-melted and magnetic-floatation-melted TiAl-based alloy, remelting has been conduted to the large magnetic-floatation-melted alloy. The TiAl-based specimen produced by magnetic-flotation-melting method has been cut into 10mm x 10mm x 10mm small pieces and remelted on the WKDHL-1 vacuum arc-melting machine. In order to keep the composition even, the remelting procedure has been repeated for four times.

The microstructure of the specimens cut from the large ingot after remelting is similar to that of the arc-melting produced sample, as compared in Fig. 37 and Fig. 32. It is composed of a cellular structure without the lamellae. White dendrites can be observed in the alloy. After remelting the large sample, the specimen has been heat treated at $1{,}235^0$C / 8h / FC. As shown in Fig. 38, a duplex structure can be obtained. This structure is similar to the microstructure of the arc-melted sample heat treated at 1240^0C / 5h / FC, Fig. 39.

6.3 The Reasons for the Difference Between the Small and Large Ingot

The difference in the microstructure features of the alloys is mainly due to the size of the ingot, which greatly affects the cooling rate of the TiAl-based alloy. As shown in Fig. 22, the TiAl7Nb-phase diagram, when the small ingot, produced through arc-melting, is cooled down rapidly, the as-cast microstructure of the sample is

composed of a non-equilibrium structure, and there is no strong microsegregation in the alloy. Thus, after the HIPping and homogenization treatment at a temperature of $1{,}250^0$C in the $\alpha + \gamma$ phase range, the microstructure of the alloy reaches an equilibrium condition, and there is no β phase observed in the alloy. For the large ingot produced through the magnetic-flotation-melting method, the cooling rate is suppressed due to the large ingot size, *d(*110 mm) × *l(*300 mm) [110 mm in diameter and 300 mm in length]. Thus, the high-temperature residual β phase can be observed in the as-cast condition. After the HIPping and homogenization treatment at $1{,}250^0$C, the kinetics for the atomic diffusion is not sufficient to reach an equilibrium condition. Thus, the β phase remains in the alloy.

Moreover, the chemical composition analysis conducted at ORNL can prove that there is no composition shift in the large ingot, which might be a cause of the difference in the microstructures. The chemical composition of the large ingot at the upper part, the lower part, and the bottom part has been listed in Table. 3.

6.4 Conclusions

1. Small ingot produced through arc-melting has an average grain size of approximately 50 μm, after HIPping and homogenization treatment. The microstructure of the alloy is a duplex structure. No β phase was found under this condition.

2. Large samples produced through the magnetic-flotation-melting method, has an equiaxed structure with an average grain size of 60 μ m in the as-cast condition. After the HIPping and homogenization treatment, the average grain size of the alloy increases

to 110 μm. The microstructure is composed of a near fully lamellar structure, with a significant amount of the β phase dispersed along the grain boundaries.

3. The difference in the microstructure features of the alloys is mainly due to the size of the ingot, which greatly affects the cooling rate of the TiAl-based alloy.

4. For the small ingot, which is cooled down rapidly, the as-cast microstructure of the sample is composed of a non-equilibrium structure, and there is no strong microsegregation in the alloy. After the HIPping and homogenization treatment, the microstructure of the alloy reaches an equilibrium condition, and no β phase is observed in the alloy.

5. For the large ingot, which is cooled down in a slower rate compared to the small alloy, the high-temperature remaining β phase can be observed in the as-cast condition. After the HIPping and homogenization treatment, the kinetic energy for the atomic diffusion is not sufficient to reach an equilibrium condition.

6. Similar microstructures with the small arc-melting sample can be obtained, both after heat treating the large ingot samples and remelting/casting a portion of the large ingot samples.

7. Hot Deformation of Large Ingot: Results and Discussions

7.1 Hot Simulation of the TiAl-based Alloy

The TiAl-based alloy samples were canned in the carbon steel for hot-simulation experiments. As shown in Fig. 40(a), at a compression temperature of $1{,}050^0$C, the TiAl-based alloy showed no deformation while the can had deformed. At a temperature of $1{,}100^0$C, Fig. 40(b), the TiAl-based alloy started to deform. As the temperature became higher, at $1{,}180^0$C, the alloy deformed at a relatively larger strain without any cracks initiated at its cross section, Fig. 40(c). While the hot-compression temperature reached $1{,}230^0$C, as indicated in Fig. 40(d), the can had deformed severely, and cracks had been initiated in the cross section of the TiAl-based alloy.

Below the temperature of $1{,}050^0$C, the stress for deformation is large in the TiAl-based alloy, the canned TiAl-based alloy cannot be hot deformed. At a temperature of $1{,}100^0$C, the stress for the deformation of the TiAl-based alloy starts to decrease, the canned alloy can be deformed at a temperature equal to or higher than $1{,}100^0$C. At the temperatures of $1{,}100^0$C, and $1{,}180^0$C, the TiAl-based alloy had deformed without any cracks initiated at its cross section, the deformation of the canned TiAl alloy along the compressing direction are 30% and 50%, respectively. Thus, the TiAl-based alloy can be hot-compressed by the minimum force to obtain enough deformation in this temperature range. While hot-compressed at $1{,}230^0$C, cracks had been initiated in the cross section of the TiAl-based alloy. The can had been largely deformed, and its strength decreased, resulting in losing its protection for the TiAl-based alloy. This trend shows that when using the carbon steel as canning

materials for the TiAl alloy, the hot-deformation temperature should not exceed $1{,}230^0$C. Since cracks could initiate and propagate easily in the alloy, which could lead to the failure in the hot deformation of the TiAl alloys.

Figure 41 shows the microstructures of Ti-45Al-7Nb-0.15B-0.4W alloy after being deformed at a rate of $0.02s^{-1}$ under different temperatures. At the temperature of $1{,}100^0$C, the microstructure does not change much, but the lamellae starts to stretch out. At a temperature of $1{,}150^0$C, the deformation in the alloy due to hot deformation starts to show. At a temperature of $1{,}180^0$C, the deformation of the microstructure is sufficient, the grains are flattened and elongated. At a temperature of $1{,}200^0$C, the deformation of the grains in the alloy seems not that obvious, this might be due to the invalidation of the coating of the alloy. Small grains, especially at the triangular grain boundaries, were observed due to the result of dynamic recrystallization in the alloy when hot deformed at the temperatures above $1{,}100^0$C.

The mechanism of the hot deformation in the TiAl-based alloy at different temperatures is related to the plastic deformation of the alloy. Since the plastic deformation of the alloy is a result from the movement of dislocations, only when the force operating on the dislocations reaches a critical value, P-N force, can the movement of dislocations be motivated. The movement of dislocations in crystal depends on the movement of atoms and vacancies in the alloy. Thus temperature has a large effect on the operating force of dislocations. The crystal structure of α_2 phase in the TiAl-based alloy is HCP. The crystal structure of γ-TiAl is ordered FCT with a low degree of symmetry. In TiAl-based intermetallics, metallic bond and covalent bond

can both be present in the alloy, which brings the advantage of high temperature resistance like ceramics. But because of the small width between dislocations, TiAl-based alloys are as brittle as ceramics are. The activation energy for hot deformation in TiAl-based alloy is very high. As shown in Fig.40, when the canned TiAl alloy was hot-compressed at $1{,}050^0$C, there is merely any change in the alloy; the temperature is too low for dislocation to be operated. When the TiAl alloy was hot-compressed at $1{,}100^0$C, the movement of dislocations has been triggered, the actual relative deformation reaches 30%, and lamellae start to bend under the compressive stress. The bending and twisting of lamellae generates dislocations under which the alloy became work-hardened. The bending-line type lamellae in the alloy demonstrate that the deformation of the TiAl alloy at $1{,}100^0$C is a pure procedure of dislocation movement and multiplication, there is no dynamic recovery involved and the size of grains did not change much. When the TiAl alloy was hot-compressed at $1{,}150^0$C and $1{,}180^0$C, respectively, the actual deformations are 45% and 50% respectively. The equiaxed grains were compressed along axial direction and elongated along radial direction, the grains changed from equiaxed-like shape to rod-like shape. Almost no fine grains were found, which indicates that the grains are under dynamical recovery. But at triangular grain boundaries, there are few fine gains generated due to the results of dynamic recrystallization during hot compression. The dynamic recovery of TiAl alloy during hot compression is a result of flow-softening, when flow-softening and work-hardening counteracts with each other, the force no longer increases as the displacement increases, it is kept around a stable value when the TiAl alloy is hot-

compressed at 1,150^{0}C -1,200^{0}C.

An optimal temperature range has been chosen according to which the capsule was strong enough to support the hot deformation of the samples without any cracking initiating in the specimens in this temperature range. Thus, for the carbon-steel-canned TiAl-based alloy, the temperature range for hot deformation is 1,180^{0}C - 1,200^{0}C, and the optimal temperature is 1,180^{0}C.

7.2 Hot Forging of Large Ingot

7.2.1 1st Forging Procedure

The microstructure of the as-cast Ti-45Al-7Nb-0.15B-0.4W alloy, is composed of equiaxed fully lamellar structure. A significant amount of the β phase, mainly distributing along the lamellar grain boundaries, can be observed in the alloy, as shown in Fig. 42(a). Porosities can also be observed in the as-cast condition. After the first forging process at 1,180^{0}C, with a deformation of 60%, at a strain rate of 0.02 s^{-1}, the grains in the alloy have been deformed. The β phase remains in the alloy after this deformation. The boride phase is a brittle hexagonal ceramic phase. It has low machining ability, during hot deformation the needle-shaped borides breaks into small pieces, as shown in Fig. 42(b). After first hot deformation, the as-cast microstructure of the alloy has changed. The bulky β phases have been stretched and elongated. This is due to the plastic deformation of the alloy. When the Pelerls-Nabaro force is reached in the movement of dislocations, plastic deformation occurs. The movement of dislocation is related to the movement of atoms and vacancies, thus temperature has a great effect

on the driving force of the dislocations. At the temperature of 1,180^{0}C the dislocation starts to move, the alloy begins to bend. This kind of bending generates the number of dislocations in the alloy. The dislocations interact with each other and forms substructures, which induces the work hardening of the alloy. During the hot deformation process, the deformed alloy dynamically recovers and recrystallizes, this reduces the substructure, and softens the alloy. When the alloy is hot deformed at 1,180^{0}C, dislocation generates and moves during the dynamically recovery of the alloy.

After the first deformation process heat treatments have been conducted to the hot-deformed alloy in order to benefit the rotation of the un-deformed grains in the second deformation process. During heat treatment recrystallization takes place at the grain boundaries, where energy is mostly stored during deformation of the alloy. Small equiaxed crystals are formed at this region. Heat treatment has been conducted on the hot-deformed alloy at 1,220^{0}C / 4h / air cool. The un-deformed grains, such as "A", surrounded by recrystallized small grains in Fig. 43, can rotate and deform easily in the second deformation process. The average grain size did not grow under this heat treatment. As the heat treating time increases to 7h at 1,220^{0}C, Fig. 44, the grain size tends to grow in the alloy. Thus the annealing time of the 1st deformed alloy should not exceed 4 hours at the temperature of 1,220^{0}C, in order to benefit the 2nd deformation process.

7.2.2 2nd Forging Procedure

After the heat treatment, a second hot-deformation process at a temperature of 1,180^{0}C, with a deformation of 50%, at a strain rate of 0.02 s^{-1}, has been conducted to

the alloy. Compared to the first deformation process, the grains in the alloy have been thoroughly deformed after the second deformation process, the remaining β phase have even been bended and smashed in the alloy, as indicated in Fig. 45. The β phase is a high temperature ductile phase which deformed significantly during hot deformation. Besides the protection of the coating, the ductile property of the β phase under high temperature makes it easier for the regions around the grain boundaries to deform, which makes the alloy more machineable.

Different heat treatments have been performed to the hot-deformed alloy, in order to reduce the amount of the β phase. When heat treating the TiAl-based alloy above the eutectoid temperature ($T_{e,}$ approximately $1{,}175^0$C), and under the α-phase transus temperature, T_α ($1{,}290 \pm 5^0$C), a duplex structure can be obtained. After the hot-deformation process, the amount of the β phase can be eliminated as the heat-treating temperature is hold still at a certain temperature range. As shown in Fig. 46, after heat treating the alloy at $1{,}240^0$C / 5h / FC, the microstructure of the alloy is composed of the lamellar structure and the primary γ phase. No β phase has been observed after this heat treatment. Both the heat treating temperature and the heat treating time have been reduced, as compared to the as-cast large ingot sample, when heat treatments are conduced in order to reduce the amount of the residual β phase. Since through the hot deformation, the kinetic energy has been stored in the deformed grains, the microsegregation in the alloy can be eliminated due to the fast atomic diffusion, when heat treating the alloy in the α + γ, two phase temperature range. Thus, when heat treating the deformed alloy at $1{,}240^0$C / 5h / FC, a duplex structure with a fine grain

size of ~ 30 μm, with no β phase, can be obtained. Above T_e, as the heating temperature increases, the volume fraction of the γ phase tends to decrease as the amount of the α phase increases. The grain size also tends to increase as the heat-treating temperature increases in this range. When the heat treating temperature is increased to $1{,}260^0$C / 5h / FC, shown in Fig. 47, the amount of the primary γ phase decreases significantly, and the amount of the lamellar grain tends to increases. The average grain size tends to grow large. When the heat treating temperature of the alloy is increased close to the T_α point, for instance $1{,}280^0$C, as shown in Fig. 48, the microstructure of the deformed alloy changes into a near fully lamellar structure after heat treating for 20 minutes. The average lamellar grain size increases. No β phase has been observed in the alloy after this heat treatment.

7.3 Conclusions

1. Hot forging and subsequent heat treatments are effective in refining the grain size and reducing the amount of the β phase in the alloy. The optimal hot-deformation temperature for the Ti-45Al-7Nb-0.15B-0.4W alloy is between $1{,}180^0$C – $1{,}200^0$C.

2. In order to deform and homogenize the TiAl-based alloy, which is usually brittle at room temperature, the deformation process has been divided into to two steps. Heat treatments have been preformed between the hot deformations, so as to benefit the efficiency of the procedure.

3. The residual β phase can be eliminated after hot deformation and heat treating the deformed alloy at a lower temperature and a shorter amount of time as compared to the as-cast alloy, due to the enhanced kinetics in the alloy induced by hot deformation.

8. Mechanical Properties: Results and Discussions

8.1 Hardness of the Small Arc-Melting Samples

Hardness tests have been conducted on the Ti-Al-Nb-W-B alloys with different W contents after the heat treatment at $1{,}280^0$C for 14 h. The results are presented in Fig. 49. It is clearly shown that, as the amount of W increases, the hardness of the alloy also increases. This trend indicates that W can strengthen the alloy. Hardness of the alloy is also related to the microstructure of the alloy. As the interlamellar spacing decreases in the TiAl-based alloys, the hardness of the alloys increases. This trend indicates that the hardness is sensitive to the changes in the interlamellar spacing of the alloys.

Thus, the hardness of the TiAl-based alloys is related to three factors: the interlamellar spacing, the colony size, and the alloy addition. The essential factor lies in the interlamellar spacing of the microstructure. As shown in Hall-Petch equation, $\sigma_{0.2} = \sigma_0 + k_\lambda \lambda^{-1/2}$, where $\sigma_{0.2}$ is the 0.2% offset yield strength, σ_0 and k_λ are material constants, and λ is the lamellar spacing. The yield strength of the alloy increases, as the interlamellar spacing decreases. Exhibited in Fig. 49(a), the hardnesses of the TiAl-based alloys are very sensitive to the changes in the interlamellar spacing. As the interlamellar spacing of the alloys slightly decreases, the hardness of the alloys increases. Alloy additions, such as W, in the TiAl-based alloys can increase the hardness of the alloy, shown in Fig. 49(b). W can effectively refine the microstructure of the alloys. As the amount of W increases, the colony size of the alloy decreases,

leading to an increase in the hardness of the alloy. Thus, W strengthens the alloy by solution strengthening and grain-size refinement.

8.2 Tensile Test of the large Magnetic-Floatation-Melting Ingot

Heat treatments have been conducted to the large ingot in order to understand the microstructure evolution of the TiAlNbWB alloy. It has been conclude in the previous work that the duplex structure of the TiAl-based alloy usually has a better room temperature tensile ductility than the fully-lamellar structure. This is mainly due to the reason that a duplex structure has a smaller average grain size than the fully-lamellar structure. But since the fully-lamellar structure has a higher creep resistance under the high-temperature application, it is important to obtain a fine-grain sized, fully-lamellar structure after heat treatments. The large amount of the high temperature residual β phase, which is observed in the large ingot alloy, can deter the room-temperature ductility, since it is quite brittle at ambient temperature. The β phase can be reduced and eliminated after different kinds of heat treatments. At a temperature of $1{,}310^0$C, and heat treated for 8 hrs, the amount of the β phase can significantly be reduced, and almost no residual β phase can be observed. But since the heat-treating temperature has exceeded the T_α point, the average grain size of this fully-lamellar structure is large. Hence, in order to obtain the fine-grain-sized lamellar structure, the heat treating temperature can not be higher than T_α. At a heat-treating temperature of $1{,}280^0$C, a temperature, which is very close to the T_α point, a near fully-lamellar structure can be obtained with a smaller average grain size. Since at $1{,}280^0$C, the

microstructure tends to transform into the single α-phase region, which can later develop into a large fully-lamellar structure after cooling, the heat treating time needs to be carefully controlled, in order to control the growth of the grains. Based on the above concerns, the heat-treating temperature needs to be controlled at a temperature slightly under the T_α point, and the heat-treating time should be carefully scheduled.

In the preparation for the tensile tests, four kinds of heat treatments have been designed, in order to understand the relationship between the microstructure of the alloy and the mechanical properties. Heat treatments have been conducted at 1,130^{0}C / 24 h / FC, 1,130^{0}C / 24 h + 1,280^{0}C / 20 min. / FC, 1,280^{0}C / 20 min. / FC, 1,280^{0}C / 40 min. / FC. As shown in Fig. 50, after heat treating the alloy at 1,130^{0}C / 24 h / FC, a duplex structure, with an average grain size of 80 μm, can be obtained. It is noteworthy that the amount of the β phase is significant in the alloy. This results from the fact that the heat-treating temperature is not high enough so as to supply enough kinetic energy for the elimination of the β phase. Therefore, a 1,280^{0}C / 20 min. / FC heat treatment has been scheduled following the 1,130^{0}C / 24 h heat treating. As shown in Fig. 51, the microstructure of the alloy after this heat treatment is composed of a near fully lamellar structure, with an average grain size of 88 μm. Compared to Fig. 50, the amount of the residual β phase in the alloy has been largely reduced, this trend is mainly due to the increase in the annealing temperature. If the TiAl-based is heat treated at 1,280^{0}C / 20 min. / FC alone, the microstructure of the alloy is composed of a near fully-lamellar structure, with an average grain size of 85 μm. Compared to the 1,130^{0}C / 24 h + 1,280^{0}C / 20 min. / FC, the microstructures are

similar, except that for the alloy with pre-heat treating at 1,130^{0}C / 24 h, the grain size tends to be slightly larger. When heat treating the alloy at 1,280^{0}C / 40 min. / FC, the microstructure of the alloy is almost same as the 1,280^{0}C / 40 min. / FC sample, except for the grain size extended a little to an average grain size of 90 μm.

Tensile tests have been conducted to the 1,130^{0}C / 24 h / FC and 1,130^{0}C / 24 h + 1280^{0}C / 20 min. / FC samples at room temperature, 300^{0}C, 600^{0}C, and 800^{0}C. For the 1280^{0}C / 20 min. / FC and 1280^{0}C / 40 min. / FC samples, tensile tests have been performed at room temperature. The geometry of the specimen for the tensile tests is shown in Fig. 53. The overall results are shown in Table 4. The tensile property, especially the room-temperature ductility of the TiAl-based alloy, is sensitively related to the grain size of the alloy, and the amount of the β phase. Listed in Table 5, comparing the 1,130^{0}C / 24 h / FC heat-treated sample with the 1,130^{0}C / 24 h + 1280^{0}C / 20 min. / FC sample, the previous one has a larger amount of the β phase, thus the tensile ductility of the alloy is poorer than the later one. For the 1,130^{0}C / 24 h + 1280^{0}C / 20 min. / FC and 1280^{0}C / 20 min. / FC heat treated samples with the same near-lamellar structure, the later one, with a smaller grain size exhibits better room-temperature tensile ductility. As compared to other TiAl-based alloys reported from previous works, exhibited in Table 6, the Ti-45Al-7Nb-0.15B-0.4W alloy shows a superior tensile ductility of 1.9%. Since for the as-cast alloys, the room-temperature ductility is usually less than 0.5%, and in general a 1.1% ductility is required for industrial applications. The Ti-45Al-7Nb-0.4W-B, with a tensile ductility of 1.9%, is a breakthrough in the design of TiAl-based alloys for structural uses in the cast

conditions. In order to obtain such high tensile ductility, the optimum heat treatment is designed at 1280^0C / 20 min. / FC, a temperature slightly below the T_α point, so as to prevent the growth of the grain size, and to effectively reduce the amount of the β phase. This newly developed TiAl-based alloy, composed of a fine near fully lamellar structure with a yield strength of 650 MPa, and an excellent room temperature ductility of 1.9%, is very important for structural use of cast TiAl hardwares, such as turbo-charger rotors, for industrial applications. The yield strength of the alloy does not change too much with the increase of the tensile testing temperature, while the ductility of the alloy increases with the increase of the temperature, as stated in Table 7.

The fracture surface of the TiAl-based alloy heat-treated at $1{,}130^0$C / 24 h + $1{,}280^0$C / 20 min. / FC, tensile tested at room temperature (RT), 300^0C, 600^0C, and 800^0C, have been shown in Fig. 54. The fracture mode is brittle, exhibiting a transgranular fracture predominately. Needle-shaped borides are frequently observed on the fracture surface of the alloy both at RT and higher temperatures. Borides often contain defects. These defects are likely to cause the stress concentration within the borides especially when they lie in a tensile specimen with their broad surface perpendicular to the tensile axis. Most of the borides have been pulled out of the metal matrix during failure, leaving indentations on the fracture surface. The inside surfaces of the indention are very smooth, indicating a debonding process along the interface between the boride and the matrix. As shown in Fig. 55, the cracks in the alloy propagates mainly through the lamellar colonies, the microcracks are formed along the

interfaces of the boride/matrix, Fig. 56, and the β/matrix, Fig. 57. The deformation incompatibility of the β phase and the matrix will induce microcracks between their interfaces and reduce the ductility of the alloy. The cracks in the poorly-oriented boride can spread through their whole lengths instantaneously due to their brittle nature. The low ductility of the TiAl-based alloy is related to these boride phases. The addition of the boron has contradictory effects on the tensile ductility of the alloy. Since the finer grain induced by boron addition can increase the ductility of the alloy, while large boride precipitation can deter the ductility of the alloy.

At the tensile testing temperatures of RT, 300^0C, and 600^0C, a delamenation and interlamellar fracture can be observed in the alloy with numerous cleavage planes. As the temperature of the tensile test increases to 800^0C, besides the transgranular fracture, the cracks start to propagate along the grain boundaries, as indicated in Fig. 58. The fracture mode of the alloy tends to change from the transgranular fracture into a combination of the transgranular and the intergranular mode along the grain boundaries. Suggesting that the brittle-ductile temperature, T_{BD}, of the alloy is around 800^0C.

As a summary, the fracture mechanism of the T-Al-based alloy is shown in Fig. 59. At lower temperatures, below 800^0C, cracks in the alloy are mainly imitated at the needle-shaped boride phases or at the bulky β phases. The cracks propagate in a direction parallel to the lamellae in a transgranular fracture mode. At higher temperatures, above 800^0C, the cracks start to propagate along the grain boundaries, indicating the existence of both transgranular fracture mode and intergranular fracture mode.

8.3 Tensile Test of the Hot-Deformed Large Ingot

Through the hot-deformation procedure, the grain size of the alloy has been refined, the microsegregation in the alloy has been eliminated. Hence when different heat treatments have been conducted to the alloys, a β-free microstructure can be obtained. The sample heat treated at $1{,}260^0$C / 5 h / FC, has a fine grain size of 60 μm. The microstructure of the alloy is composed of a duplex structure. The sample heat treated at $1{,}280^0$C / 20 min. / FC, has a near fully-lamellar structure. Tensile tests at room temperature have been conducted on the alloys. Results are shown in Table 4. For the hot deformed alloy with near fully-lamellar structure, the tensile elongation is 1.8%, which is comparable with the as-cast ones with the same microstructure, as shown in Table 8. Therefore, for this typical TiAl-based alloy, a good ductility can be obtained without any hot deformation process. As compared with other thermomechanically deformed TiAl-based alloys, indicated in Table 9, the Ti-45Al-7Nb-0.15B-0.4W alloy has a good room temperature ductility combined with a higher yield strength than that reported in literature.

8.4 Conclusions

1. The hardness of the alloy increases with increasing the W concentration. This trend indicates that W strengthens the TiAl-based alloys by the solution strengthening and grain-size refinement.

2. The tensile ductility of the alloy is very sensitive to the grain size of the alloy. It

increases, as the grain size decreases.

3. The β phase is a high-temperature residual phase, which can deter the tensile ductility of the alloy. Thus, by reducing the amount of the β phase, the tensile ductility of the alloy can be improved.

4. A significant improvement in the tensile ductility, reaching 1.9%, can be obtained in the as-cast and heat-treated Ti-45Al-7Nb-0.4W-B alloy.

5. The hot deformed alloy with a near fully lamellar structure shows a ductility of 1.8%, which is comparable with the as-cast material with the optimal heat treatment.

6. From the fracture surface of the TiAl-based alloy, fractures mainly initiate along the β phase or at the TiB_2 boride phase.

7. The TiAl-based alloy exhibits a transgranular fracture mode at room temperature, and both transgranular and intergranular fracure modes at elevated temperatures.

9. Overall Conclusions

Based on the "composition-microstructure-property" relationship, in order to understand the microstructure-mechanical property relationship of the TiAl-based alloy, the Ti-Al-Nb-B-W alloy system has been carefully studied.

Through the alloy design of small arc-melting samples, the phase compositions and microstructural relations of the Ti-Al-Nb-B-W alloys have been investigated. With the increasing amount of W in the TiAl-based alloy, the non-equilibrium structures, such as dendrites, in the as-cast condition became more obvious. After the HIP and homogenization treatments, a refined microstructure can be obtained. It has been concluded that with the additional amount of W, the grain size and the interlamellar spacing of the TiAl-based alloy can be effectively refined. But as the additional amount of W reaches 0.7 at.%, the β phase can be observed in the TiAl-based alloy. The grain size of the TiAl-based alloy grows as the heat-treating temperature increases. The grain size increases dramatically at the T_α point. Thus, in order to control the growth of the grain size, the heat-treating temperature should be scheduled under the T_α point. Through the understanding of the alloying effects on the phase structure, the interlamellar spacing, grain size, and hardness of the alloys, the Ti-45Al-7Nb-0.15B-0.4W is a newly-developed TiAl-based alloy, which can possess good mechanical properties after simple low-cost procedures of HIPping and heat treatments.

Casting technique can affect the microstructures of the TiAl-based alloy. For the Ti-45Al-7Nb-0.15B-0.4W alloy produced through the magnetic-flotation-melting method, there is a large difference in the microstructures compared with the small arc-

melting alloy. The difference in the microstructure features of the alloys is mainly due to the size of the ingot, which greatly affects the cooling rate of the TiAl-based alloy. Under certain circumstances, such as remelting samples cut from the large ingot, similar microstructures can be obtained in the small and large ingots. The large casting alloy shows a slow cooling rate and the formation of the meta-stable β phase, which cannot be eliminated at around $1{,}200^0$C. The high-temperature residual β phase can deter the room-temperature tensile ductility of the alloy. By heat treatments and hot deformations, the β phase can be eliminated.

In order to conduct the hot deformation on the TiAl-based alloys, hot simulation has been performed on the alloys to obtain the optimum parameter for hot forging. The hot deformation of the TiAl-based alloy can refine the grain structure, and increase the kinetics of the alloy, which results in the elimination of the meta-stable β phase at around $1{,}200^0$C.

The ductility of the TiAl-based alloy is strongly related to the grain size of the alloy. A fine near fully-lamellar structure can achieve high ductility. The study of the microstructures and mechanical properties of the large ingot leads to a design of the optimal heat treatment, which is $1{,}280^0$C / 20 min., in order to obtain fine microstructure and minimize the amount of the β phase. The ductility of the Ti-45Al-7Nb-0.15B-0.4W alloy, with a fine near fully-lamellar structure, can reach 1.9%, which is a breakthrough in the design and application of the TiAl-based alloy. Since for most as-cast alloys, the room temperature ductility is very limited (< 0.5%).

10. Future Work

The newly-developed Ti-45Al-7Nb-0.15B-0.4W shows an outstanding tensile elongation at room temperature. Thus, it is a good candidate for industrial applications. With the additional amount of Nb, B, and W in the TiAl-base alloy, the microstructure of the alloy tends to be refined. The phase composition in the as-cast alloy contains meta-stable β phase in the mass production. A fine near fully-lamellar structure can achieve excellent room temperature ductility, but how it benefits the creep resistance of the alloy at higher temperatures is still unknown. Thus, a more complete understanding of the mechanical properties of the alloy at elevated temperatures needs to be conducted.

Since the applications of the TiAl-based alloys are usually under high temperatures, the future research work will focus on the creep and fatigue experiments of the alloys. Fatigue experiments will be conducted at both low-cycles and high-cycles. The key factors that control the deformation and fracture behavior of the alloys will be identified. The oxidation and corrosion behavior of the alloy at elevated temperatures will also be studied.

A complete microstructure-mechanical properties relationship will be developed at both room temperature and elevated temperatures for this newly-developed alloy.

References Cited

1) C. T. Liu, J. H. Schneibel, P. J. Maziasz, J. L. Wright, and D. S. Easton, “Tensile Properties and Fracture Toughness of TiAl Alloys with Controlled Microstructures”, Intermetallics, 1996, 4, 429 ~ 440.

2) C. M. Austin and T. J. Kelly, “Gas Turbine Engine Implementation of Gamma Titanium Aluminide,” Superalloys, Pennsylvania, TMS, 1996, 539～548.

3) D. E. Davidson, “Designing with Gamma Titanium CAESAR Program Titanium Aluminide Component Application,” Superalloys, Pennsylvania, TMS, 1996, 545～557.

4) M. Nazmy and V. Lupinc, “Gamma TiAl Intermetallic for Gas Turbine Applications,” Materials for Advanced Power Engineering, 1998, 933～941.

5) G. L. Chen, and J. P. Lin, “Physical Metallurgy of the Ordered Structural Intermetallic Compounds,” Metallurgy Industry Publish. Co., 1999.

6) K. Hashimoto, H. Doi, and T. Tsujimoto, “Re-Examination of the Ti-Al-V Ternary Phase Diagram,” Transactions of the Japan Institute of Metals, 1986, 27(10), 741～749.

7) S. C. Huang, E. L. Hall, and M. F. Gigliotti, “Rapidly Solidified Binary TiAl Alloys,” High-Temperature Ordered Intermetallic Alloys II Symposium, 1987, 481～486.

8) Y. W. Kim, “Trends in the development of gamma TiAl alloys,” Gamma Titanium Aluminides, 1995, 637～654.

9) P. L. Martin, M. G. Mendiratta, and H. A. Lipsitt, “Creep Deformation of TiAl and TiAl with W Alloys,” Metallurgical Transactions A, 1983(14), 2170～2174.

10) M. Nazmy, C. Noseda, M. Staubli, B. Phillipsen, N. S. Stoloff, and R. H. Jones eds. "Processing and Design Issues in High Temperature Materials," The Minerals, Metals Materials Society, Switzerland, 1997, 159.

11) R. Yua, L. L. Hea, Z. Y. Cheng, J. Zhu, and H. Q. Yea, "B_2 Precipitates and Distribution of W in a Ti-47Al-2W-0.5Si Alloy," Intermetallics, 2002, 10(7), 661～665.

12) G. H. Chen, A. Frefer, and F. H. Froes, "Structural Evolution of Mechanically Alloyed Ti-Al alloys," Materials Science & Engineering A, 1992, 158(1), 93～101.

13) W. R. Chen, L. Zhao, and J. Beddoes, "Precipitation Hardening of the Fully Lamellar Structure of Investment Cast Ti-47Al-2Nb-1Mn-0.5Mo-0.5W-0.2Si Alloy," Scripta Materialia, 1999, 41(6), 597～603.

14) W. M. Yin, J. T. Guo, "Microstructure Analyses on a New Creep Resistant TiAl Alloy," Acta Metallurgical Material, 1999, 35(1), 176~182.

15) Y. R. Zheng and X. P. Wang, "β_2 Phase in TiAl-Cr Alloy," Nonferrous Met. Soc., 1998, 18(1), 1～6.

16) W. D. Liu, "Valence Electronic Structure and Mechanical Properties of Ti_3Al and TiAl Alloy," Ph.D. Dissertation, North Western University, 2002.

17) Y. W. Kim, "Ordered Intermetallic Alloy, Gamma-Titanium Aluminides," JOM, 1994, 46(7), 30～39.

18) Y. W. Kim and D. M. Dimiduk, "Designing Gamma TiAl Alloys: Fundamentals, Strategy and Production," Proceedings of the Second International Symposium on Structural Internetallics. TMS, 1997, 531～543.

19) Y. W. Kim, “Effects of Microstructure on the Deformation and Fracture of γ-TiAl Alloys,” Materials Science & Engineering A, 1995, 192-193(2), 519～533.

20) A. Menand, A. Huguet, and A. N. Partaix, “Interstitial Solubility in γ and α_2 Phases of TiAl-Based Alloys,” Acta Materialia, 1996, 44(12), 4729～4737.

21) M. Yamaguchi, H. Inui, K. Kishida, M. Matsumuro, and Y. Shirai, “Gamma Titanium Aluminide Alloys,” Materials Research Society Symposium – Proceedings. 1995, 364(1), 3～16.

22) S. C. Huang, “Microstructure and Property Tradeoffs in Wrought TiAl-Base,” Metallurgical Transactions A (Physical Metallurgy and Materials Science), 1992, 23A (1), 375～377.

23) G. Wegmann and K. Maruyama, “On the Microstructure Stability of TiAl/Ti_3Al Polysynthetically Twinned Crystals under Creep Conditions,” Phil. Mag. A, 2000(80), 2283.

24) R. Gnanamoorthy, Y. Mutoh, N. Masahashi, and M. Matsuo, “High Temperature Strength and Fracture Toughness in γ-phase Titanium Aluminides,” Journal of Materials Science, 1993, 28(24), 6631～6638.

25) C. T. Liu, P. J. Maziasz, and J. L. Wright, “Key Microstructures Controlling the Mechanical Properties of Two Phase TiAl alloys with Lamellar Structures,” In MRS Procs., High Temperature Intermetallic Alloys VII, 1997, 460, 83～90.

26) D. A. Lukasak and D. A. Koss, “Flow and Fracture of a Ti_3Al-Nb Alloy,” Metallurgical Transactions A (Physical Metallurgy and Materials Science), 1990, 21A (1), 135～143.

27) S. C. Huang, “Microstructure and Property Tradeoffs in Wrought TiAl-Based Alloys,” Metall. Trans., 1992, 23A, 375.

28) G. Wegmann and K. Maruyama, “On the Microstructure Stability of TiAl/Ti_3Al Polysynthetically Twinned Crystals under Creep Conditions,” Phil. Mag. A, 2000, 80, 2283.

29) W. O. Soboyejo, J. E. Deffeyes, and P. B. Aswath, “Investigation of Room-and Elevated-Temperature Fatigue Crack Growth in Ti-48Al,” Materials Science & Engineering A (Structural Materials: Properties, Microstructure and Processing), 1991, 138 (1), 95～101.

30) L. M. Hsiung and T. G. Nieh, “Microstructures and Properties of Powder Metallurgy TiAl Alloys,” Materials Science and Engineering A, 2004, 364(1-2), 1～10.

31) M. R. Shagiev, O. N. Senkov, G. A. Salishehev, and F. H. Fores, “High Temperature Mechanical Properties of a Submicrocrystalline Ti-47Al-3Cr Alloy Produced by Mechanical Alloying and Hot Isostatic Pressing,” Journal of Alloy and Compounds, 2000, 313 (1-2), 201～208.

32) F. Sun and T. L. Lin, “Superplastic Phenomenon in a Large-grained TiAl Alloy,” Scripta. mater., 2001, 44 (4), 665～670.

33) H. Clemens, I. R. Umberg, and P. Schwantes, “Characterization of Ti-48Al-2Cr Sheet Material,” Intermetallics, 1994, 2(3), 179～184.

34) Y. W. Kim and D. M. Dimiduk, “Progress in the Understanding of Gamma Titanium Aluminides,” JOM, 1991, 43(8), 40～47.

35) Y. W. Kim, R. Wagner, M. Yamaguchi, H. lemens, W. Glatz, P. Schretter, C. Koeppe, A. Bartecs, R. Behr, and A.Wanner, in Gamma Titanium Aluminides and Alloys, eds., TMS, Warrendale, PA, 1995, 717～726.

36) Y. W. Kim and D. M. Dimiduk, "Progress in the Understanding of Gamma Titanium Aluminides," JOM, 1991, 43(8), 40～47.

37) C. Q. Peng, "Effects of Cyclic Heat Treatment on the Microstructure and Mechanical Properties of TiAl Base Alloy," Ph.D. Dissertation, Central South University, 2001.

38) R. Gerling, A. Bartels, H. Clemens, H. Kestler, and F. P. Schimansky, "Structural Characterization and Tensile Properties of a High Niobium Containing Gamma TiAl Sheet Obtained by Powder Metallurgical Processing," Intermetallics, 2004, 12(3), 275～280.

39) D. Hu, "Effect of Boron Addition on Tensile Ductility in Lamellar TiAl Alloys," Intermetallics, 2002, 10(9), 851～858.

40) T. T. Cheng, "The Mechanism of Grain Refinement in TiAl Alloys by Boron Addition - An Alternative Hypothesis," Intermetallics, 2000, 8(1), 29～37.

41) Y. Mizuhara, K. Hashimoto, and N. Masahashi, "Microstructure and Phase Stability of TiAl-W Ternary Alloy," Intermetallics, 2003, 11(8), 807～816.

42) R. Yu, L. L. He, Z. Y. Cheng, J. Zhu, and H. Q. Ye, "B_2 Precipitates and Distribution of W in a Ti-47Al-2W-0.5Si Alloy," Intermetallics, 2002, 10(7), 661～665.

43) F. Appel, M. Oehring, and R. Wagner, “Novel Design Concepts for Gamma-base Titanium Aluminide Alloys,” Intermetallics, 2000, 8(9-11), 1283～1312.

44) D. Arrel, H. M. Flower, and D. R. West, “Effect of Si on Microstructure of Ti_3Al Alloys Containing Niobium,” Mater. Sci. Techno., 1996,12(8), 617～622.

45) T. T. Cheng and M. H. Loretto, “The Decomposition of the Beta phase in Ti-44Al-8Nb and Ti-44Al-4Nb-4Zr-0.2Si Alloys,” Acta Metall. Mater., 1998, 46(13), 4801～4819.

46) Z. C. Liu, Y. W. Kim, S. J. Li, W. J. Zhang, J. P. Lin, and G. L. Chen, “Effect of Nb and Al on High Temperature Strength of γ-TiAl,” Chin. J. Nonferrous Met. Soc., 2000, 10(4), 470～475.

47) X. Y. Chen, X. J. Wan, and J. N. Shen, “Effect of Alloy Element Nb on High Temperature Oxidation Behavior of TiAl Alloy,” Corrosion and Protection, 2002, 22(2), 69～71.

48) Y. Shida and H. Anada, “Role of W, Mo, Nb and Si on Oxidation of TiAl in Air at High Temperature,” Mater Trans, JIM, 1994, 35(9), 623～631.

49) D. J. Larson, C. T. Liu, and M. K. Miller, “Tungsten Segregation in $\alpha_2 + \gamma$ Titanium Aluminides,” Intermetallics, 1997, 5(7), 497～500.

50) C. T. Liu, P. J. Maziasz, and D. J. Larson, “Effect of B and W Addition on Microstructures and Mechanical Properties of Dual Phase Lamellar TiAl Alloys,” In: Interstitial and Substitutional Solute Effects in Intermetallics, Eds, T. Baker, P. D. Noebe and E. P. George, TMS Publication, Warrendale, PA, 1998, 179～188.

51) J. Beddoes, L. Zhao, P. Au, and W. Wallace, “The Brittle-ductile Transition in HIP Consolidated Near γ-TiAl + W and TiAl + Cr Powder Alloys,” Materials Science and Engineering A, 1995, 192-193, 324～332.

52) V. Recina and B. Karlsson, “Tensile Properties and Microstructure of Ti-48Al-2W-0.5Si γ-titanium Aluminide at Temperature between Room Temperature and 800^0C,” Mater. Sci. Techno., 1999, 15(1), 57～66.

53) Y. W. Kim, “Gamma Titanium Aluminides: Their Status and Future,” JOM, 1995(7), 39～41.

54) H. Anada and Y. Shida, “Effect of W Addition on the Oxidation Behavior of TiAl Intermetallic Compound,” J. Japan Institute Metals, 1994, 58(9), 1036～1043.

55) D. J. Larson, C. T. Liu, and M. K. Miller, “Boron Solubility and Boride Compositions in α_2 + γ Titanium Aluminides,” Intermetallics, 1997, 5(6), 411～414.

56) W. L. Gao, H. Zhang, E. L. Zhang, and S. Y. Zeng, “Morphology of TiB_2 in TiAl-B Alloy,” Cast Tech., 2003, 24(3), 176～178.

57) W. L. Gao, H. Zhang, J. P. He, Y. X, Jin, and S. Y. Zeng, “Growth of Fine Rod-like TiB_2 Cross in TiAl-B Alloy,” Rare Met. Mater. Eng., 2003, 32(3), 179～182.

58) S. H. Kim, H. H. Chung, S. G. Pyo, S. J. Hwang, and N. J. Kim, “Effect of B on the Microstructure and Mechanical Properties of Mechanically Milled TiAl Alloys,” Metallurgical and Materials Transactions, 1998, 29A (9), 2273～2283.

59) Z. J. Pu and K. H. Wu, “Investigation on Boron Distribution in a TiAl-based Alloy Using Particle-Cracking,” Scripta. Metall. Mater., 1996, 34(1), 169～174.

60) C. T. Liu, “Recent Advances in Ordered Intermetallics,” Materials Chemistry and Physics, 1995, 42(2), 77～86.

61) P. J. Maziasz, R. V. Ramanujan, C. T. Liu, and J. L. Wright, “Effects of B and W Alloying Additions on the Formation and Stability of Lamellar Structures in Two-Phase γ-TiAl,” Intermetallics, 1997, 5(2), 83～95.

62) Y. H. He, B. Y. Huang, X. H. Qu et.al., “Effect of Carburization on Enhancing the High-Temperature Oxidation Resistance of the TiAl-Based Alloys,” J. Mater. Res., 1996, 10(6), 603～607.

63) F. Appel, M. Oehring, and R. Wagner, “Novel Design Concepts for Gamma-base Titanium Aluminide Alloys,” Intermetallics, 2000, 8(9-11), 1283～1312.

64) R. T. Zheng, Y. G. Zhang, and C. Q. Chen, “Effect of Circle Heat Treatment on Microstructure of Duplex γ-TiAl Alloys,” Heat-treatments of Metals, 2002, 31(6), 472～475.

65) Z. C. Liu, H. J. Li, G. P. Lin, and G. L. Chen, “Refinement Mechanism of Cyclic Heat Treatment on Ti-46Al-8.5Nb-0.2W,” Rare Metals, 2000, 24(4), 251～255.

66) Z. Q. Pan, C. X. Han, “Effects of Iso-thermal Forging on Microstructures of Ti-47Al-5 (Cr + V + Mo + Nb) Intermetallics,” Rare Materials and Engineering, 1996, 25(3), 22～25.

67) C. T. Liu, J. L. Wright, and S. C. Deevi, "Microstructures and Properties of a Hot-Extruded TiAl Containing no Cr ," Materials Science and Engineering, 2002, 329A, 416～423.

68) S. J. Li, Z. C. Liu, and G. L. Chen, "Refinement of Microstructures of Forged Ti-46Al-8.5Nb-0.2W," Material Science and Technology, 2000, 8(3), 46～49.

69) L. Huang, P. K. Liaw, and C. T. Liu, "Microstructural Control of Ti-Al-Nb-W-B Alloys," Metallurgical and Materials Transactions A, 2007, 38(A), 2290～2297.

70) X. J. Xu, G. L. Chen, and D. Y. Zhang, "Microstructure and tensile properties of as-cast Ti–45Al–(8–9)Nb–(W, B, Y) alloy," Journal of Alloys and Compounds, 2006(414):131～136.

71) D. Hu, X.H. Wu, and M.H. Loretto, "Advances in optimisation of mechanical properties in cast TiAl alloys," Intermetallics, 2005(13): 914～919.

Appendices

Appendix A

Tables

Table 1 Development of the γ-TiAl-based Alloys (at.%) [5]

Generation	Compositions (at.%)	Processing
1st	Ti-48Al-1V-0.3C	Exploratory
2nd	Ti-47Al-2(Cr,Mn)-Nb Ti-(45-47)Al-2Nb-2Mn-0.8 TiB_2 Ti-47Al-2W-0.5Si	Cast Cast Cast
3rd	Ti-47Al-5(Cr,Nb,Ta) Alloy K5 (Ti-46.2Al-2Cr-3Nb-0.2W) Ti-(45-47)Al-(1-2)Cr-(1-5)Nb-(0-2)(W,Ta,Hf,Mo,Zr)-(0.02)B-(0-2)(W,Ta,Hf,Mo,Zr)-(0-0.2)B-(0.03-0.3)C-(0.03-0.2)Si-(0.15-0.25)O-X	Cast Wrought Wrought

Table 2 Microstructural Evolution of the TiAl-based Alloys

	900^0C/ 360 h	$1{,}265^0$C/ 18 h	$1{,}280^0$C/ 14 h	$1{,}295^0$C/ 10 h	$1{,}310^0$C/ 5 h
0 at.% W	γ, $\alpha_2+\gamma$, boride	γ, $\alpha_2+\gamma$, boride	γ, $\alpha_2+\gamma$, boride	$\alpha_2+\gamma$, boride	$\alpha_2+\gamma$, boride
0.2 at.% W	γ, $\alpha_2+\gamma$, boride	γ, $\alpha_2+\gamma$, boride	γ, $\alpha_2+\gamma$, boride	$\alpha_2+\gamma$, boride	$\alpha_2+\gamma$, boride
0.4 at.% W	γ, $\alpha_2+\gamma$, boride	γ, $\alpha_2+\gamma$, boride	γ, $\alpha_2+\gamma$, boride	$\alpha_2+\gamma$, boride	$\alpha_2+\gamma$, boride
0.7 at.% W	γ, $\alpha_2+\gamma$, β, boride	γ, $\alpha_2+\gamma$, β, boride	γ, $\alpha_2+\gamma$, β, boride	$\alpha_2+\gamma$, β, boride	$\alpha_2+\gamma$, boride

Table 3 Chemical Analysis of the Large Ingot

Content	Ti (at.%)	Al (at.%)	Nb (at.%)	W (at.%)
Upper Part	47.18	45.31	6.95	0.400
Middle Part	46.33	45.75	7.36	0.410
Bottom Part	47.52	44.87	7.04	0.416

Table 4 Mechanical Behavior of the Ti-45Al-7Nb-0.15B-0.4W Alloy

Heat Treatment Condition	Tensile Test Temperature	Yield Strength (MPa)	Tensile Ductility (%)
1,130^{0}C / 24 h / FC	RT	590	0.8
1,130^{0}C / 24 h / FC	300^{0}C	578	1.0
1,130^{0}C / 24 h / FC	600^{0}C	561	2.4
1,130^{0}C / 24 h / FC	800^{0}C	483	3.0
1,130^{0}C / 24 h + 1,280^{0}C / 20 min. / FC	RT	620	1.7
1,130^{0}C / 24 h + 1,280^{0}C / 20min. / FC	300^{0}C	590	1.9
1,130^{0}C / 24 h + 1,280^{0}C / 20min. / FC	600^{0}C	560	2.2
1,130^{0}C / 24 h + 1,280^{0}C / 20min. / FC	800^{0}C	485	3.8
1,280^{0}C / 20min. / FC	RT	650	1.9
1,280^{0}C / 40min. / FC	RT	640	1.6
Hot-Deformed + 1,260^{0}C / 5 h / FC	RT	690	2.0
Hot-Deformed + 1,280^{0}C / 20 min. / FC	RT	640	1.8

Table 5 Mechanical Behavior of the Ti-45Al-7Nb-0.15B-0.4W Alloy at Room Temperature

Heat Treatment Condition	Tensile Test Temperature	Yield Strength (MPa)	Ductility (%)
1,130^{0}C / 24 h / FC	RT	590	0.8
1,130^{0}C / 24 h + 1,280^{0}C / 20 min. /FC	RT	620	1.7
1,280^{0}C / 20 min. / FC	RT	650	1.9

Table 6 Comparison in the Mechanical Behavior of the TiAl-based Alloys

TiAl-based Alloys	Condition	Yield Strength (MPa)	Ductility (%)
Ti-46Al-8Nb[70]	Cast + HIP @ 1,320^{0}C / 150 MPa / 4 h	482	0.2
	Cast + HIP @ 1,320^{0}C / 150 MPa / 4 h + 1,360^{0}C / 1 h / Saltbath @ 850^{0}C	523	0.5
Ti-47Al-2Nb-1Mn-0.2Si-1W[70]	Cast + 900^{0}C / 4 h / AC	278	0.6
	Cast + HIP @ 1,320^{0}C / 150 MPa / 4 h	402	0.5
	Cast + HIP @ 1,320^{0}C / 150 MPa / 4 h + 1,375^{0}C / 1 h / OQ	398	1.0
Ti-45Al-7Nb-0.15B-0.4W	Cast + HIP @ 1,250^{0}C / 130 MPa / 5 h + 1,280^{0}C / 20 min. / FC	650	1.9

Table 7 Mechanical Behavior of the Ti-45Al-7Nb-0.15B-0.4W Alloy at Higher Temperatures

Heat Treatment Condition	Tensile Test Temperature	Yield Strength (MPa)	Ductility (%)
1,130^{0}C / 24 h / FC	300^{0}C	578	1.0
1,130^{0}C / 24 h / FC	600^{0}C	561	2.4
1,130^{0}C / 24 h / FC	800^{0}C	483	3.0
1,130^{0}C / 24 h + 1,280^{0}C / 20 min. / FC	300^{0}C	590	1.7
1,130^{0}C / 24 h + 1,280^{0}C / 20 min. / FC	600^{0}C	560	2.2
1,130^{0}C / 24 h + 1,280^{0}C / 20 min. / FC	800^{0}C	485	3.8

Table 8 Comparison of the Mechanical Behavior of the As-cast and Hot-Deformed Alloys

Condition	Yield Strength (MPa)	Ductility (%)
As-cast + 1,280^{0}C / 20 min. / FC	650	1.9
Hot-Deformed 1,280^{0}C / 20 min. / FC	640	1.8

Table 9 Comparison of the Mechanical Behavior of the thermomechanically Deformed TiAl-based Alloys

TiAl-based Alloys	Condition	Yield Strength (MPa)	Ductility (%)
Ti-48Al-2Nb-2Cr-1B[71]	Hot Forging + 1,380^{0}C / 1 h / FC	545	1.8
Ti-44Al-8Nb-1B[71]	Extrusion + 1,320^{0}C / 2 h / FC + 900^{0}C/ 4h / AC	570	1.6
Ti-45Al-7Nb-0.15B-0.4W	Hot Forging + 1,280^{0}C / 20 min. / FC	640	1.8

Appendix B

Figures

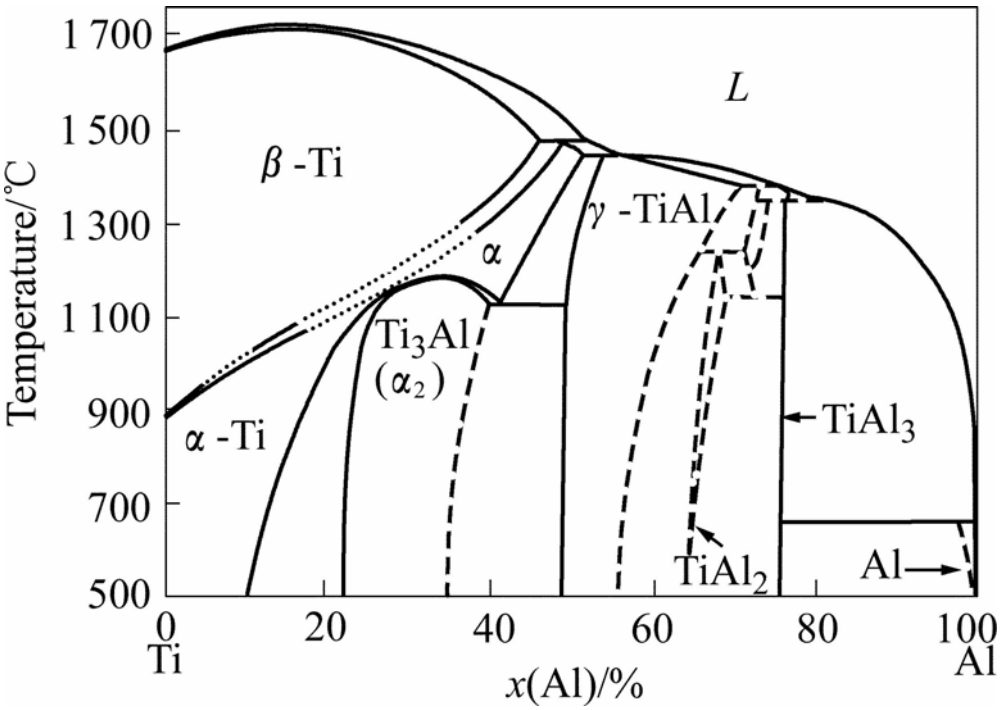

Figure 1 Binary phase diagram of the Ti-Al alloys [6]

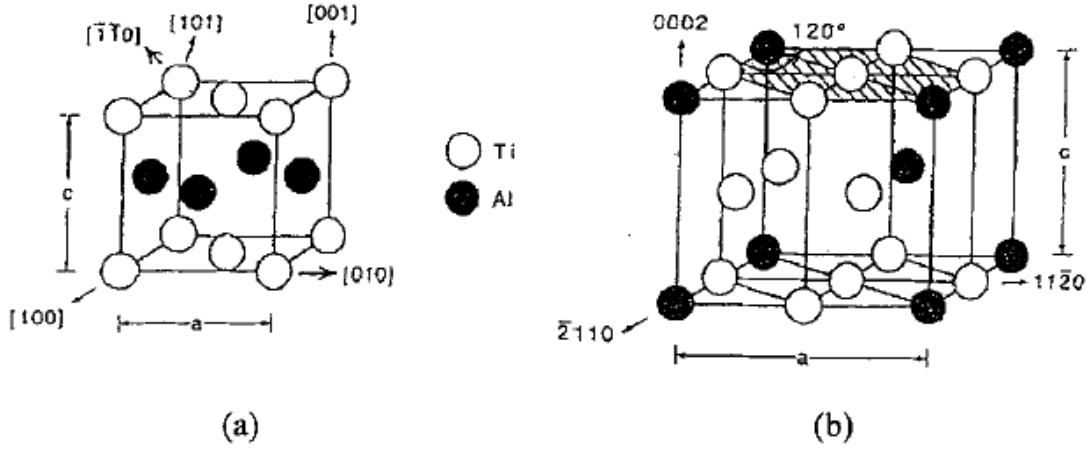

(a) γ phase (Ll_0) structure (b) α_2 phase ($D0_{19}$) structure

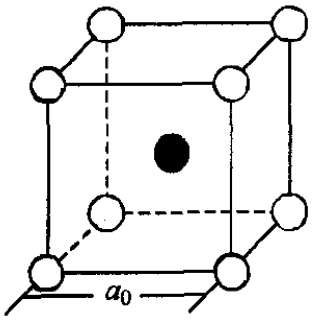

(c) β phase BCC structure

Figure 2 TiAl crystal structures (a) γ phase structure, (b) α_2 phase structure, (c) β phase structure [6]

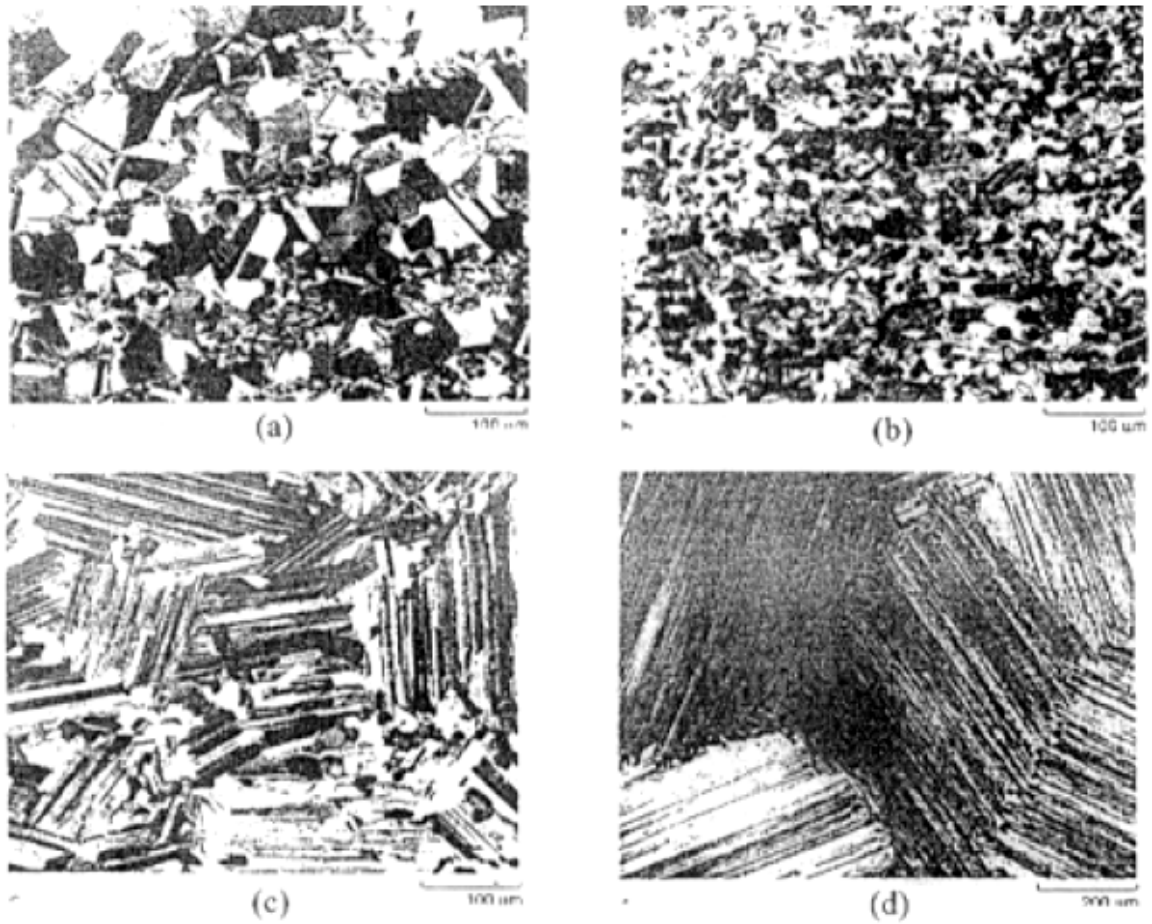

Figure 3 Four typical microstructures of the γ-TiAl-based alloys after heat treatments, (a) Near-gamma structure, (b) Duplex structure, (c) Nearly-lamellar structure, and (d) Fully-lamellar structure [8]

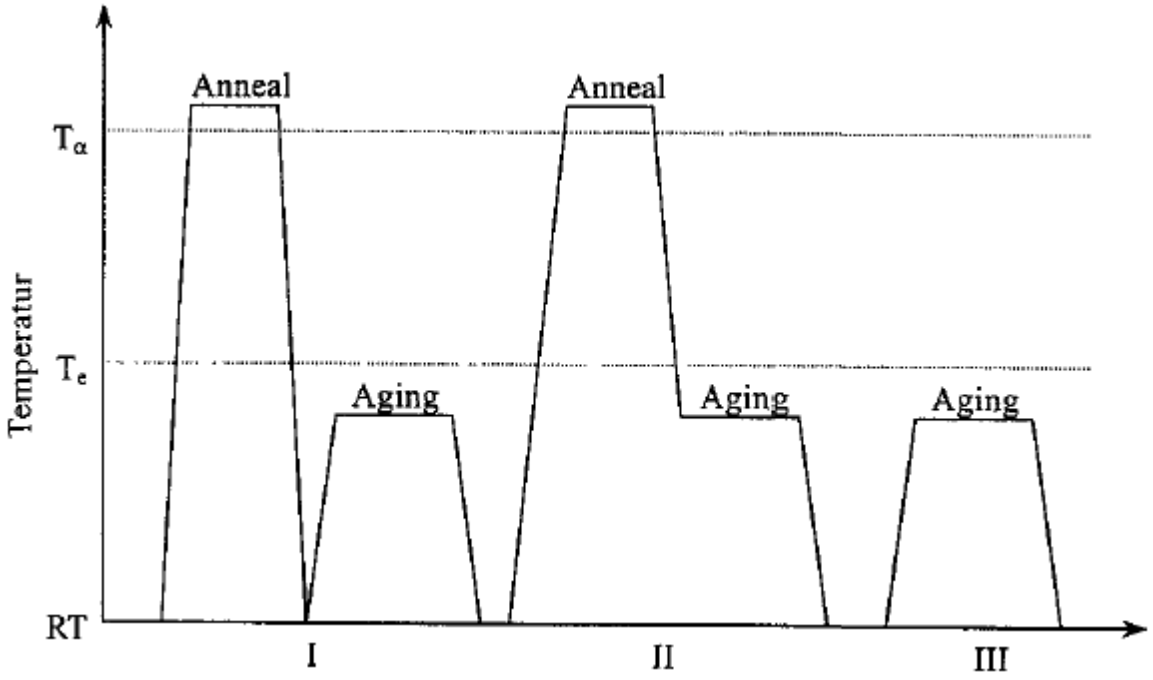

Figure 4 Three typical heat-treating processes of the γ-TiAl alloys [8] (Type I, Π, and Ш)

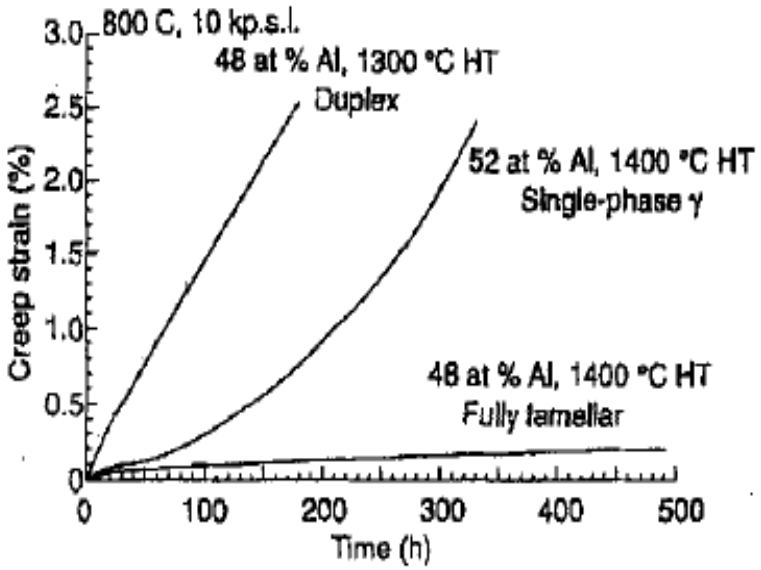

Figure 5 Creep curves of different TiAl alloys with different microstructures [26]

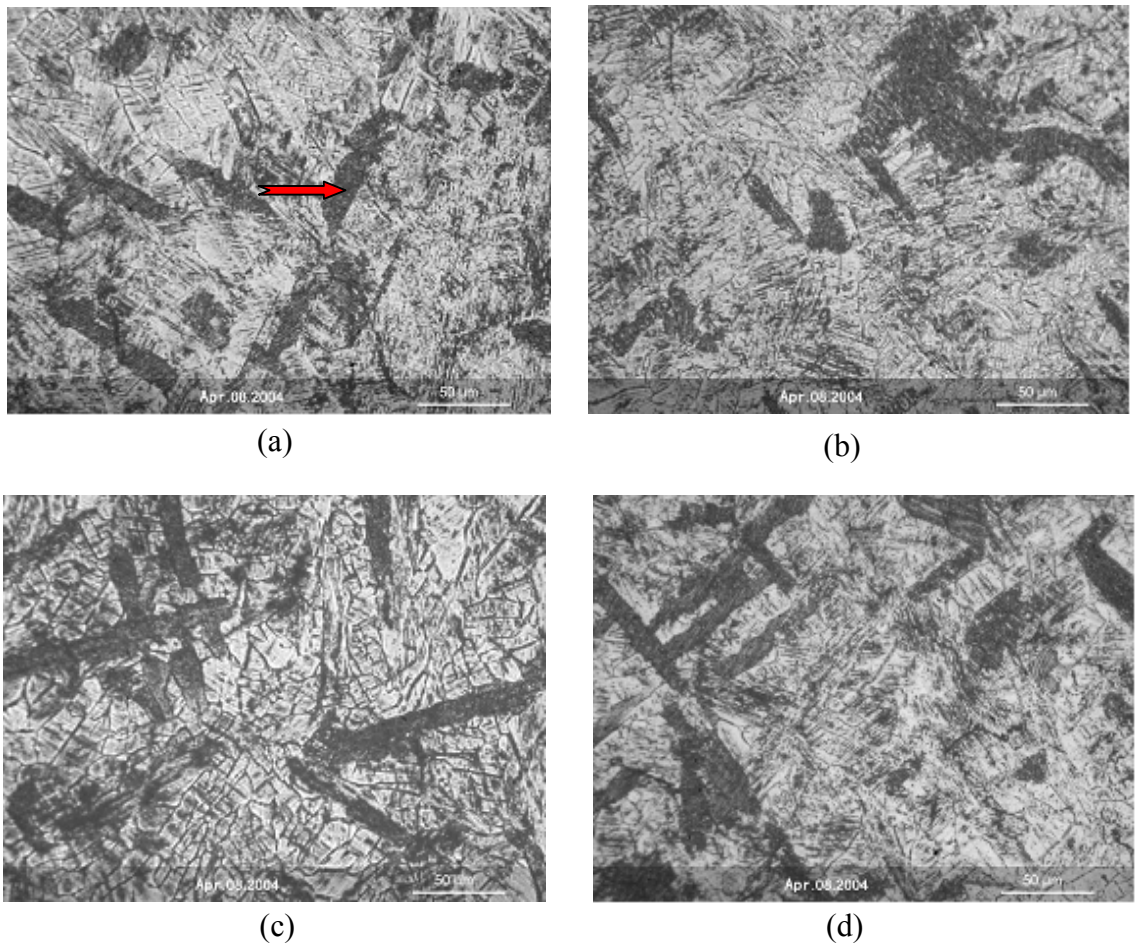

Figure 6 Optical microstructures of the as-cast Ti-Al-Nb-W-B alloys
(The arrows in (a) indicate the dendrites.)
(a) Ti-45Al-7Nb-0.15B, (b) Ti-45Al-7Nb-0.15B-0.2W, (c) Ti-45Al-7Nb-0.15B-0.4W, and (d) Ti-45Al-7Nb-0.15B-0.7W

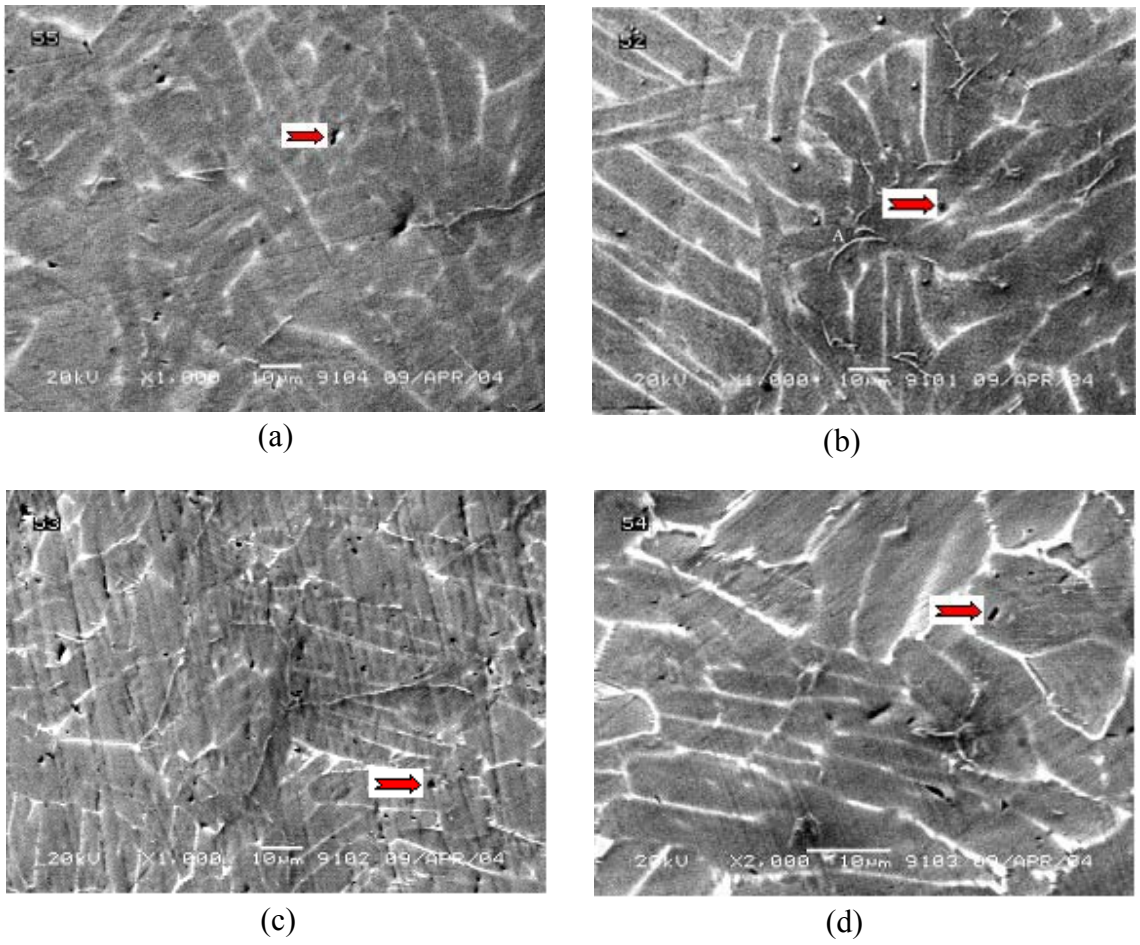

(a) (b)

(c) (d)

Figure 7 Backscattered electron images of the as-cast Ti-Al-Nb-W-B alloys (The arrows show the porosities. Point A in (b) shows the ribbon-shaped Ti-B boride phase.)
(a) Ti-45Al-7Nb-0.15B, (b) Ti-45Al-7Nb-0.15B-0.2W, (c) Ti-45Al-7Nb-0.15B-0.4W, and (d) Ti-45Al-7Nb-0.15B-0.7W

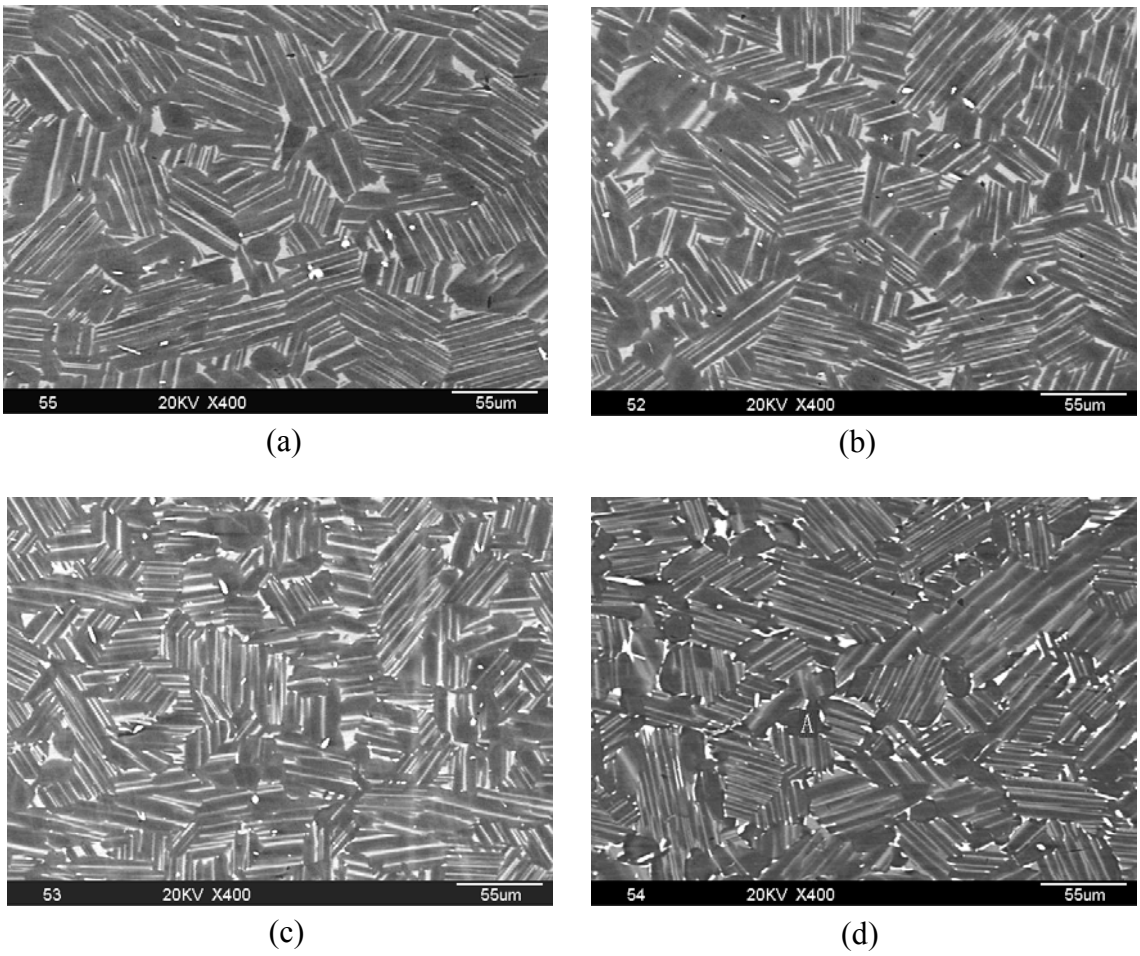

Figure 8 Backscattered electron images of the Ti-Al-Nb-W-B alloys after HIPping and homogenization (Area A in (d) shows the γ phase), (a) Ti-45Al-7Nb-0.15B, (b) Ti-45Al-7Nb-0.15B-0.2W, (c) Ti-45Al-7Nb-0.15B-0.4W, and (d) Ti-45Al-7Nb-0.15B-0.7W

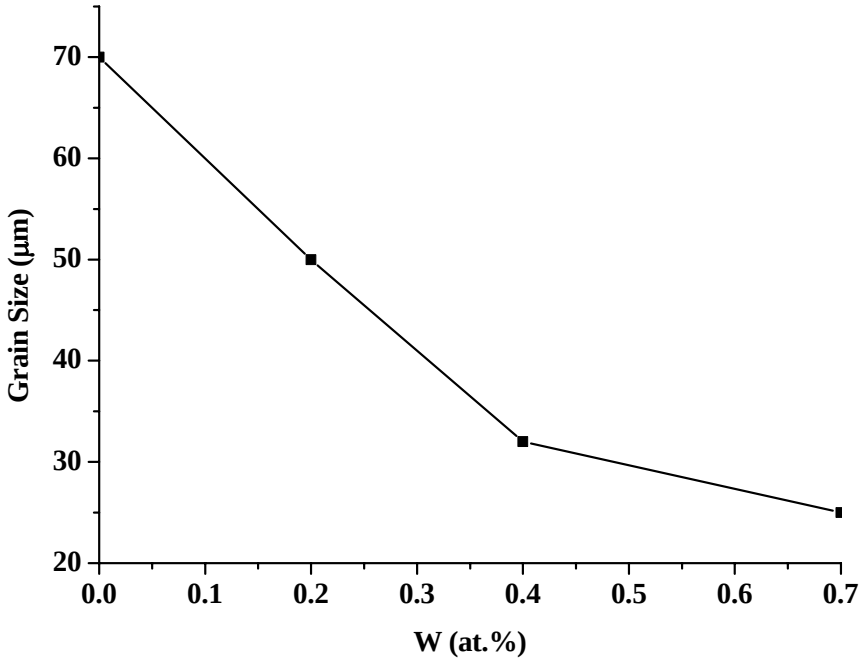

(a)

Figure 9 Effect of W on the (a) grain size, and (b) lamellar spacing of the Ti-Al-Nb-W-B alloys after HIPping and homogenization

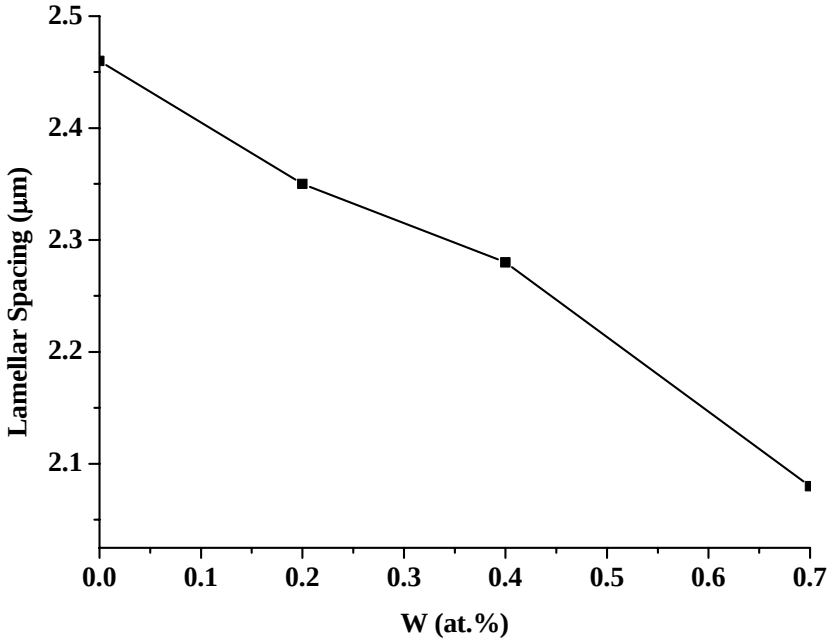

(b)

Figure 9 Continued

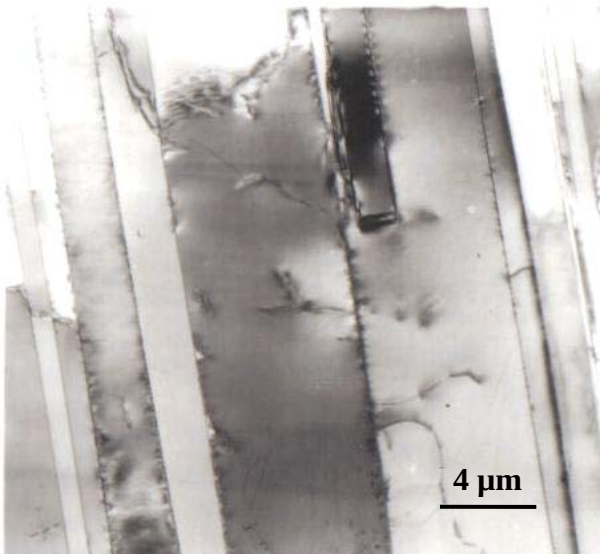

(a)

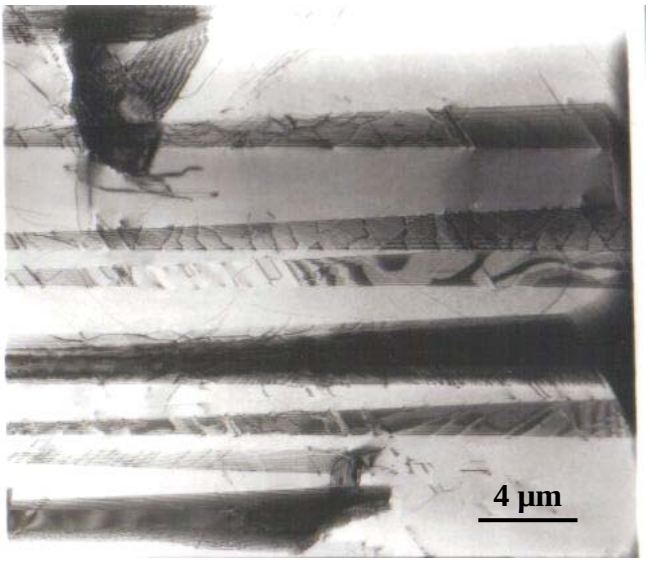

(b)

Figure 10 TEM analyses of the Ti-Al-Nb-W-B alloys after HIPping and homogenization, (a) Ti-45Al-7Nb-0.15B-0.2W, (b) Ti-45Al-7Nb-0.15B-0.4W, and (c) Ti-45Al-7Nb-0.15B-0.7W

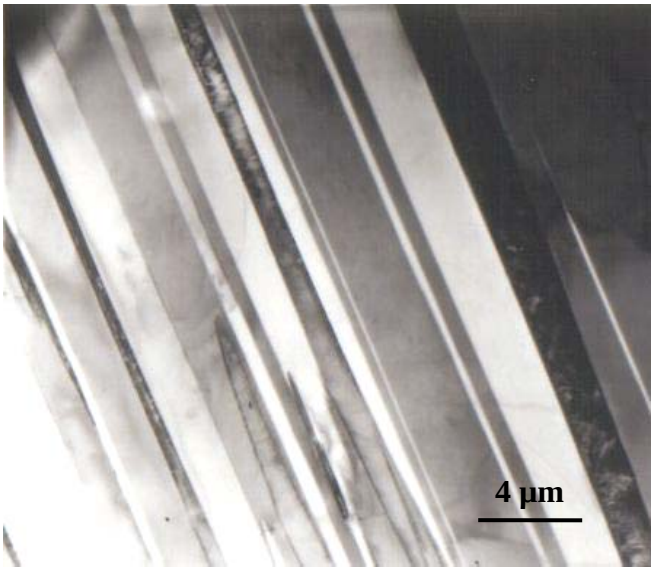

(c)

Figure 10 Continued

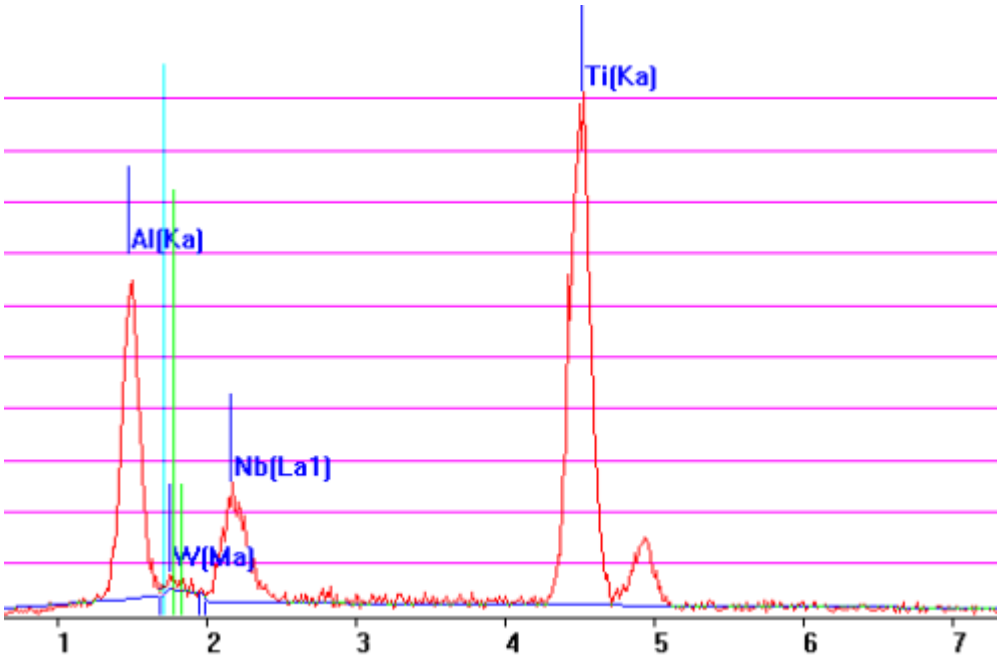

Figure 11 Energy-Dispersive X-ray Spectroscopy (EDS) of the γ phase in the Ti-45Al-7Nb-0.15B-0.7W alloy after HIPping and homogenization

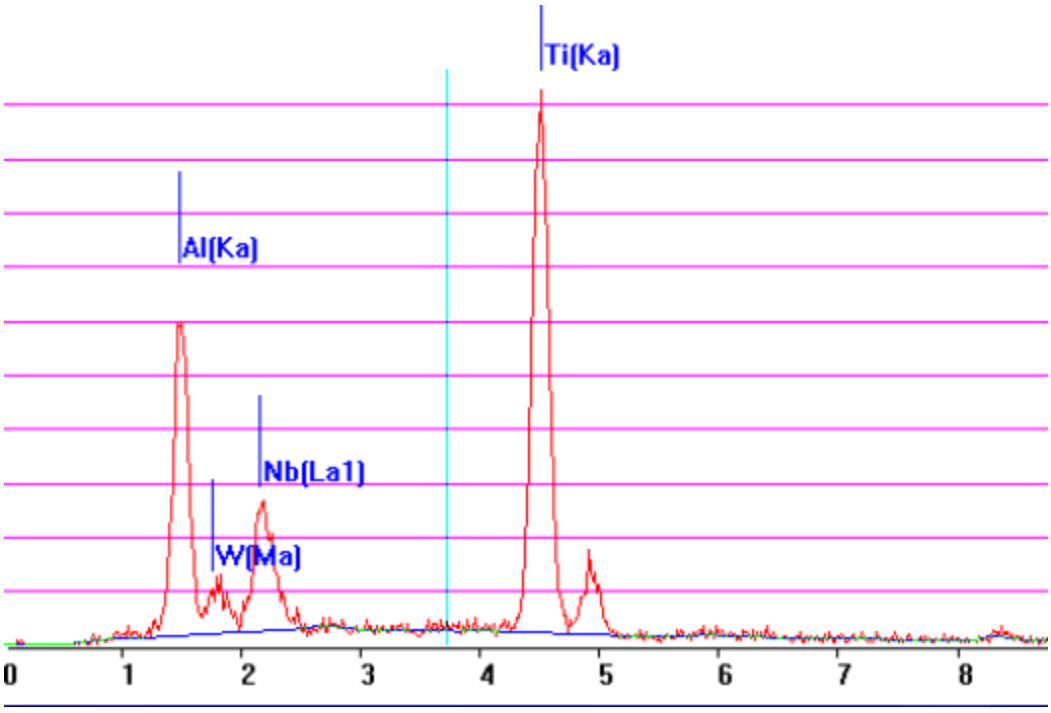

Figure 12 EDS of the α_2 phase in the Ti-45Al-7Nb-0.15B-0.7W alloy after HIPping and homogenization

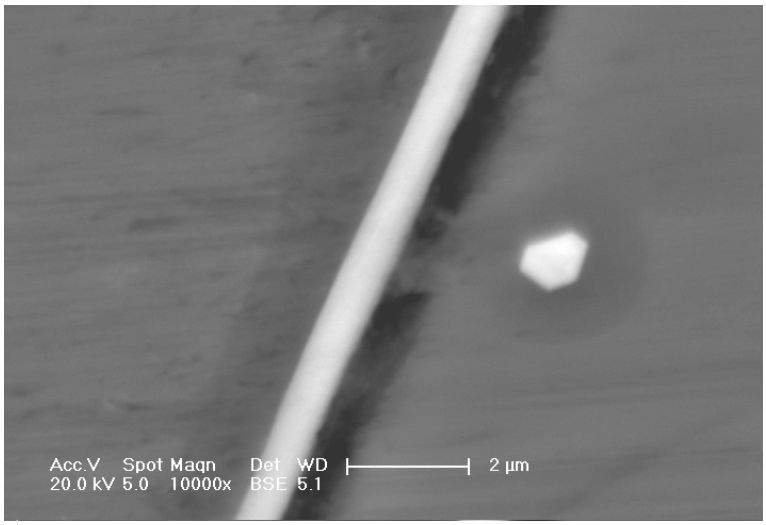

(a)

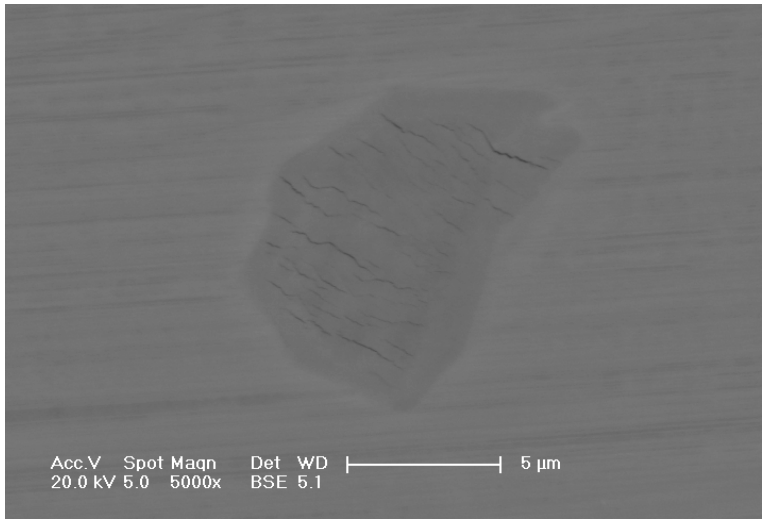

(b)

Figure 13 Backscattered images of the Ti-45Al-7Nb-0.15B-0.7W alloy after HIPping and homogenization, (a) TiB_2 needles, (b) γ-phase, and (c) formation of the γ-twin caused by TiB_2 (shown in area A)

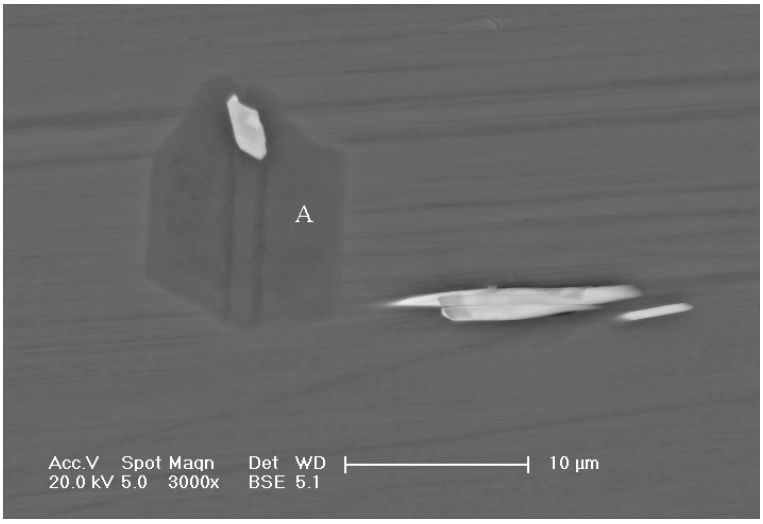

(c)

Figure 13 Continued

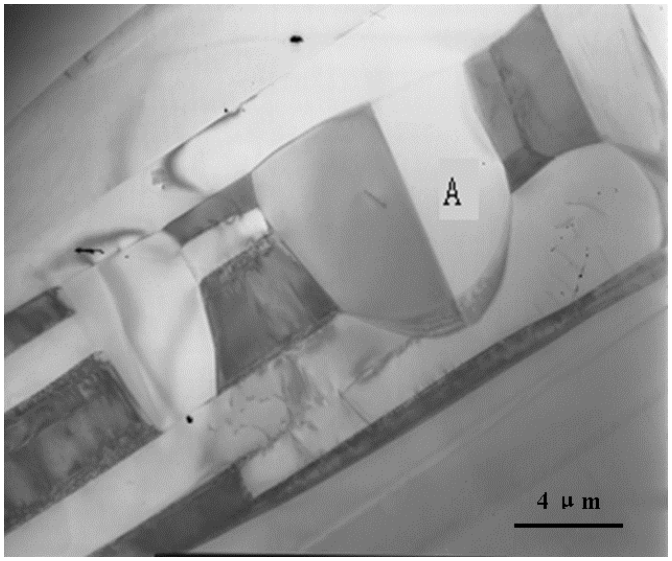

(a)

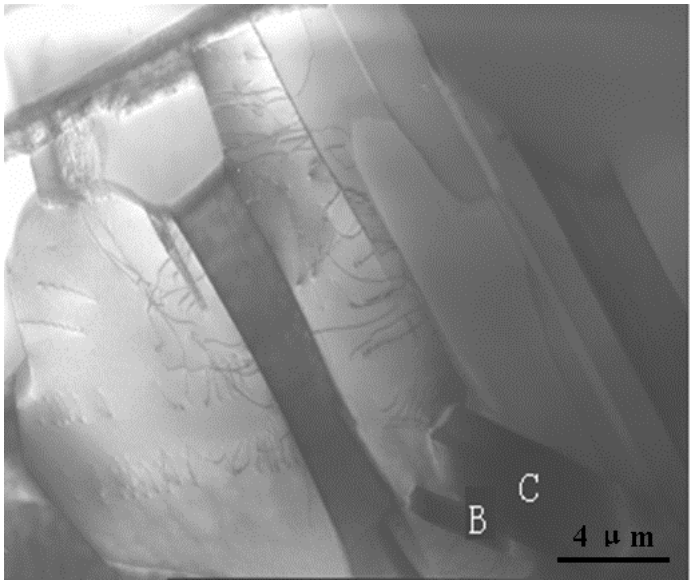

(b)

Figure 14 TEM analyses of the Ti-45Al-7Nb-0.15B-0.4W alloy after HIPping and homogenization, (a) γ-twin separated from the α_2/γ lamellae (shown in area A), and (b) TiB_2 and γ-twin (shown in area B and area C)

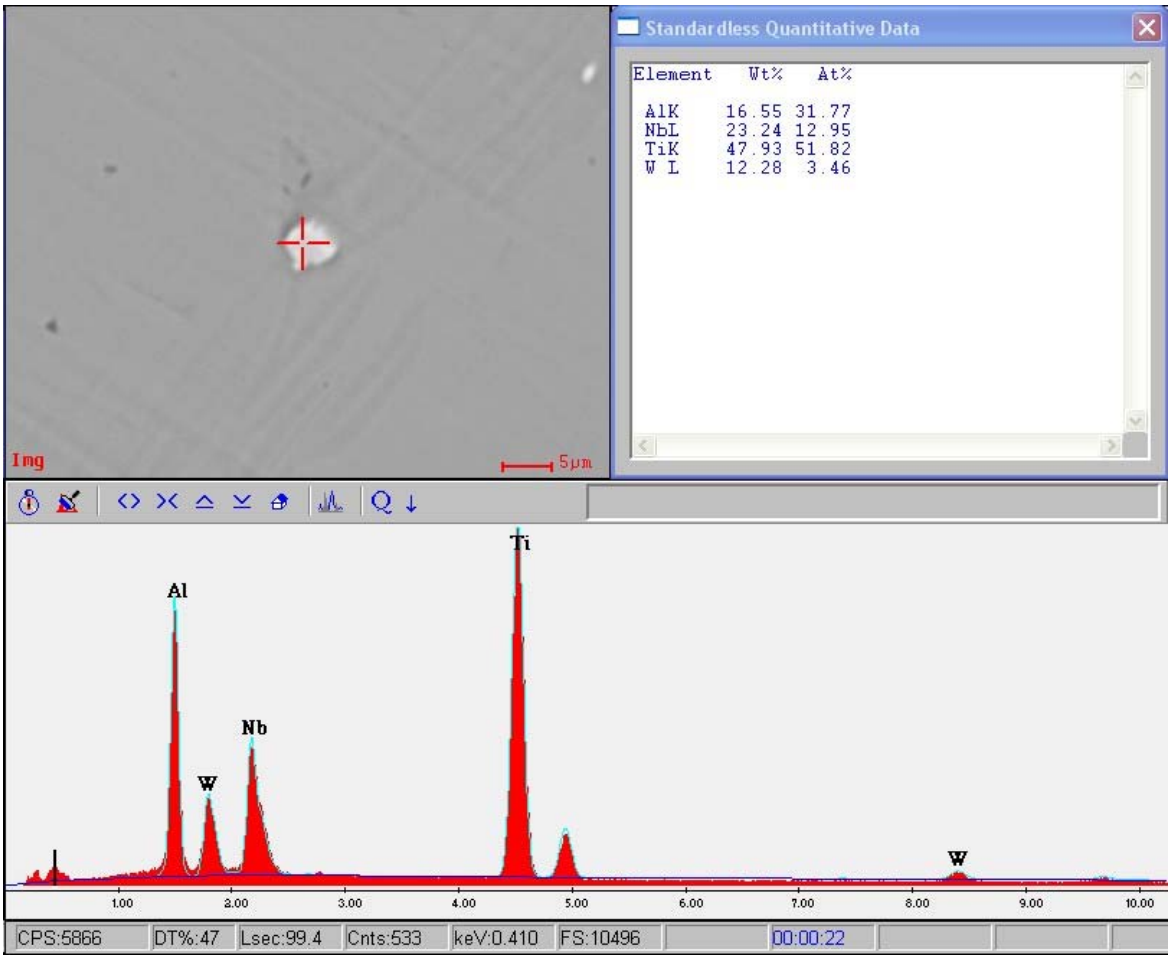

Figure 15 Topograph and composition analyses of the β phase

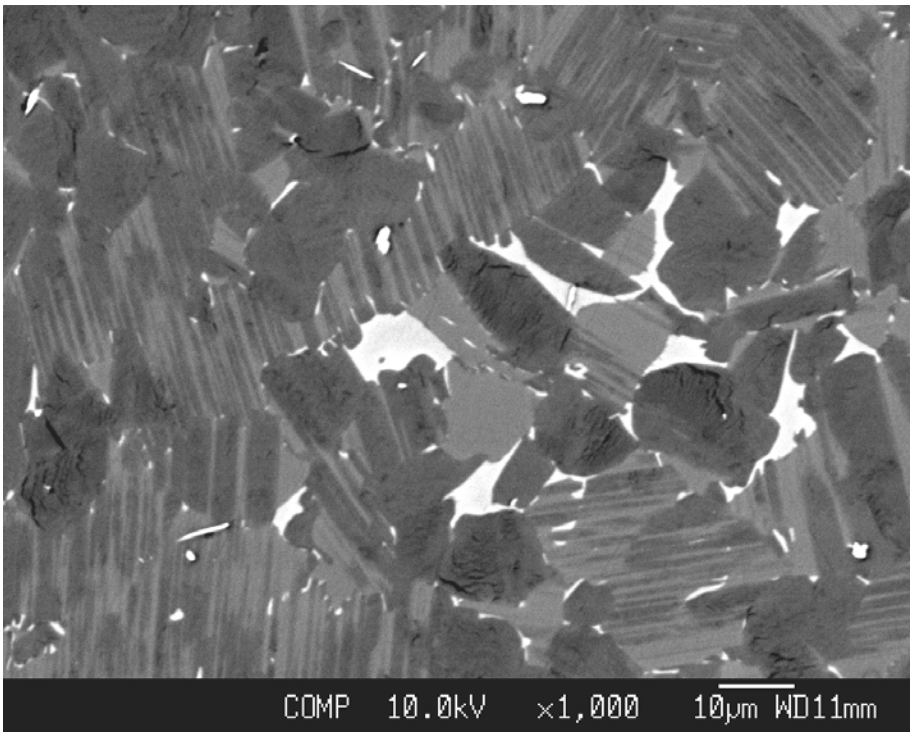

Figure 16 Microstructure of the Ti-45Al-7Nb-0.15B-0.7W alloy after HIPping and homogenization

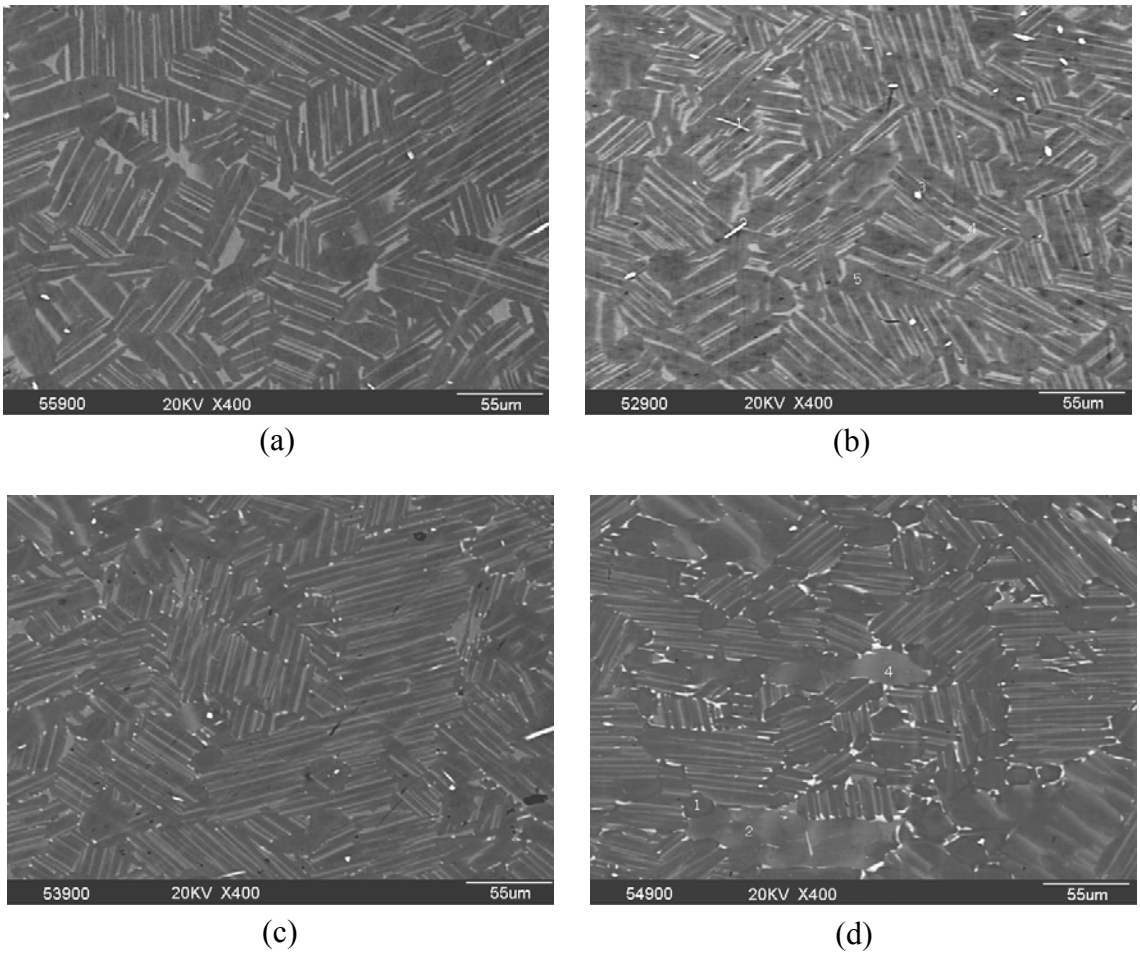

Figure 17 Microstructures of the Ti-Al-Nb-W-B alloys heat treated at 900^0C, 360 h, (a) Ti-45Al-7Nb-0.15B, (b) Ti-45Al-7Nb-0.15B-0.2W, (c) Ti-45Al-7Nb-0.15B-0.4W, and (d) Ti-45Al-7Nb-0.15B-0.7W

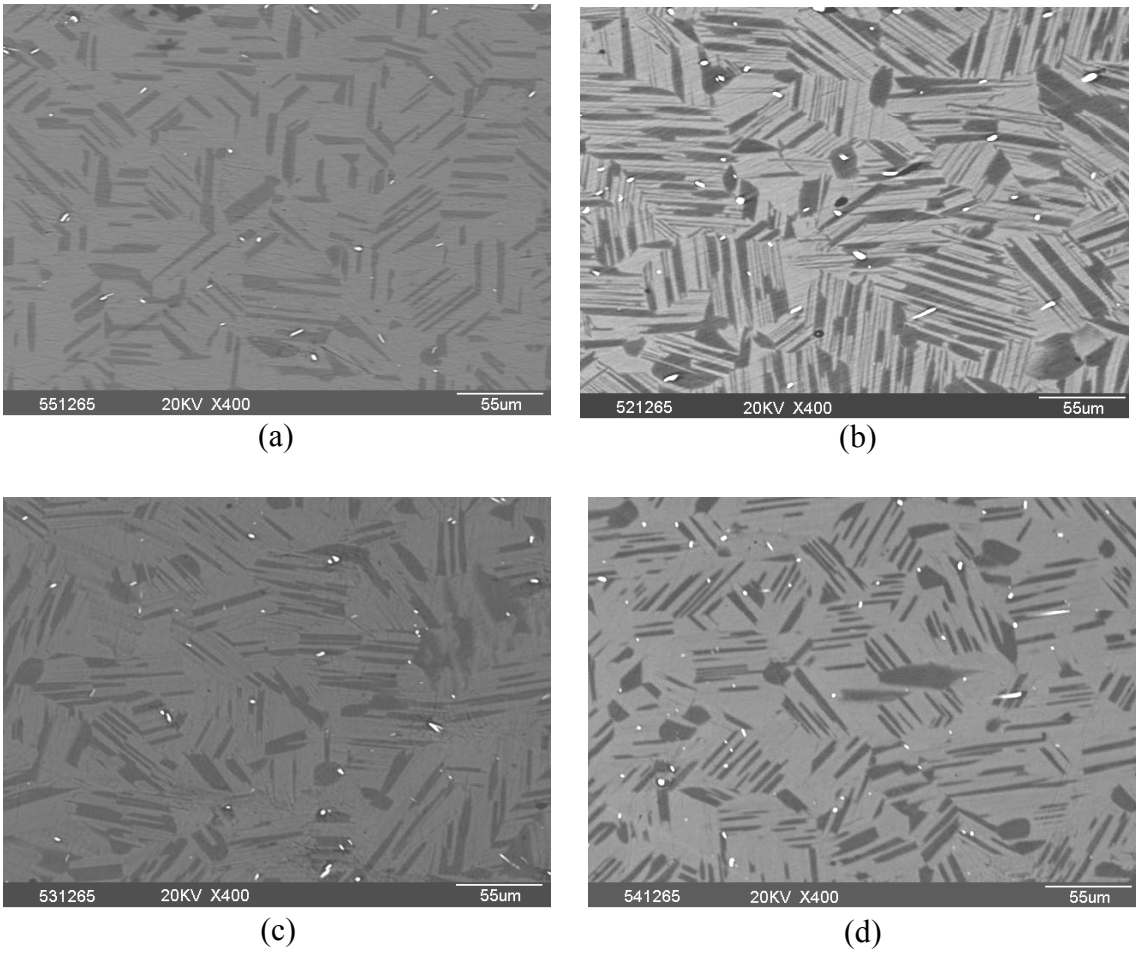

Figure 18 Microstructures of the Ti-Al-Nb-W-B alloys heat treated at 1,265^{0}C, 18 h, (a) Ti-45Al-7Nb-0.15B, (b) Ti-45Al-7Nb-0.15B-0.2W, (c) Ti-45Al-7Nb-0.15B-0.4W, and (d) Ti-45Al-7Nb-0.15B-0.7W

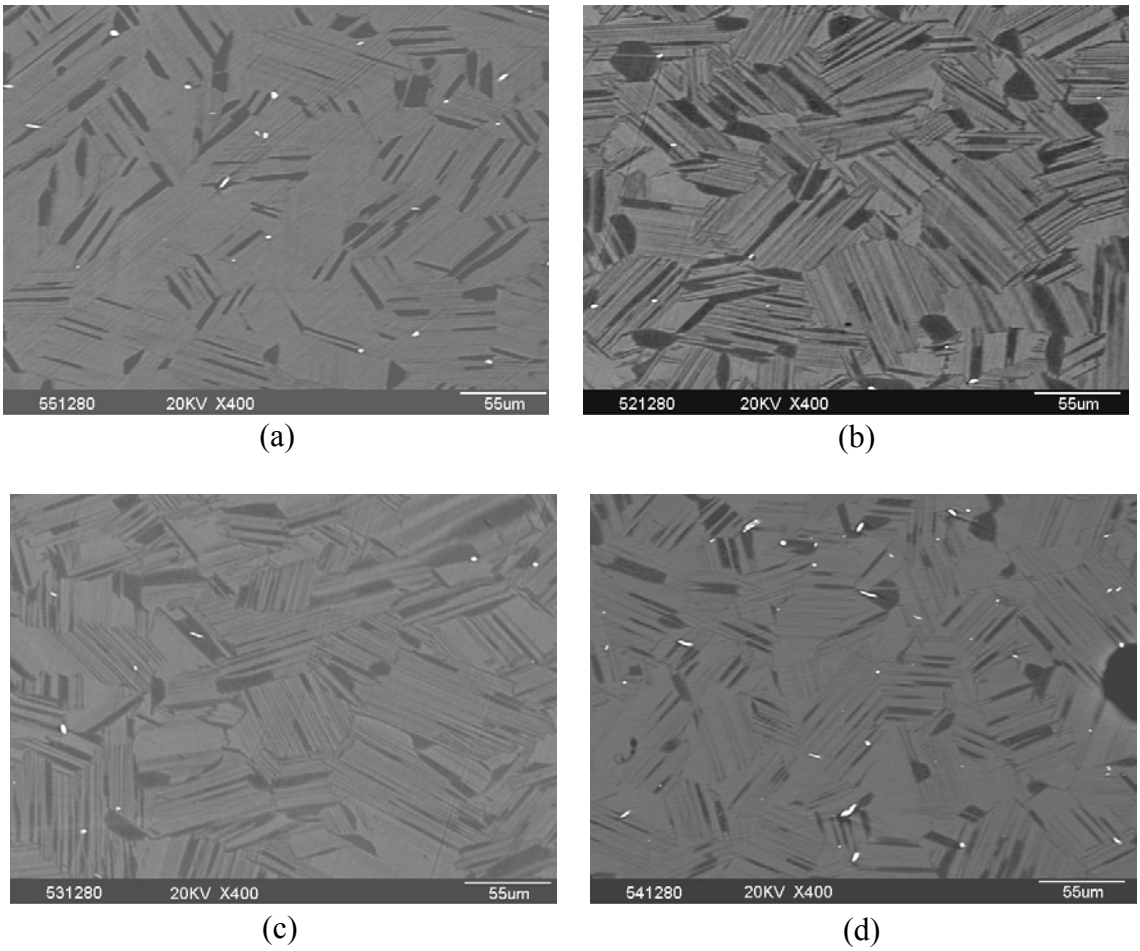

Figure 19 Microstructures of the Ti-Al-Nb-W-B alloys heat treated at 1,280^{0}C, 14 h, (a) Ti-45Al-7Nb-0.15, b) Ti-45Al-7Nb-0.15B-0.2W, (c) Ti-45Al-7Nb-0.15B-0.4W, and (d) Ti-45Al-7Nb-0.15B-0.7W

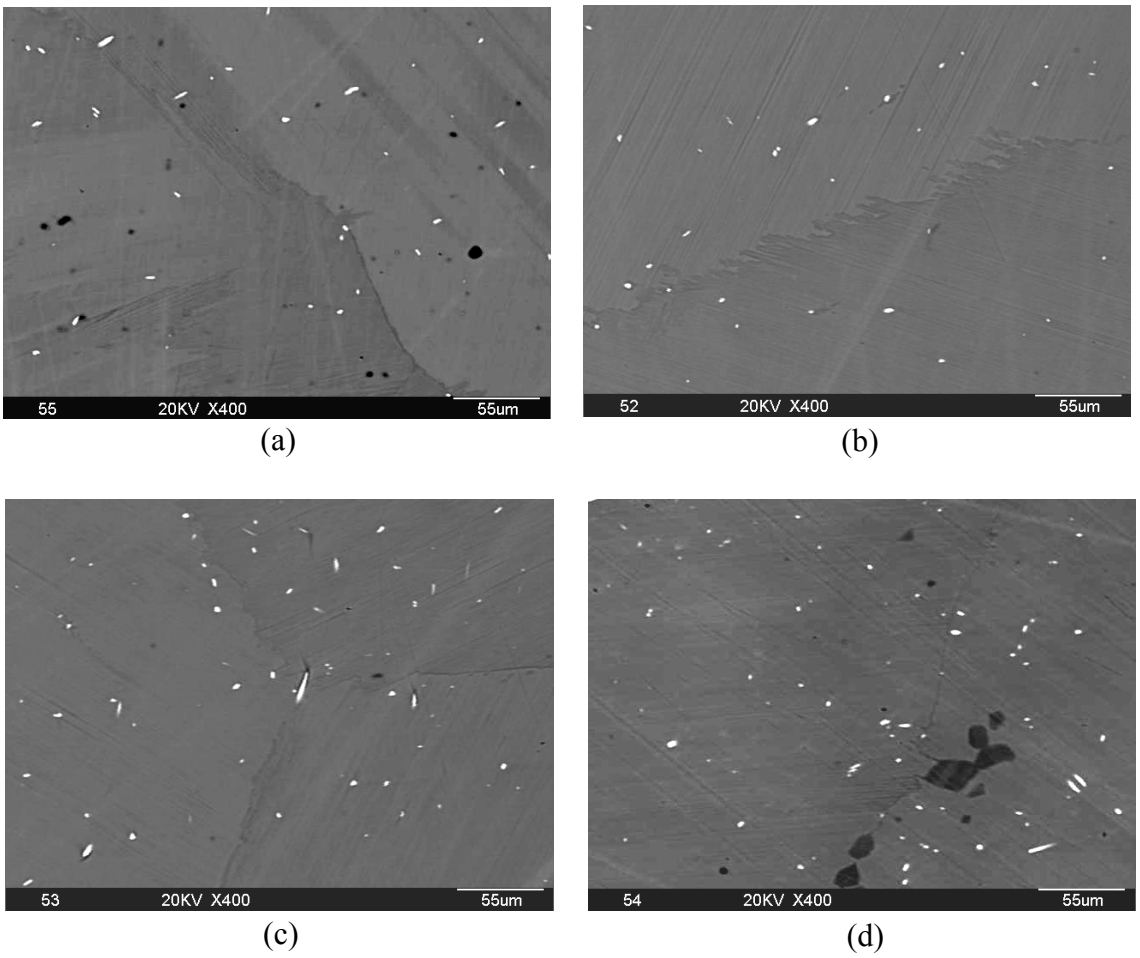

Figure 20 Microstructures of the Ti-Al-Nb-W-B alloys heat treated at 1,295^{0}C, 10 h, (a) Ti-45Al-7Nb-0.15B, (b) Ti-45Al-7Nb-0.15B-0.2W, (c) Ti-45Al-7Nb-0.15B-0.4W, and (d) Ti-45Al-7Nb-0.15B-0.7W

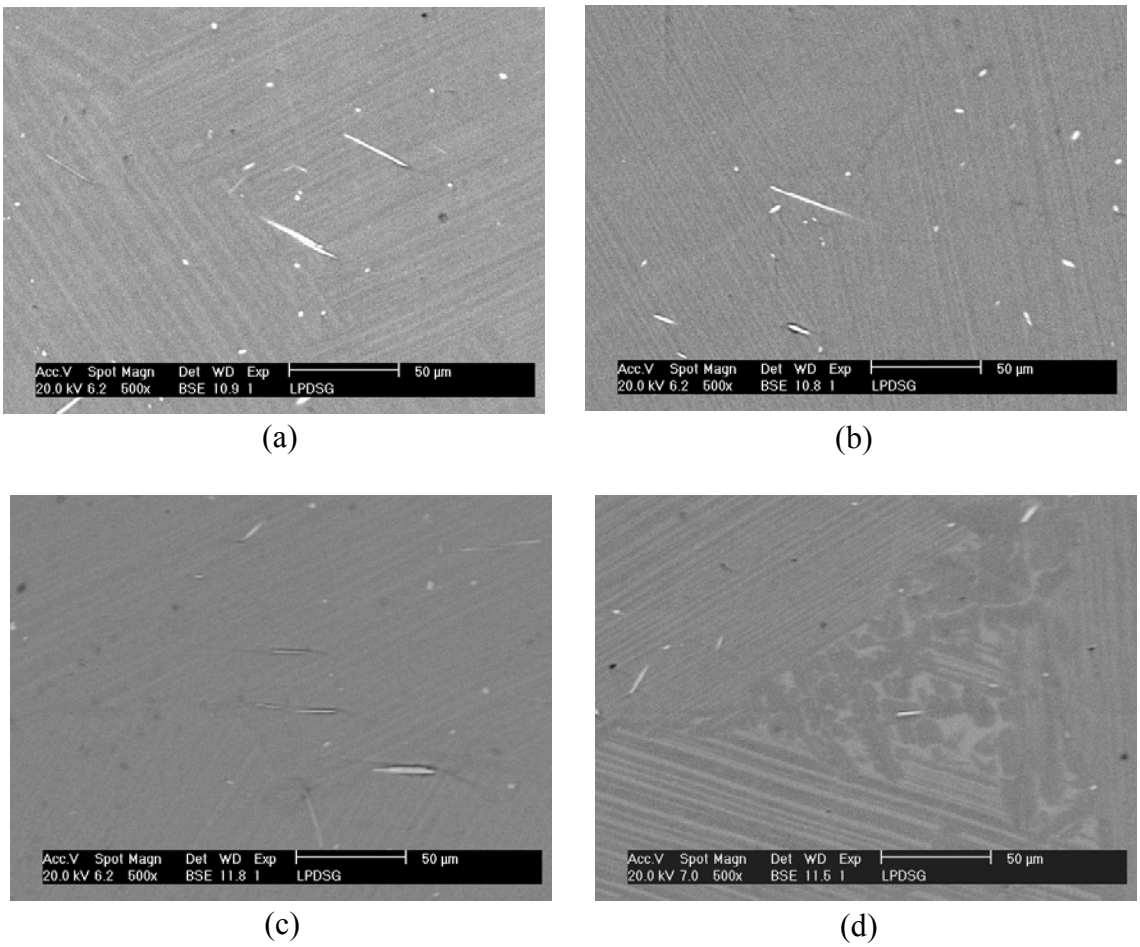

Figure 21 Microstructures of the Ti-Al-Nb-W-B alloys heat treated at 1,310^{0}C, 5 h, (a) Ti-45Al-7Nb-0.15, (b) Ti-45Al-7Nb-0.15B-0.2W, (c) Ti-45Al-7Nb-0.15B-0.4W, and (d) Ti-45Al-7Nb-0.15B-0.7W

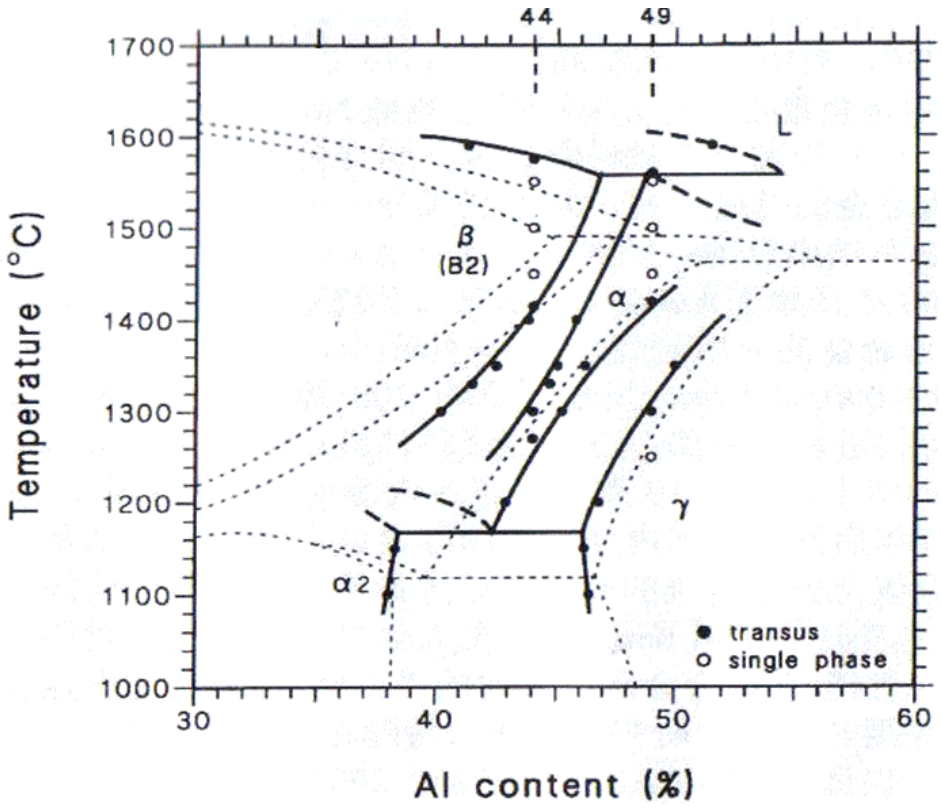

Figure 22 Ti-Al-7Nb phase diagram [70]

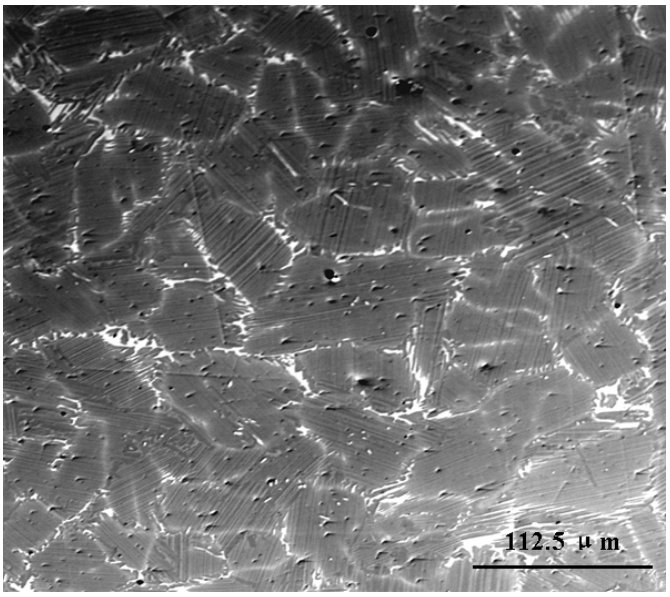

(a)

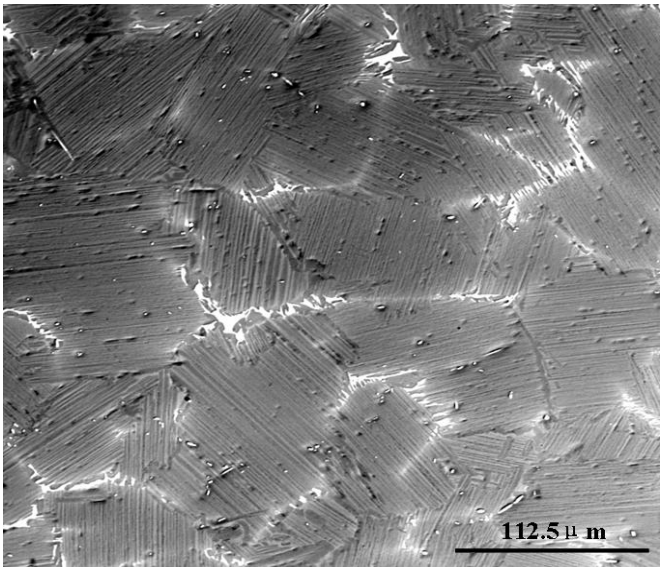

(b)

Figure 23 Microstructure of the (a) as-cast Ti-Al-Nb-W-B alloy produced by magnetic flotation melting, (b) as-cast condition + HIP, and (c) as-cast condition + HIP + homogenization

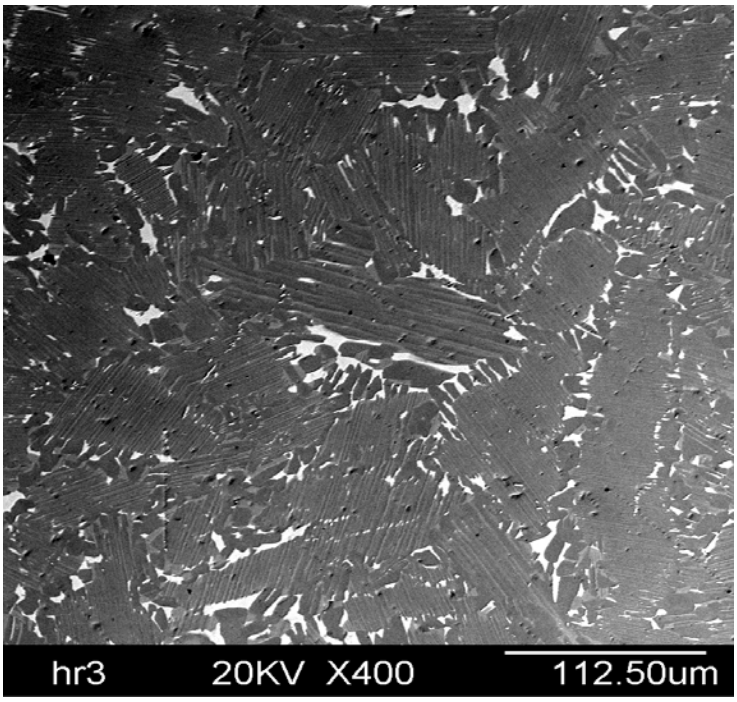

(c)

Figure 23 Continued

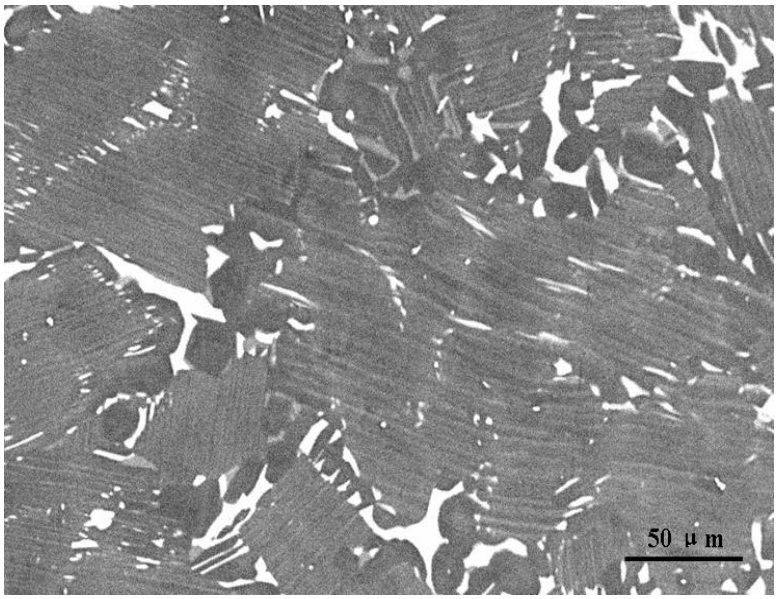

Figure 24 Ti-Al-Nb-W-B alloy heat treated at 1,240^{0}C, 16 h, furnace cooled (FC), indicating the existence of the β phase

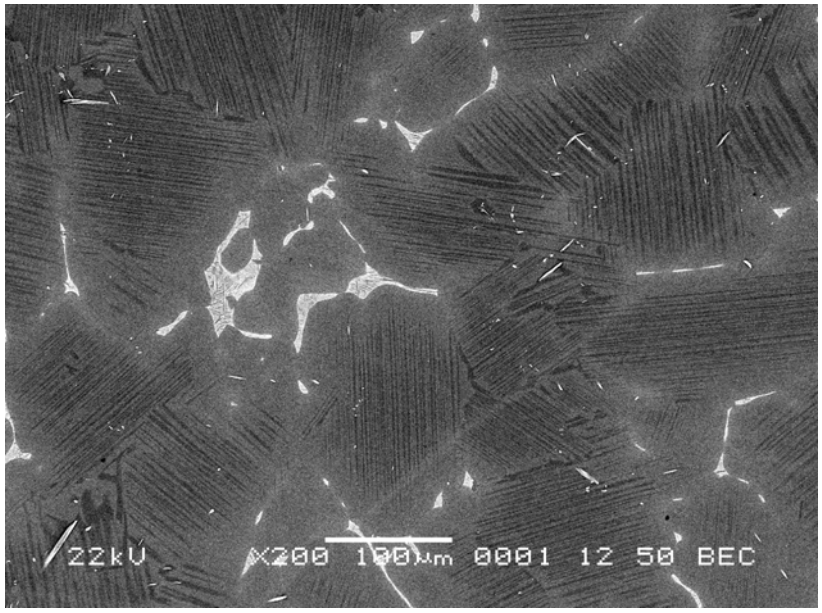

Figure 25 Ti-Al-Nb-W-B alloy heat treated at 1,280^{0}C, 30 min., FC, indicating the reduction of the amount of the β phase

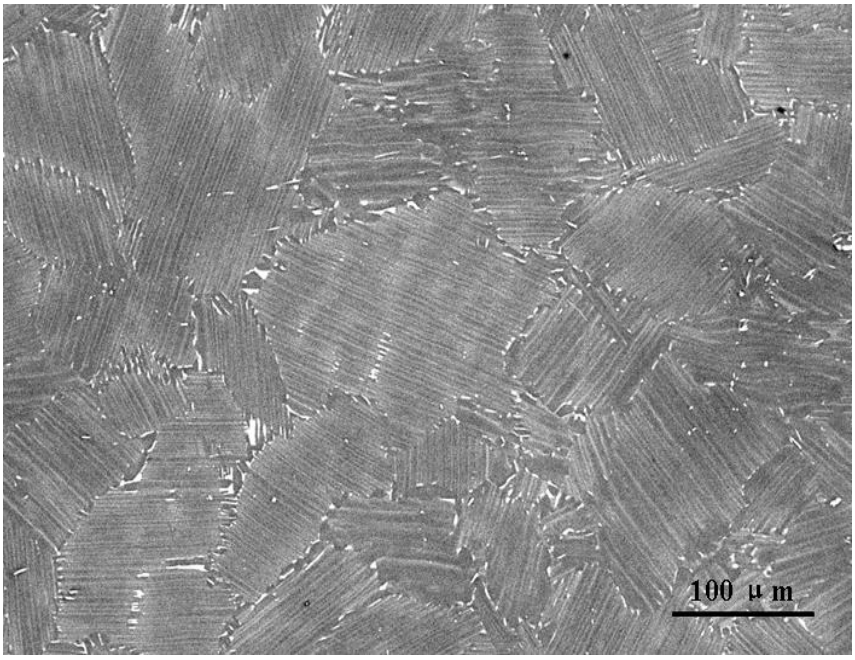

Figure 26 Ti-Al-Nb-W-B alloy heat treated at 1,310^{0}C, 8 h, FC, indicating the elimination of the β phase

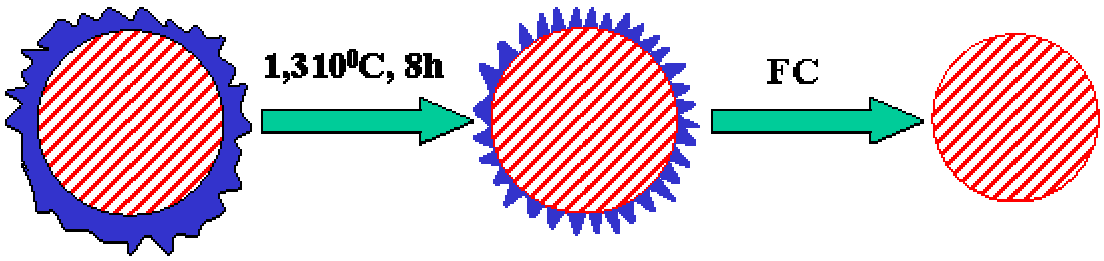

Figure 27 The transformation of the β phase in the Ti-Al-Nb-W-B alloy after the heat treatment

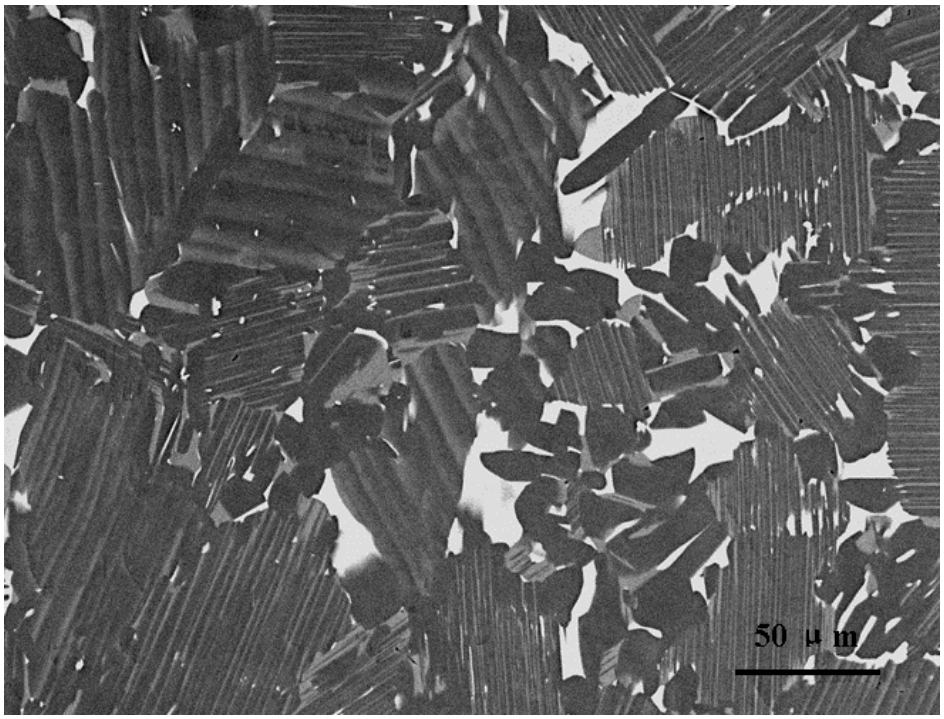

Figure 28 Microstructure of the Ti-Al-Nb-W-B alloy heat treated at 1,190^{0}C, 14 h, air cooled

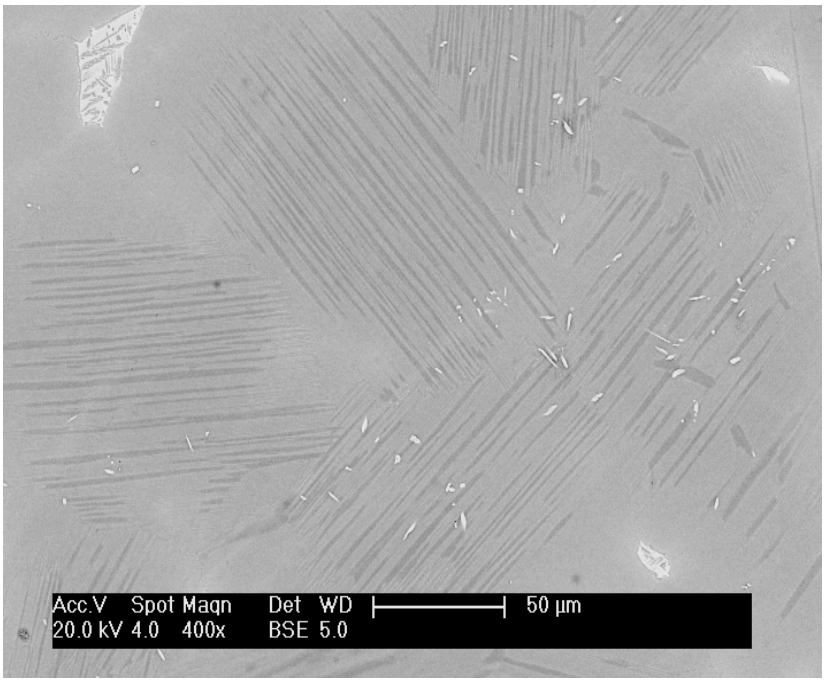

Figure 29 Microstructure of the Ti-Al-Nb-W-B alloy heat treated at 1,290^{0}C, 8 h, air cooled

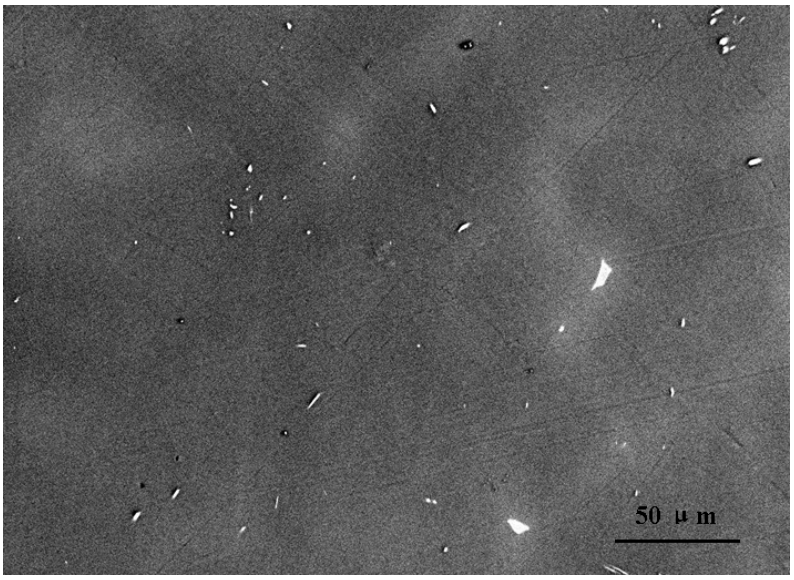

(a)

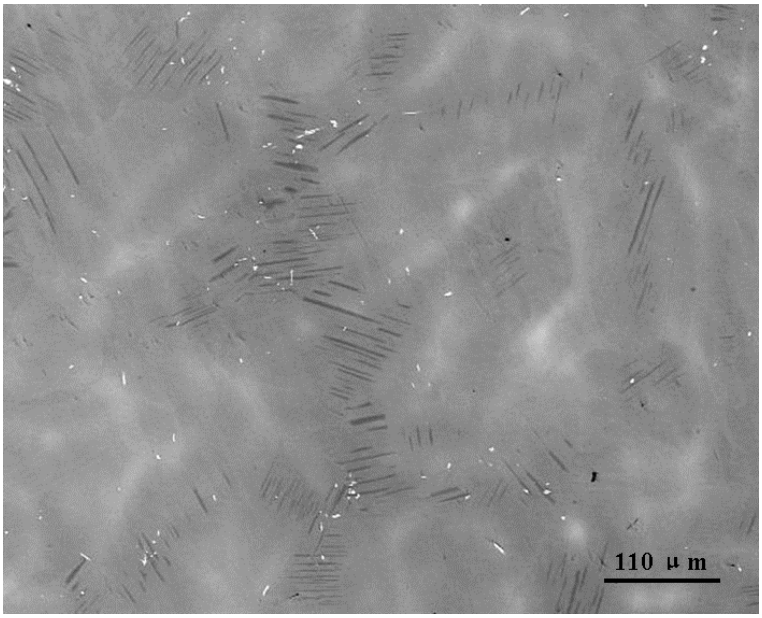

(b)

Figure 30 Microstructure of the Ti-Al-Nb-W-B alloy heat treated at 1,310^{0}C, 8 h, (a) salt ice water cooled, (b) oil cooled, (c) fan cooled, (d) air cooled, and (e) furnace cooled

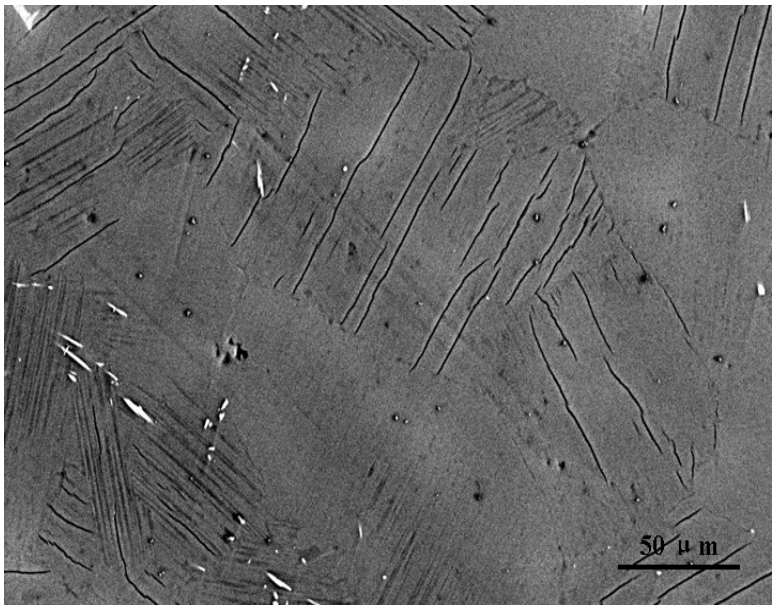

(c)

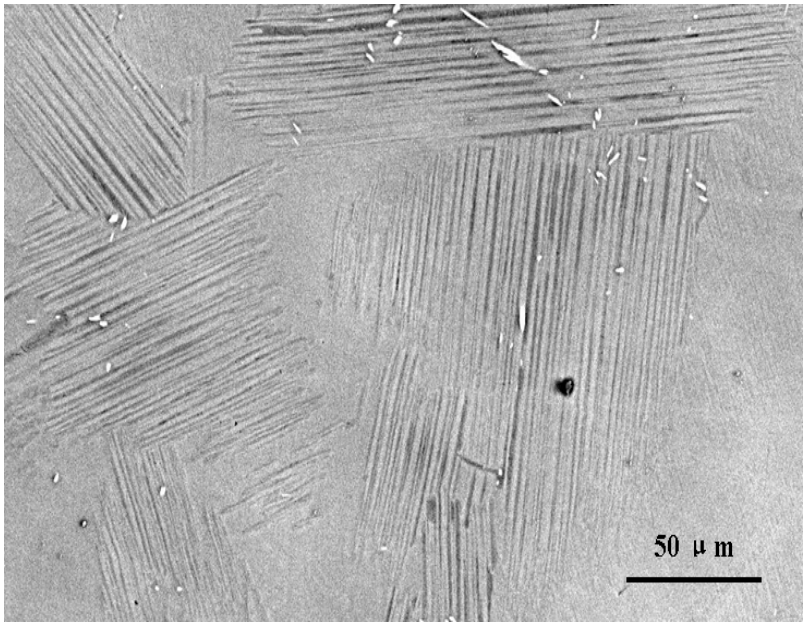

(d)

Figure 30 Continued

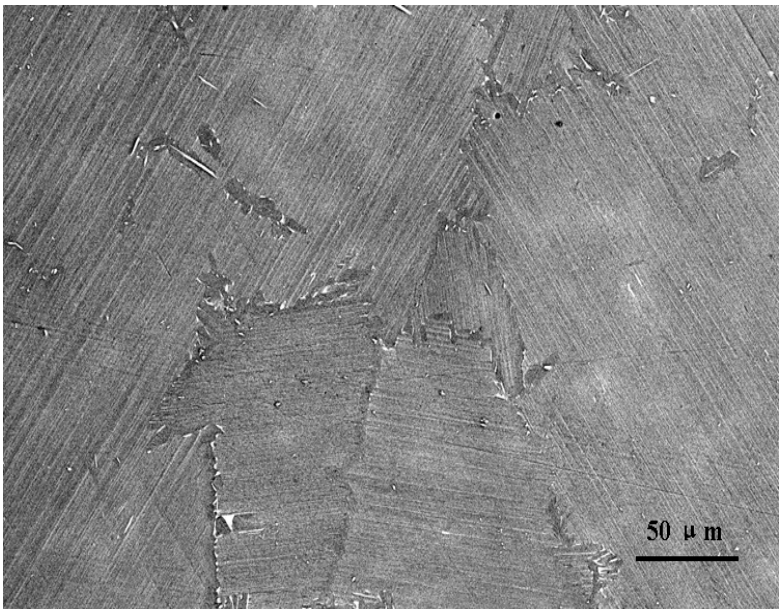

(e)

Figure 30 Continued

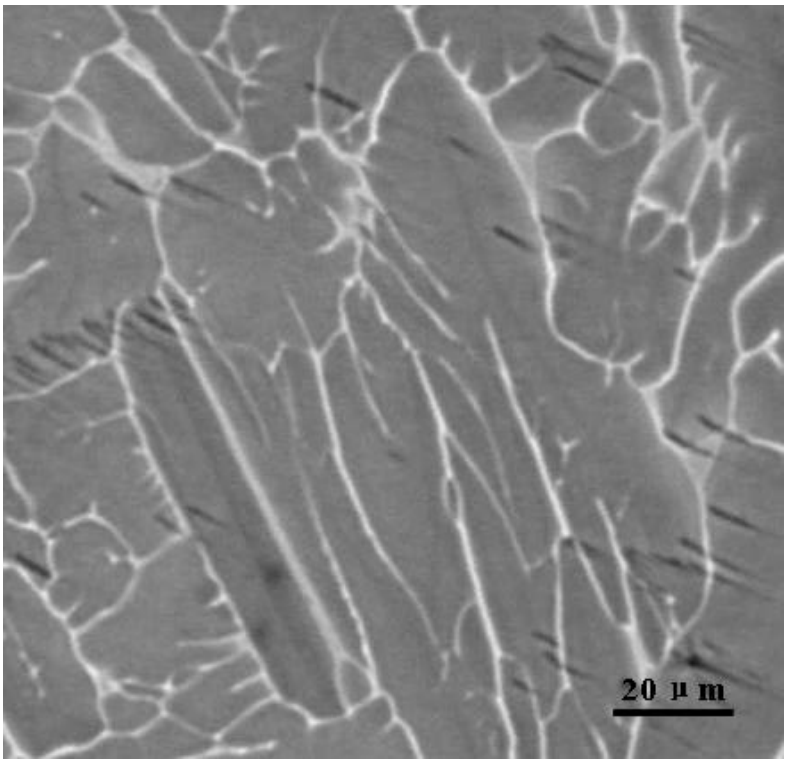

Figure 31 Microstructure of the Ti-Al-Nb-W-B alloy produced by magnetic floatation melting and heat treated at 1,450^{0}C, 2 h, salt-ice-water cooled

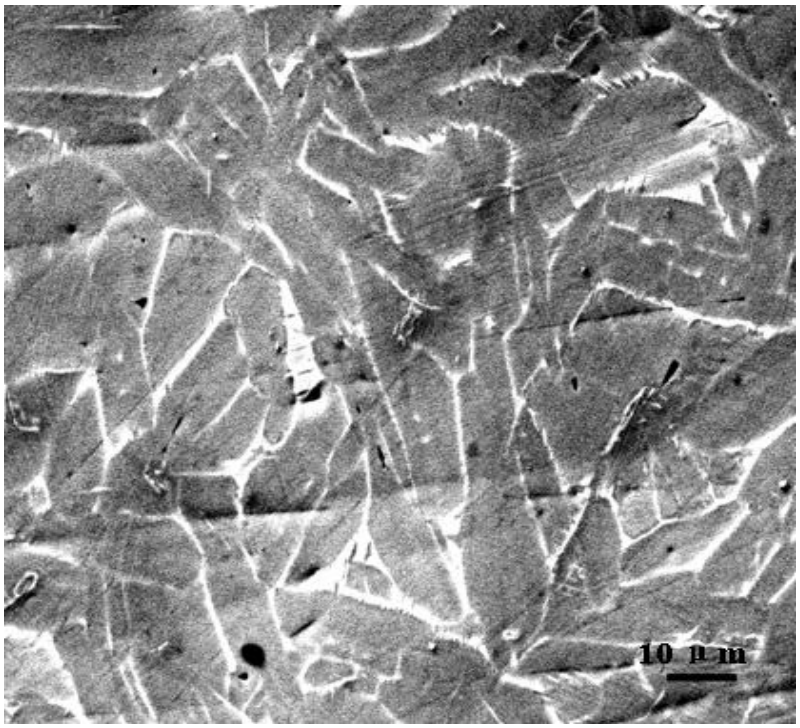

Figure 32 Microstructure of the as-cast Ti-Al-Nb-W-B alloy produced by drop casting

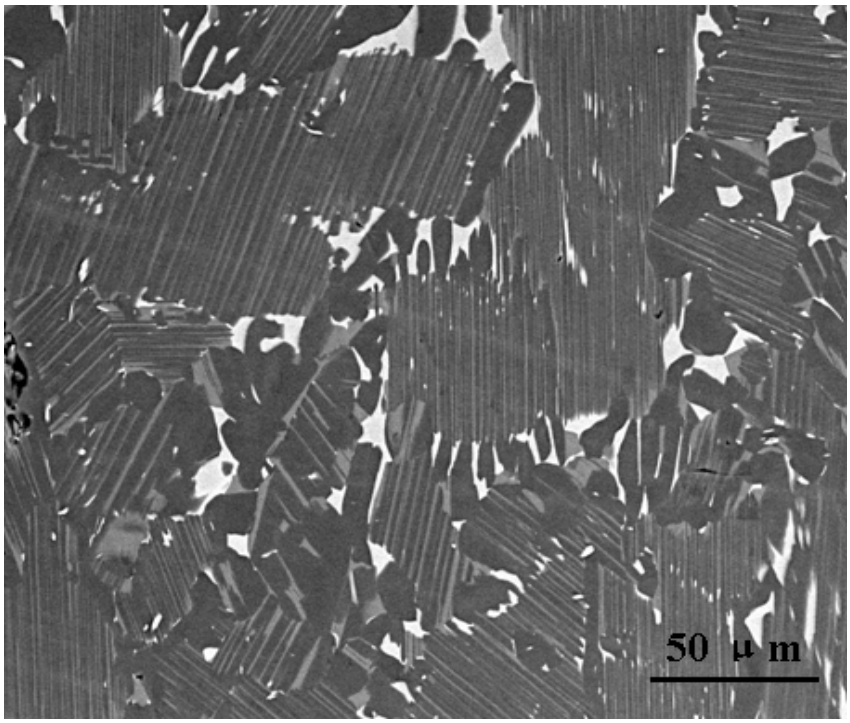

Figure 33 Microstructure of the Ti-Al-Nb-W-B alloy heat treated at 1,450^{0}C, 2 h, salt ice water cooled, then annealed at 1,260^{0}C, 14 h, FC

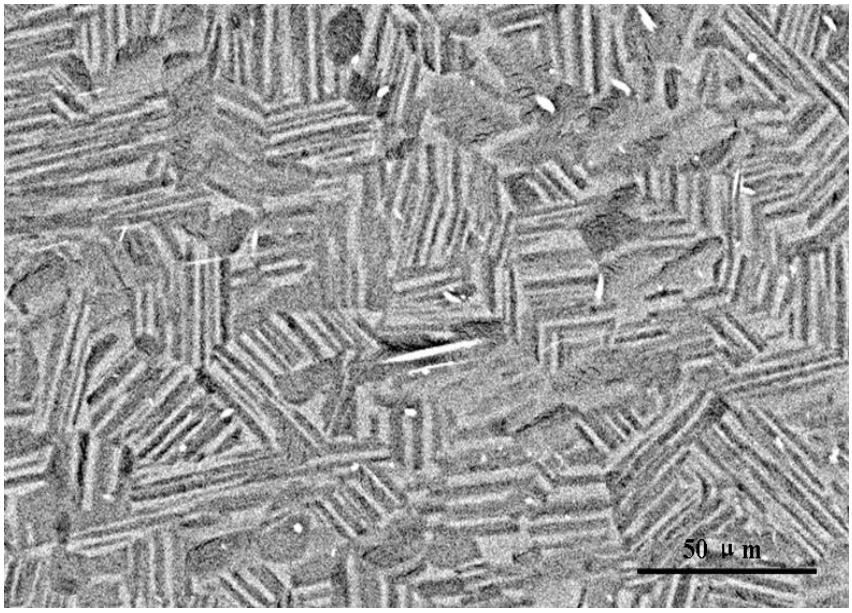

Figure 34 Microstructure of the arc-melted Ti-Al-Nb-W-B alloy heat treated at $1{,}250^{0}$C, 16 h, air cooled

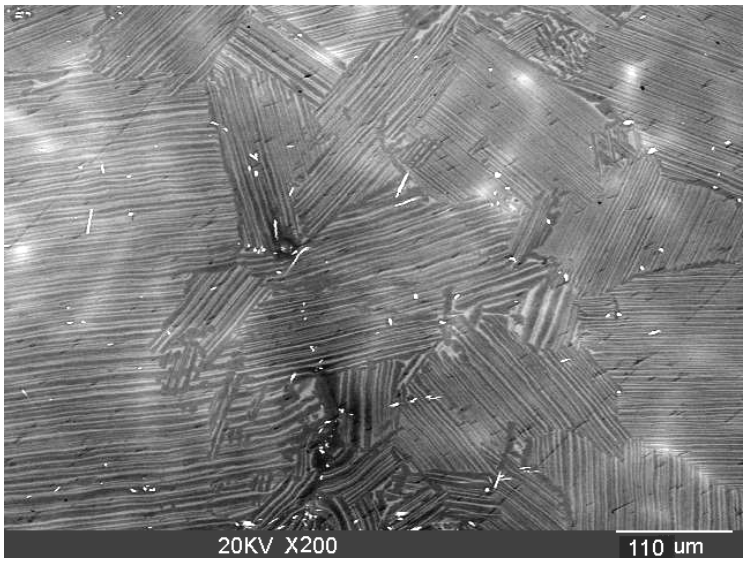

Figure 35 Microstructure of the Ti-Al-Nb-W-B alloy produced by magnetic floatation melting and heat treated at 1,295^{0}C, 10 h, air cooled

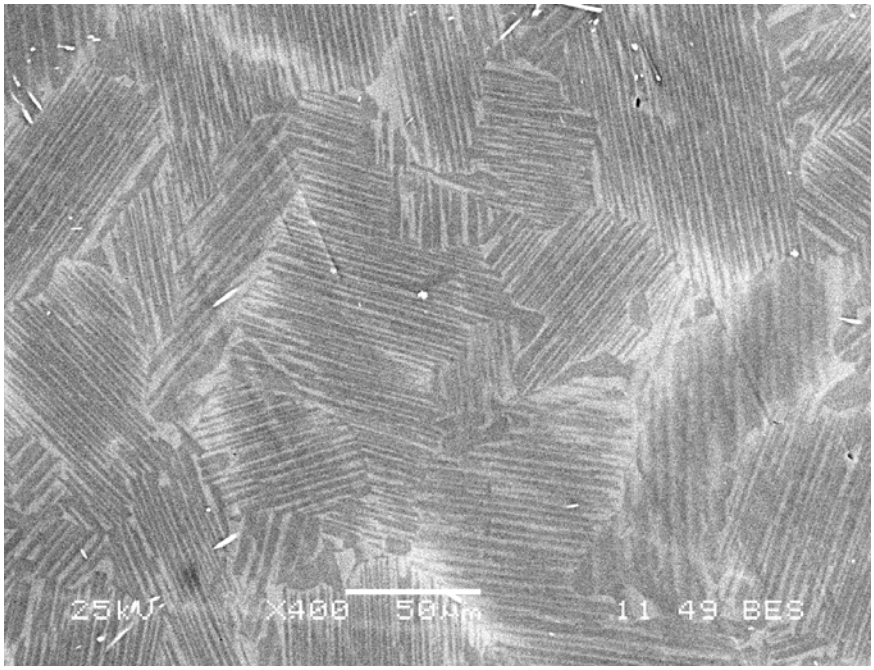

Figure 36 Microstructure of the arc-melted Ti-Al-Nb-W-B alloy heat treated at $1{,}295^{0}$C, 10 h, air cooled

.

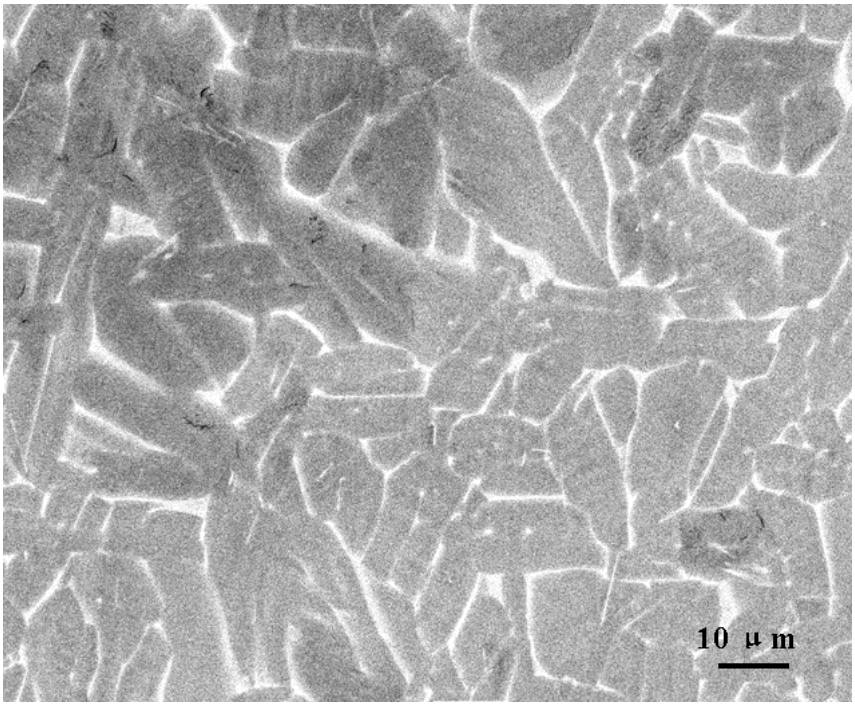

Figure 37 Backscattered electron image of the Ti-Al-Nb-W-B alloy produced by magnetic floatation melting and then remelting

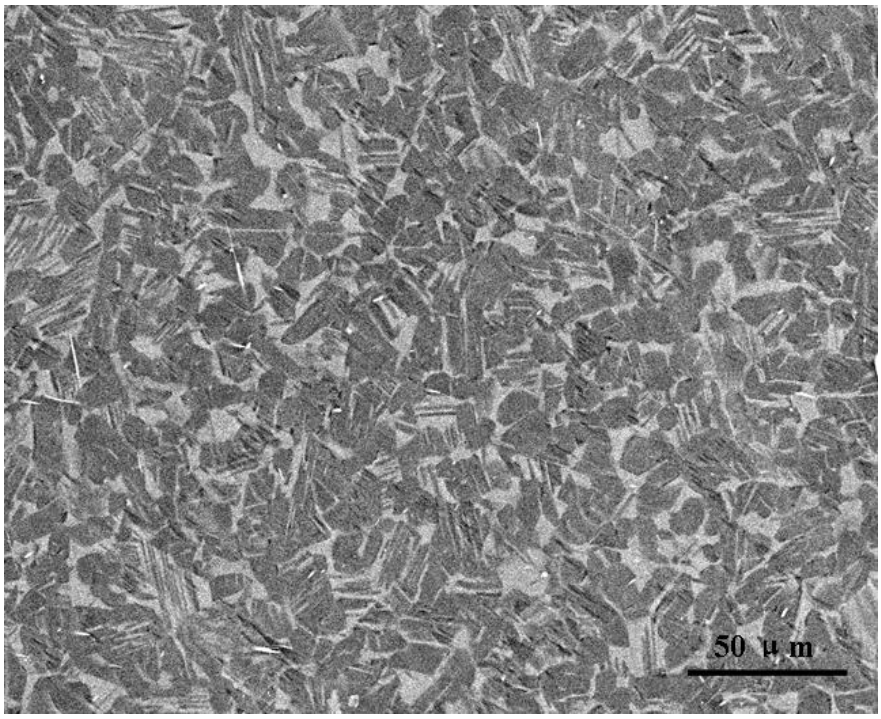

Figure 38 Microstructure of the Ti-Al-Nb-W-B alloy produced by magnetic floatation melting, remelting, and heat treated at $1{,}235^{0}$C, 8 h, FC

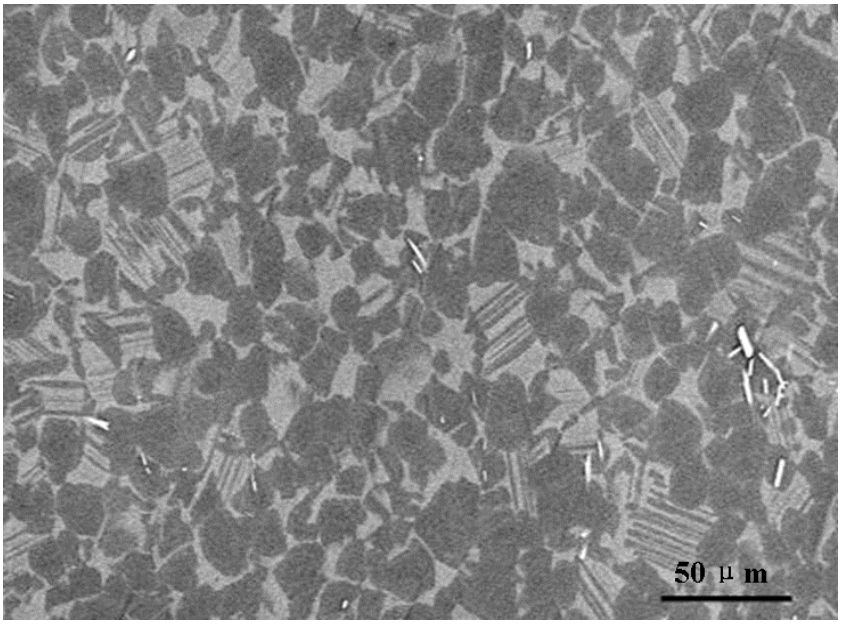

Figure 39 Microstructure of the Ti-Al-Nb-W-B alloy produced by arc-melting, heat treated at 1,240^{0}C, 5 h, FC

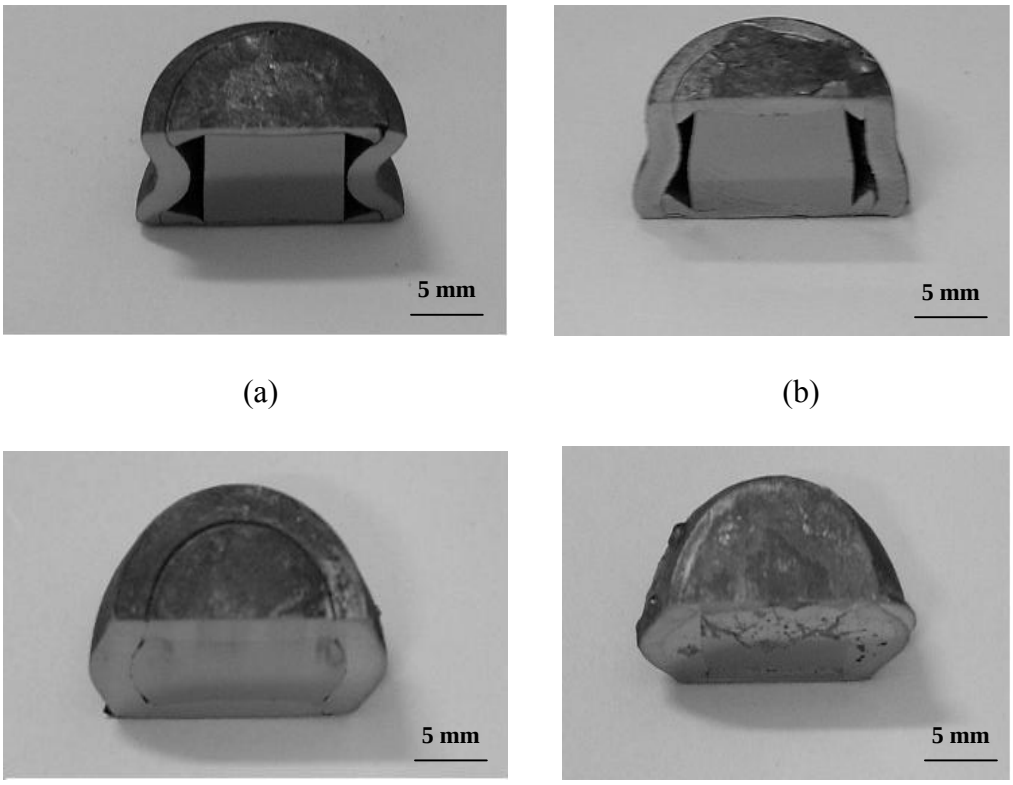

Figure 40 Canned Ti-Al-Nb-W-B alloy after the hot-compression tests at (a) $1{,}050^0$C, (b) $1{,}100^0$C, (c) $1{,}180^0$C, and (d) $1{,}230^0$C

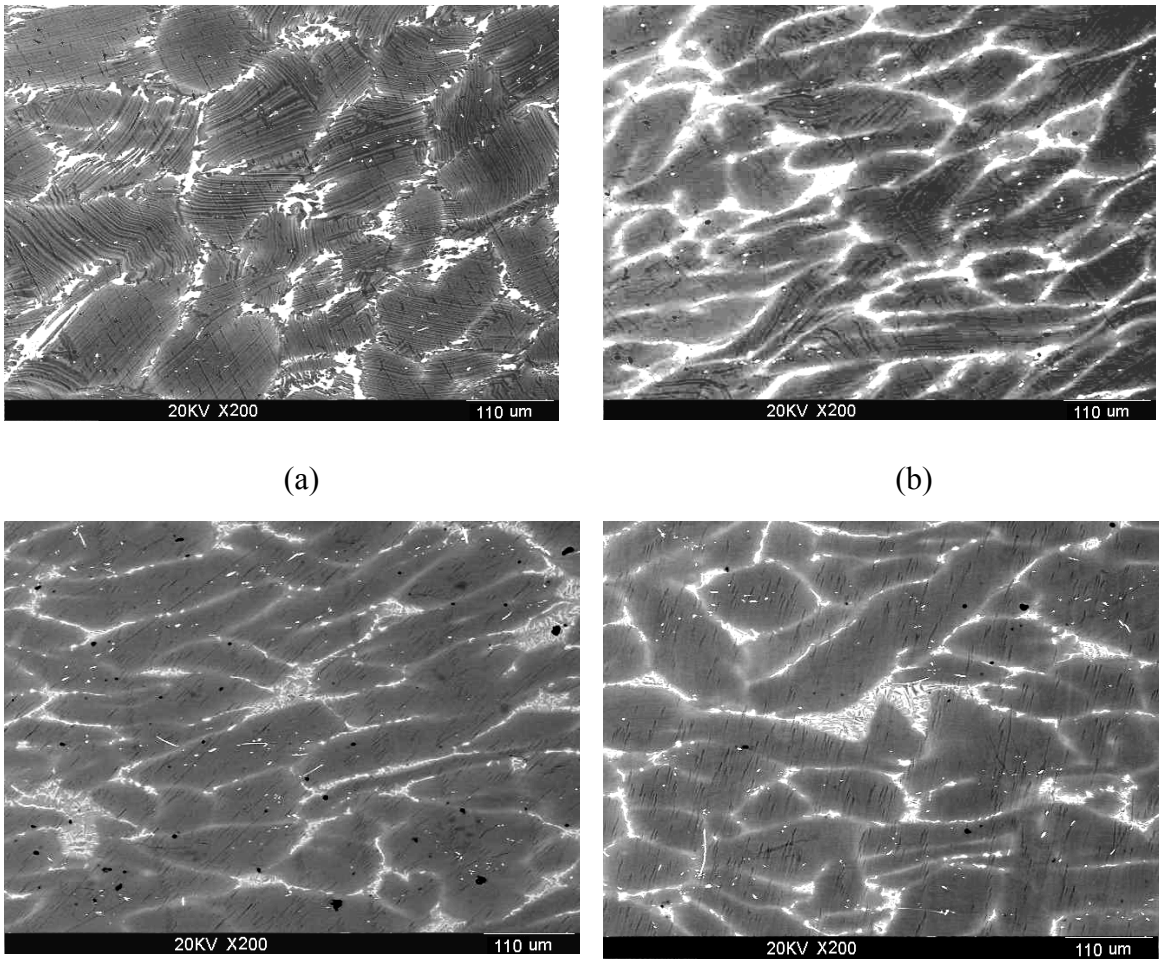

Figure 41 Microstructures of the Ti-Al-Nb-W-B alloys deformed at (a) 1,100^{0}C, (b) 1,150^{0}C, (c) 1,180^{0}C, and (d) 1,200^{0}C

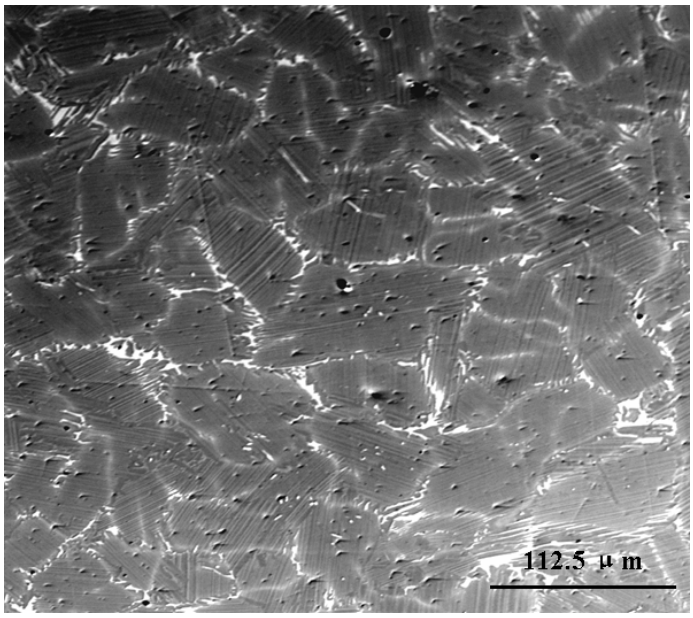

(a)

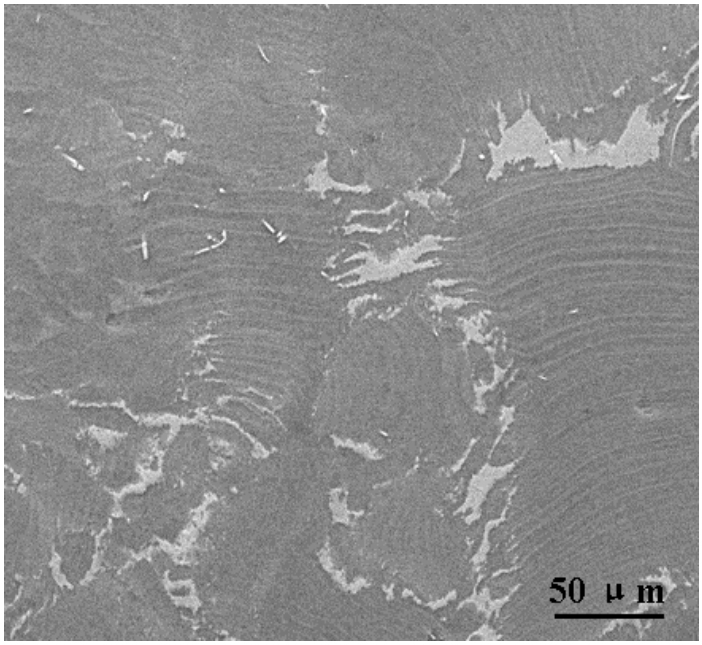

(b)

Figure 42 Microstructure of the (a) as-cast Ti-Al-Nb-W-B alloy produced by magnetic floatation melting, and (b) after deforming at $1{,}180^{0}$C with the deformation of 60%

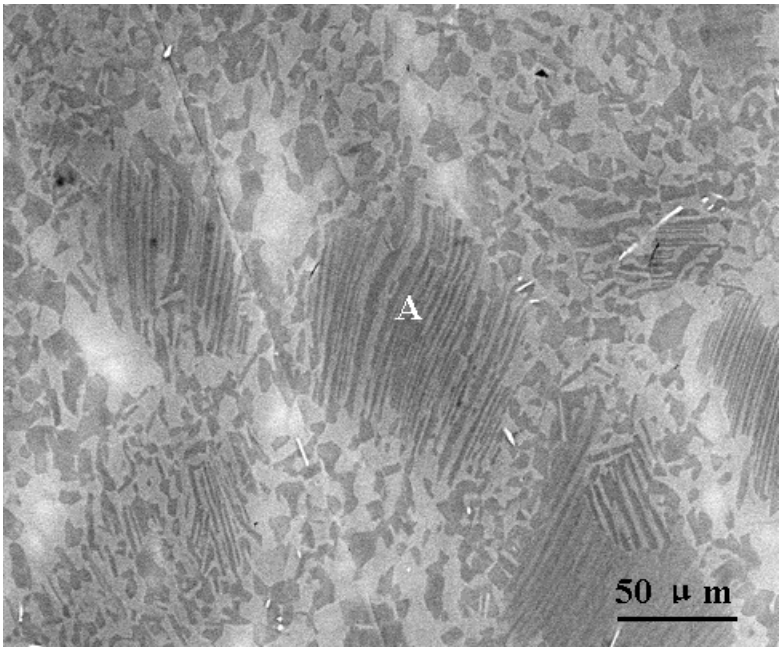

Figure 43 Microstructure of the deformed Ti-Al-Nb-W-B alloy heat treated at $1{,}220^{0}$C, 4 h, air cooled, area A indicates the undeformed lamellar grain

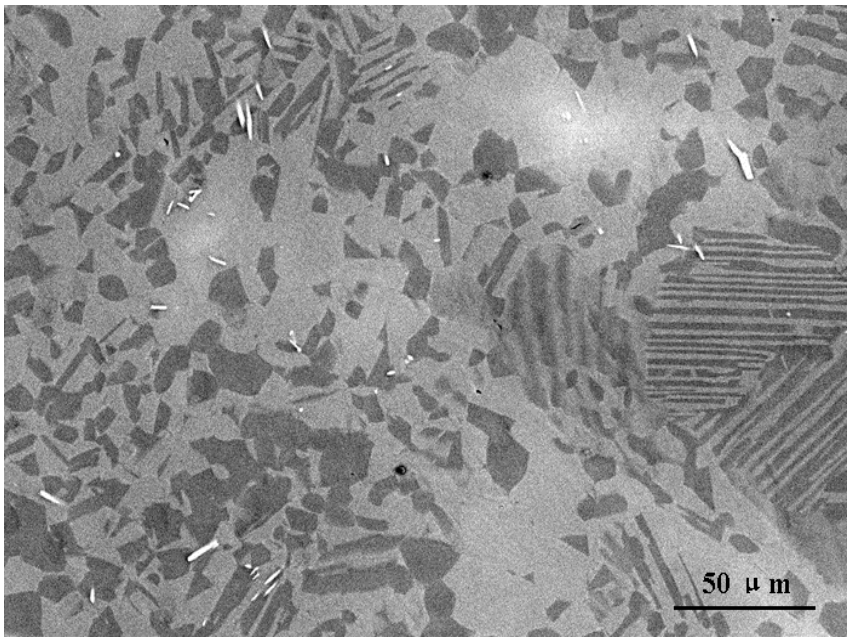

Figure 44 Microstructure of the deformed Ti-Al-Nb-W-B alloy heat treated at $1{,}220^{0}$C, 7 h, air cooled

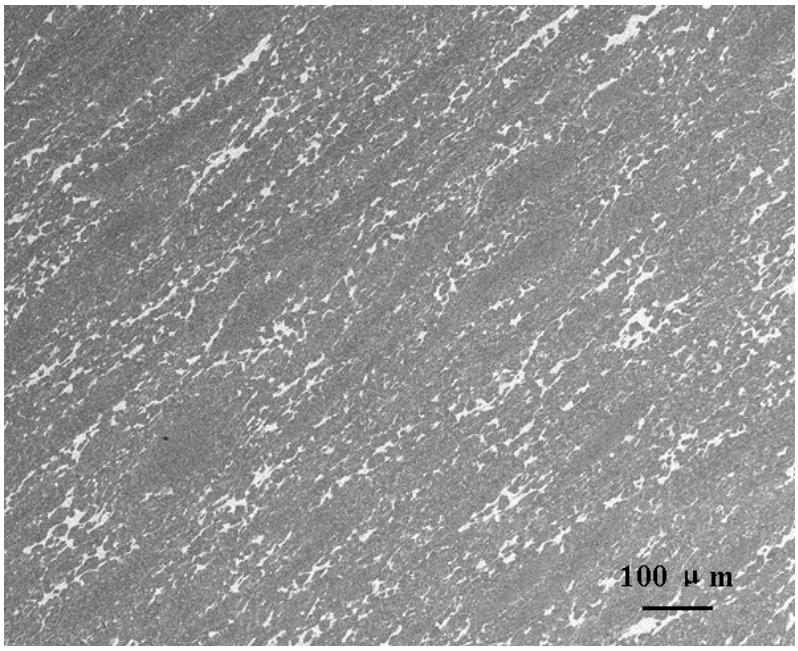

(a)

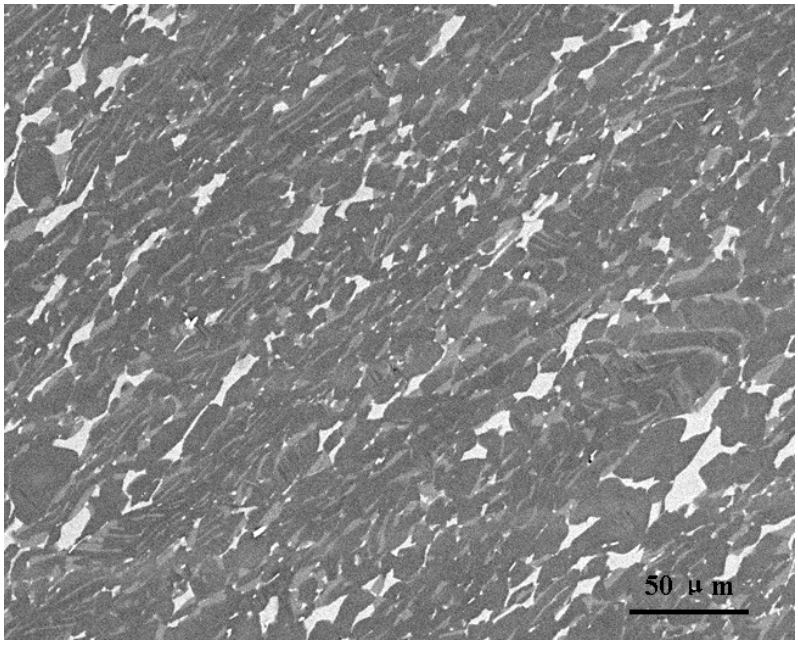

(b)

Figure 45 Microstructure of the Ti-Al-Nb-W-B alloy after the second deformation

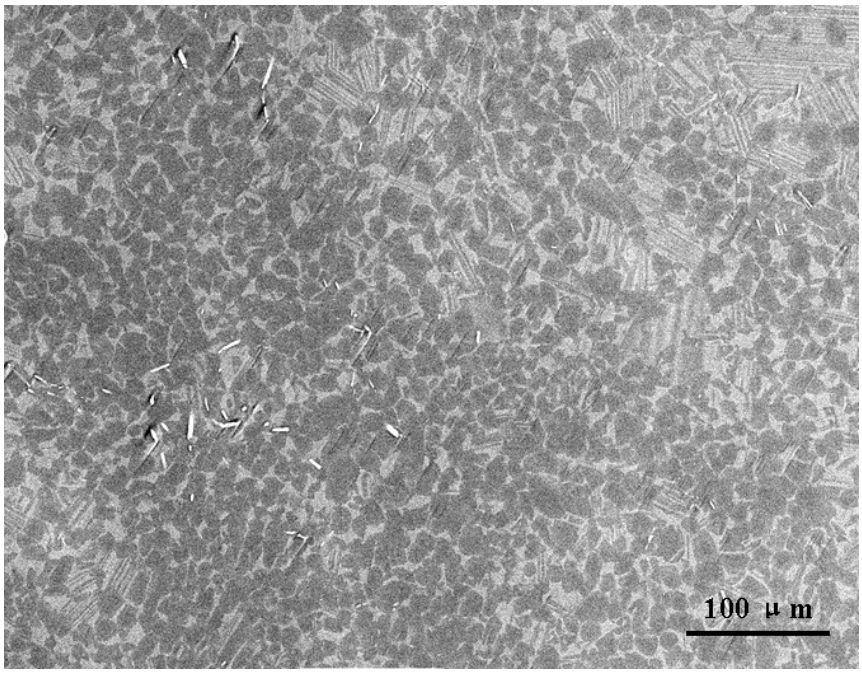

Figure 46 Microstructure of the Ti-Al-Nb-W-B alloy after the second deformation, and then heat treated at 1,240^{0}C, 5 h, FC

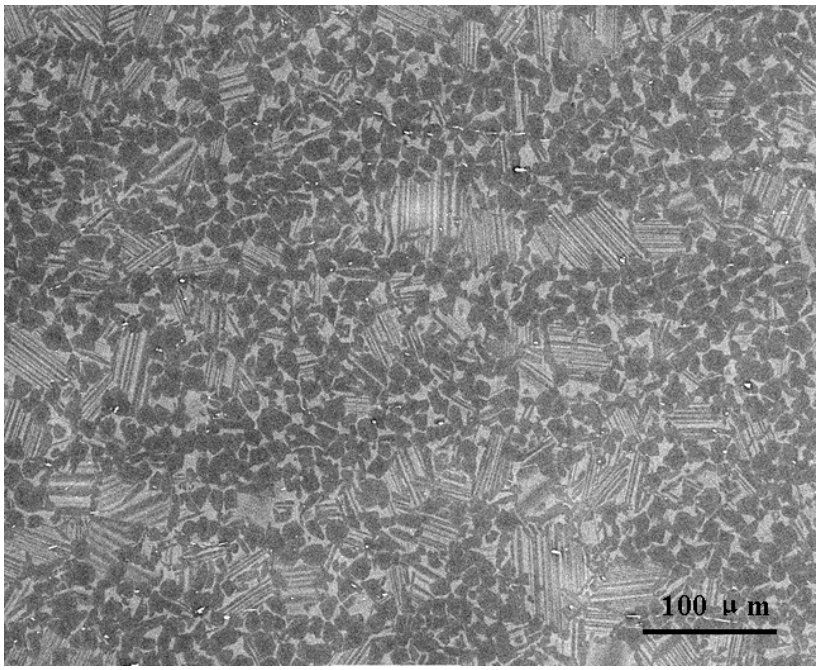

Figure 47 Microstructure of the Ti-Al-Nb-W-B alloy after the second deformation, and then heat treated at $1{,}260^{0}$C, 5 h, FC

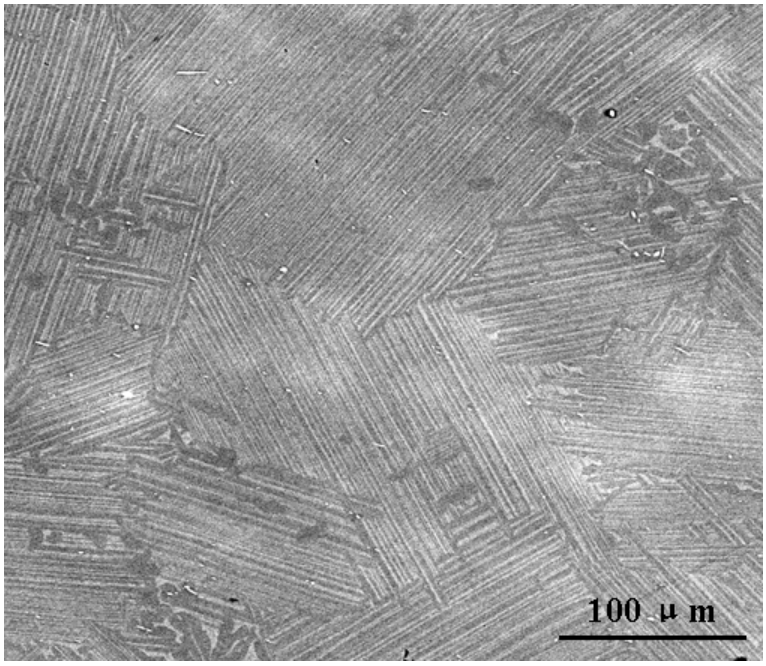

Figure 48 Microstructure of the Ti-Al-Nb-W-B alloy after the second deformation, and then heat treated at $1{,}280^{0}$C, 20 min., FC

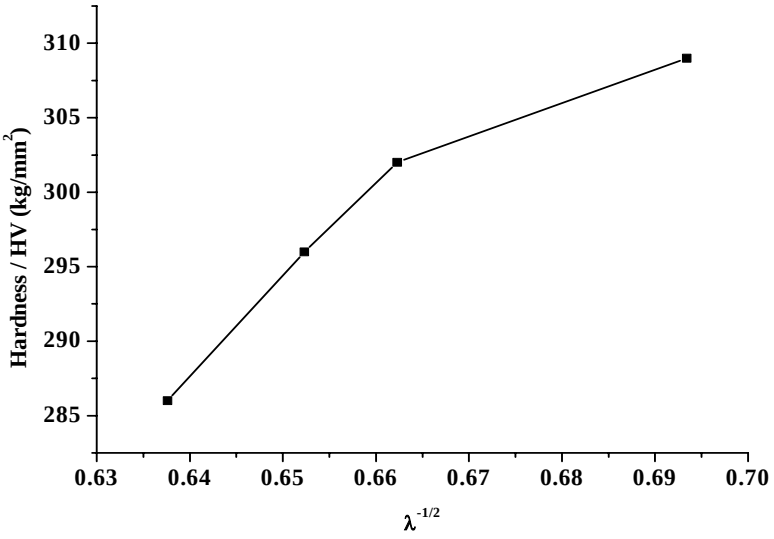

(a)

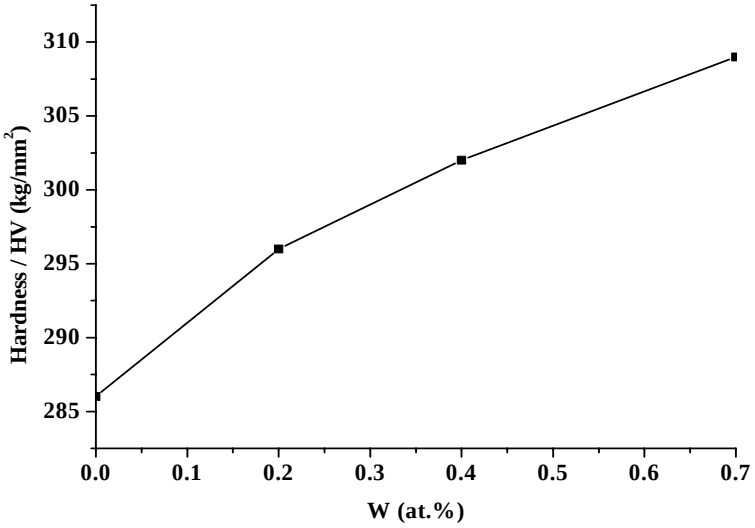

(b)

Figure 49 Effects of (a) interlamellar spacing and (b) W content on the hardness of the Ti-Al-Nb-B-W alloys after heat treating at 1,280^{0}C, 4 h, the hardness of the alloy increases, when the interlamellar spacing of the alloy decreases and the amount of W content of the alloy increases

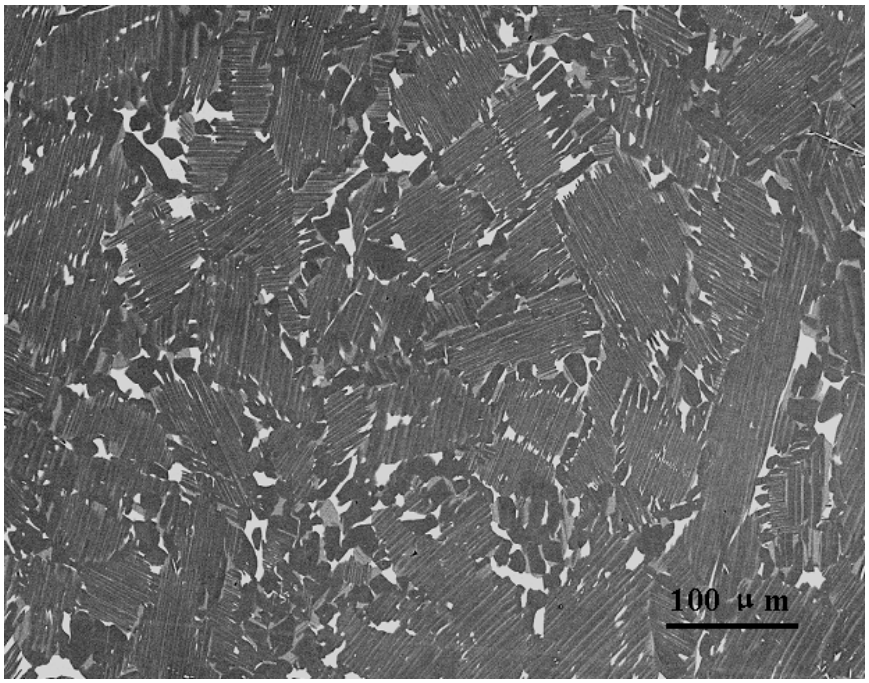

Figure 50 Microstructure of the Ti-Al-Nb-W-B alloy heat treated at 1,130^{0}C, 24 h, FC

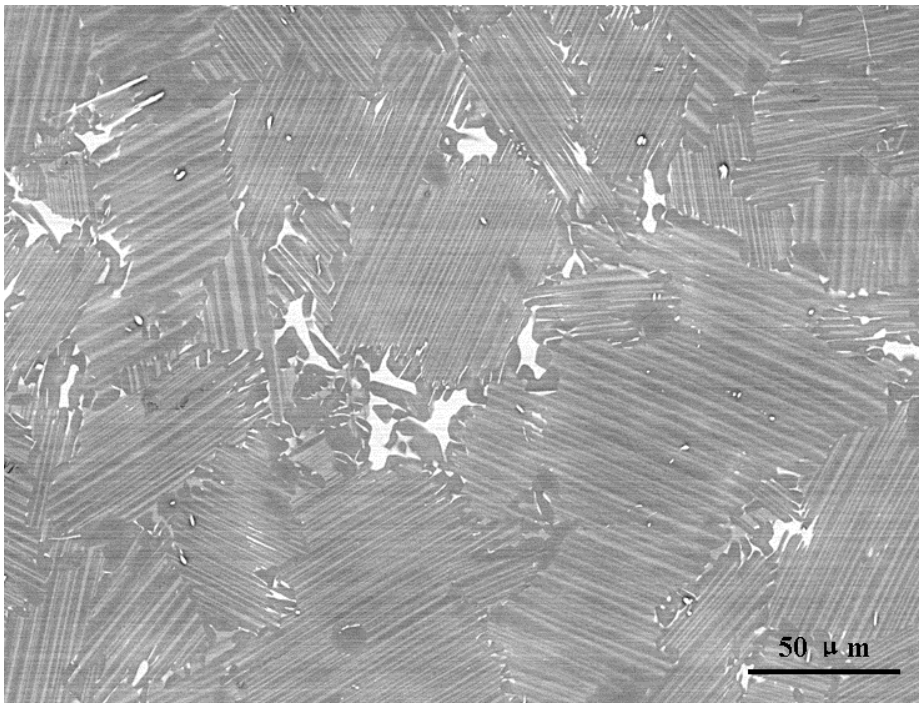

Figure 51 Microstructure of the Ti-Al-Nb-W-B alloy heat treated at 1,130^{0}C, 24 h + 1,280^{0}C, 20 min., FC

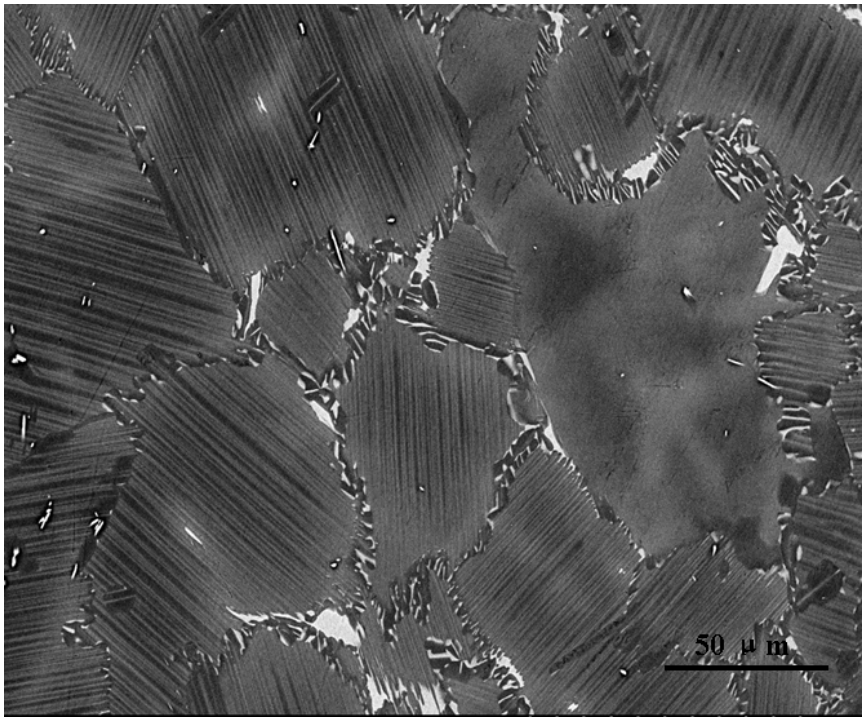

Figure 52 Microstructure of the Ti-Al-Nb-W-B alloy heat treated at 1,280^{0}C, 20 min., FC

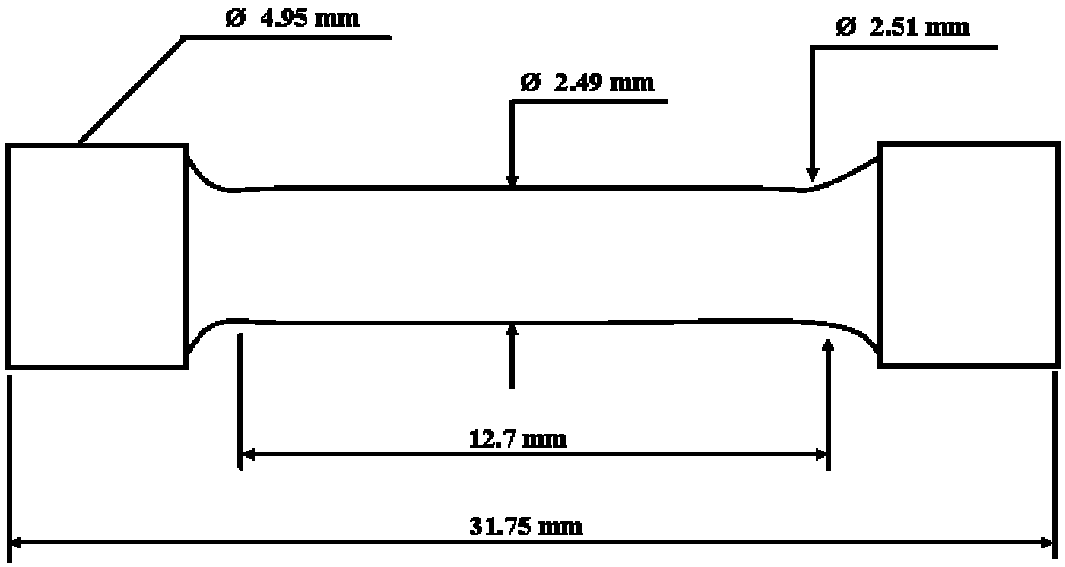

Figure 53 Geometry of the Ti-Al-Nb-W-B alloy sample for tensile test

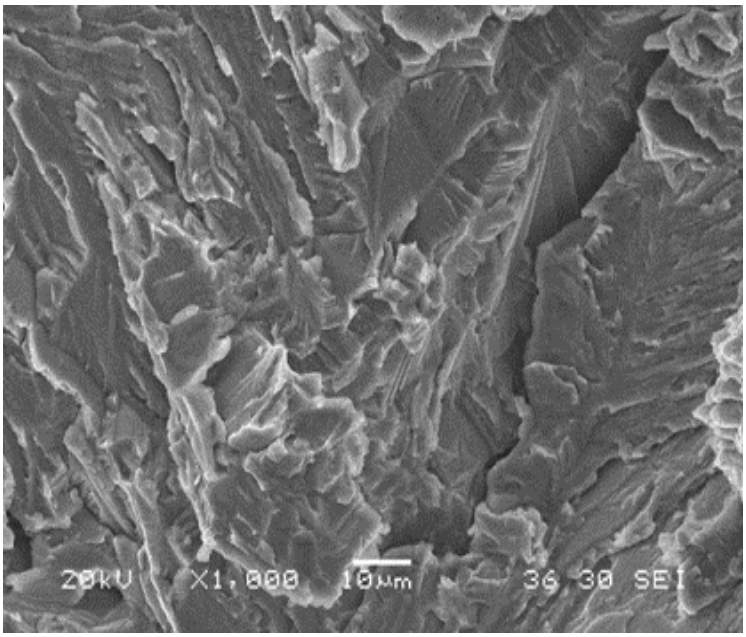

(a)

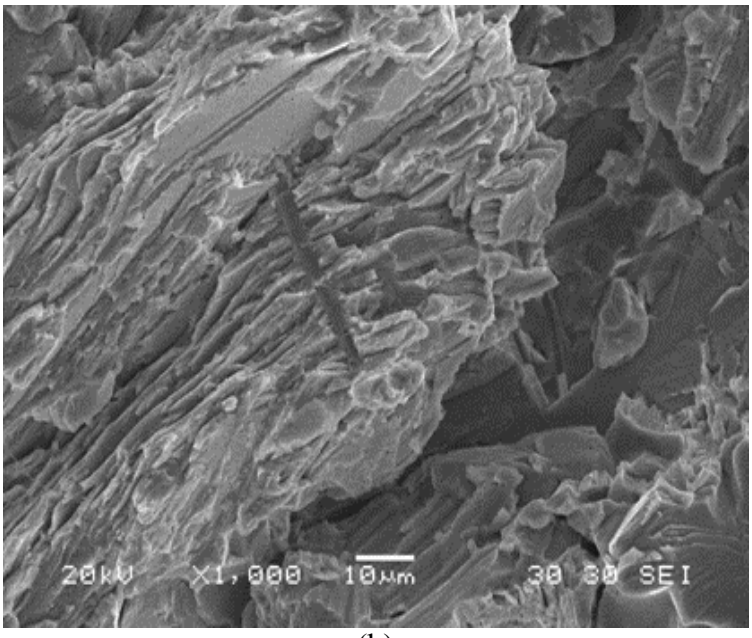

(b)

Figure 54 Fracture surface of the Ti-Al-Nb-W-B alloy heat-treated at 1,130^{0}C, 24 h + 1,280^{0}C, 20 min., FC, tensile tested at (a) room temperature, (b) 300^{0}C, (c) 600^{0}C, and (d) 800^{0}C

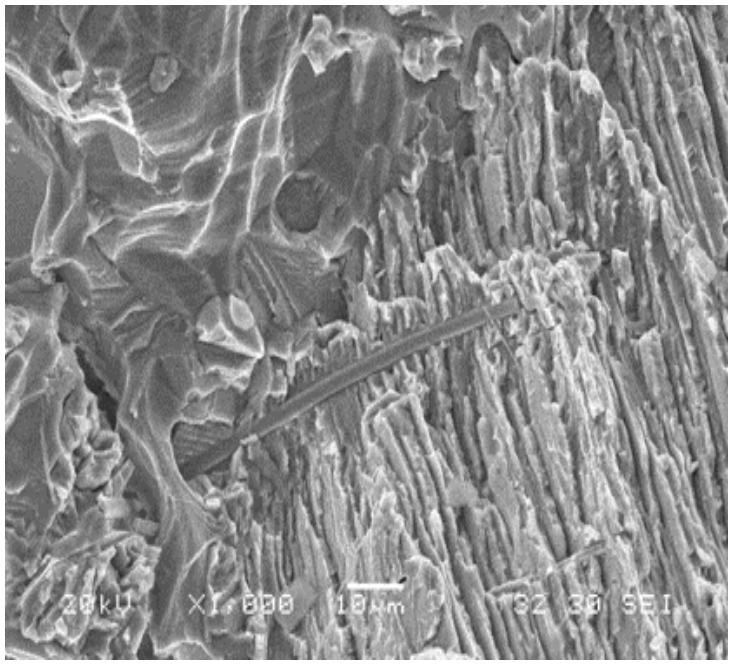

(c)

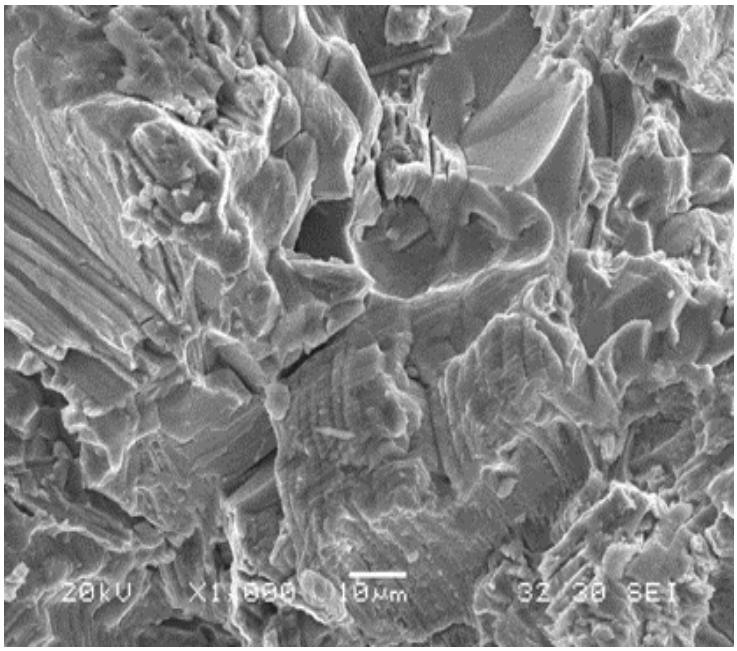

(d)

Figure 54 Continued

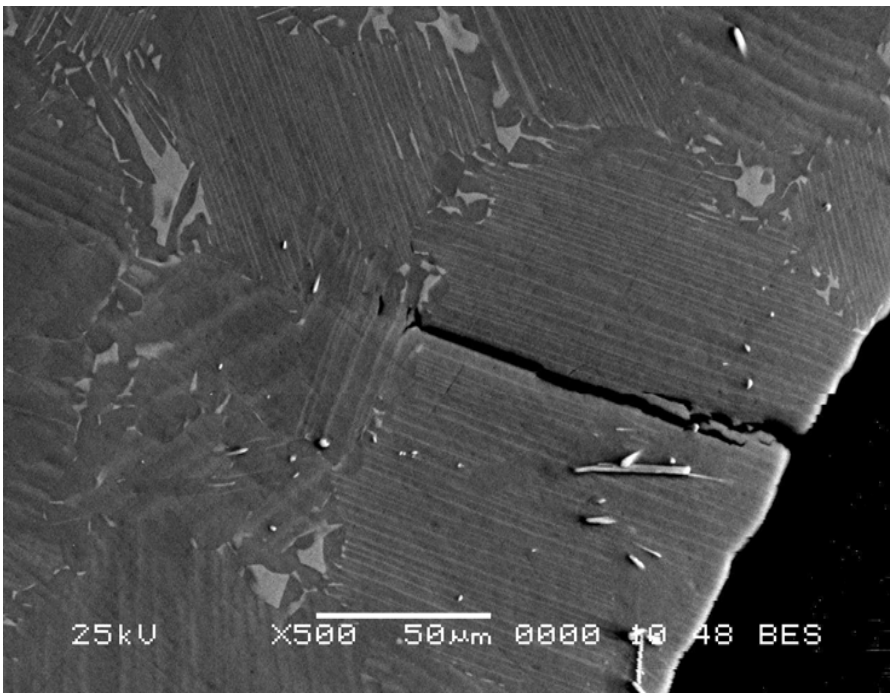

Figure 55 Fracture surface of the Ti-Al-Nb-W-B alloy heat-treated at 1,130^{0}C, 24 h + 1,280^{0}C, 20 min., FC, tensile tested at 600^{0}C

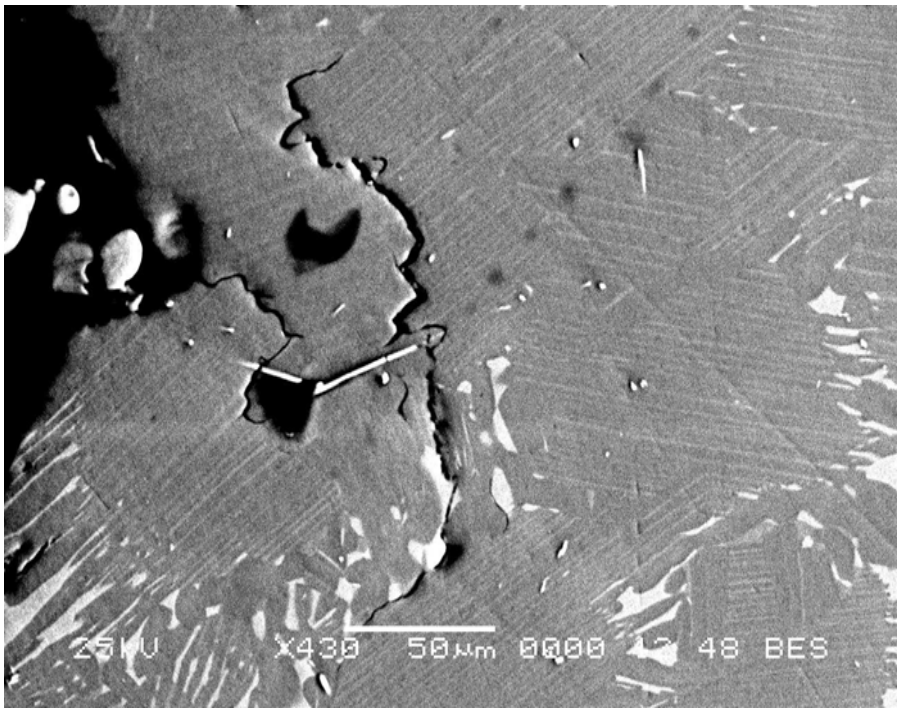

Figure 56 Microcrack at the interface of the boride and the matrix of the Ti-Al-Nb-W-B alloy heat-treated at $1{,}130^0$C, 24 h + $1{,}280^0$C, 20 min., FC, tensile tested at 600^0C

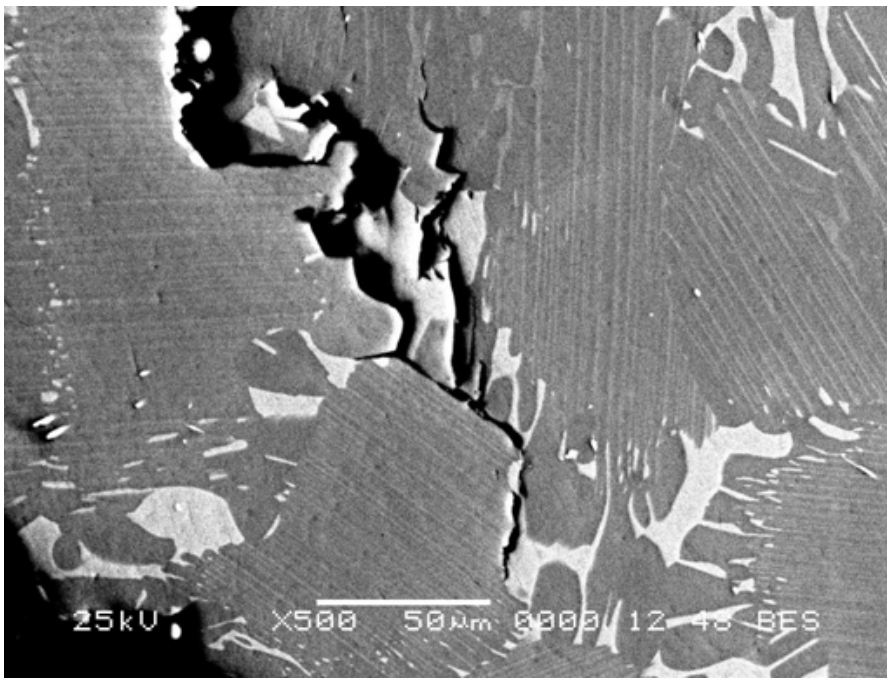

Figure 57 Microcrack at the interface of the β phase and the matrix of the Ti-Al-Nb-W-B alloy heat-treated at 1,130^{0}C, 24 h + 1,280^{0}C, 20 min., FC, tensile tested at 600^{0}C

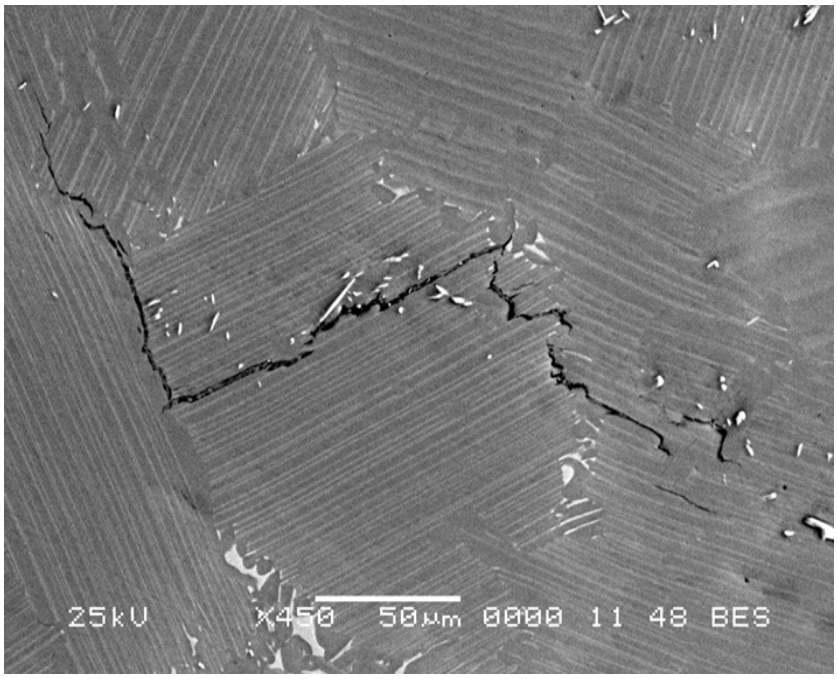

Figure 58 Fracture surface of the Ti-Al-Nb-W-B alloy heat-treated at 1,130^{0}C, 24 h + 1,280^{0}C, 20 min., FC, tensile tested at 800^{0}C

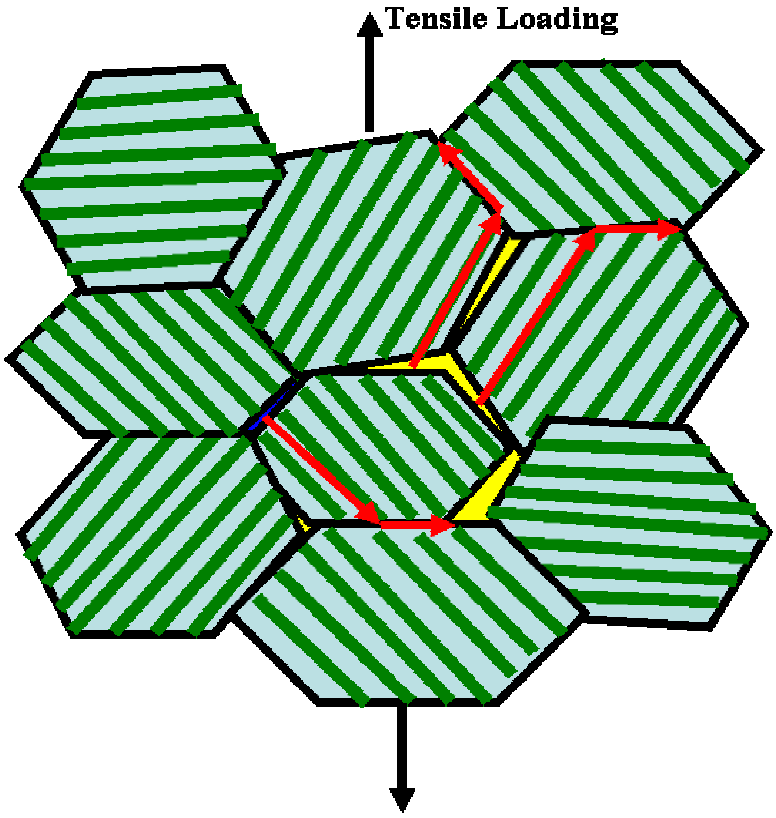

Figure 59 Fracture mechanism of the Ti-Al-Nb-W-B alloy

Vita

Lan Huang was born in Changsha, Hunan Province, People's Republic of China (PRC). During September 1997 to June 2001, she pursued her undergraduate study at the *Hunan University*, and received her Bachelor degree majoring in Computer Science.

Lan came to the *University of Tennessee* in Knoxville and enrolled in the Doctoral Program in Materials Science and Engineering Department in 2002. She received her Master degree in Materials Science and Engineering in 2005. The Doctor of Philosophy degree will be granted in 2008.